DEPOSITIONAL ENVIRONMENT AND RESERVOIR CHARACTERISTICS OF THE MEDRANO SNADSTONE, SOUTHERN OKLAHOMA HOXBAR OIL TREND (SOHOT)

By

SEAN GANES

Bachelor of Science in Geology

Oklahoma State University

Stillwater, OK

2012

Submitted to the Faculty of the
Graduate College of the
Oklahoma State University
in partial fulfillment of
the requirements for
the Degree of
MASTER OF SCIENCE
December, 2020

DEPOSITIONAL ENVIRONMENT AND RESERVOIR CHARACTERISTICS OF THE MEDRANO SNADSTONE, SOUTHERN OKLAHOMA HOXBAR OIL TREND (SOHOT)

Thesis Approved:

Dr. Jim Puckette

Thesis Adviser

Dr. Mary Hileman

Dr. Jack Pashin

ACKNOWLEDGEMENTS

I owe a tremendous amount of gratitude to my advisor, Dr. Puckette, for not only his knowledge, time, and patience that he exhibited with me throughout the thesis project, but also the everlasting impact the he has and will have on my career. I could not have crossed the finish line without Dr. Puckette's guidance throughout the process. Secondly, I am extremely thankful for my additional committee members, Dr. Pashin and Dr. Hileman, for the wealth of knowledge and experience that I was able to refer to for my research. I would also like to thank Dr. Abdelsalem for his incredible help throughout graduate school.

I would also like to thank Unit Petroleum Corporation and EOG Resources for providing much of the data used for the research. Special thanks to, in no particular order, Ed Heald (Unit Petroleum), Todd Conklin (Unit Petroleum), Samantha Dosser (Unit Petroleum), Heather Askew (Unit Petroleum), Tyler Treece (EOG Resources), and Dan Ambuehl (EOG Resources) for their help in accessing the data and setting up the project database.

Last, but certainly not least, I would like to thank my family for the overwhelming support I received throughout the research. I would like to thank my grandparents, Wilbur and Zona Cheap, for the constant encouragement I received even as I fell behind on my research by letting work take over much of my time. I also am forever indebted to my wife, Lexi Ganes, for constantly motivating and pushing me towards the finish line.

Name: SEAN GANES

Date of Degree: DECEMBER, 2020

Title of Study: DEPOSITIONAL ENVIRONMENT AND RESERVOIR CHARACTERISTICS OF THE MEDRANO SANDSTONE, SOUTHERN OKLAHOMA HOXBAR OIL TREND (SOHOT)

Major Field: GEOLOGY

Abstract:

Commercially discovered in 1936, the Medrano Sandstone, is a prolific oil and gas producer in the Cement field and surrounding areas. Deposited during Middle-Pennsylvanian time, it is a member of the Hoxbar group. The sandstone formation is located on the southwestern flank of the Anadarko basin and was most likely the sourced from the Ouachita Mountains in southeastern Oklahoma. The problem that arises when developing a field in the Southern Oklahoma Hoxbar Oil Trend (SOHOT) area with the Medrano Sandstone unit is that on conventional triple combo logs the sandstones show a strong correlation from one well to another, but taking a closer look at the reservoir using specialty NUTECH Logs, the reservoir can vary greatly. These differences (permeability, fluid saturation, etc.) in the reservoir have a direct correlation in the production of the wells. The primary objective for the study is to determine the factors that are influencing the reservoir quality of the Medrano Sandstone.

Results were based around an investigation into the depositional environment of the Medrano Sandstone, as well as an investigation into the petrology and diagenetic history of the Medrano formation. Within a predetermined geographically area public well logs, specialty NUTECH Logs, access to two cores with associated photomicrographs, SEM images, XRD, and core porosity/permeability were used to map the distribution of the Medrano sandstone and build a relationship between depositional environment and reservoir quality of the Medrano sandstone. The integrated data of core sedimentary structures and gamma-ray log motifs supported that of a prograding deltaic depositional environment, where the proposed source of the Medrano Sandstone is the Ouachita Mountains, which is supported by the major constituent of monocrystalline quartz grains and the presence of large chert grains found in core samples. Reservoir quality exhibited a relationship from structural highs of the Medrano Sandstone and also higher permeability reservoirs in the Medrano Sandstone, as determined by NUTECH Logs, are associated with distinct Electrofacies signatures of Blocky and Fining Upward log motifs.

TABLE OF CONTENTS

LIST OF TABLES

Table Page

LIST OF FIGURES

Figure Page

Figure Page

CHAPTER I

INTRODUCTION

Discovered in 1936, the Medrano Sandstone is a prolific oil and gas producing formation located in southeastern Anadarko Basin. Medrano Sandstone vertical wells have produced in excess of 10 billion cubic feet of gas. With the development of horizontal drilling techniques in recent years, an interest in the Medrano Sandstone is renewed and it is imperative that a thorough understanding of the reservoir is achieved to continue developing this oil and gas reservoir. This study will examine the depositional environment and diagenetic history to determine factors influenced the reservoir quality within the Medrano Sandstone. The study will focus on the Medrano Sandstone in south-central Oklahoma in the southeastern part of the Anadarko Basin. The study examines the tri-county area of Caddo, Grady, and Comanche counties, encompassing T.4N. through T.8N., R.7W. through R.12W. (Figure 1.1). Major oil and gas fields in the area of investigation include Cement and Chickasha, which produce from multiple horizons including the Medrano Sandstone.

Objectives

The primary objective of the study is to determine factors influencing reservoir quality within the Medrano Sandstone. A number of analyses were conducted to establish the physical and chemical properties of the sandstone following a systematic plan that included:

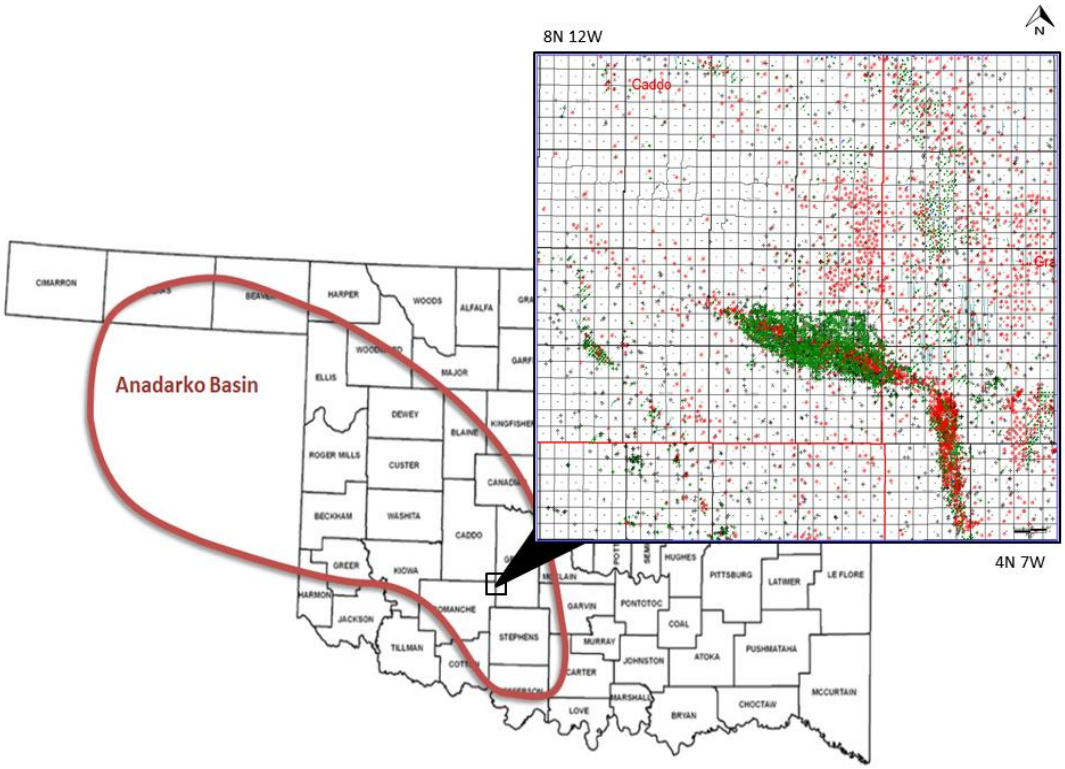

Figure 1.1. Map of Anadarko Basin and Location of Study Area.

1) Generating a system of cross sections (Figure 2.5) within the study area to establish the stratigraphic framework of the Medrano Sandstone interval and adjacent formations,

2) Constructing a structural contour map of the study area to identify major structural features,

3) Examination of cores in the study area and calibration of core to wireline logs to develop electrofacies,

4) Constructing maps showing distribution of the Medrano Sandstone electrofacies,

5) Petrographic analysis of thin sections to determine the detrital composition and diagenetic history of the Medrano Sandstone,

6) Comparison of data from wireline well logs to petrophysical Nutech Logs to identify zones of higher permeability Medrano Sandstone reservoir (Figure 1.3), and

7) Integration of all data to develop a relationship between depositional environment of the Medrano Sandstone and reservoir properties.

Background, Data Acquisition and Methods

The Medrano Sandstone is a member of the middle Pennsylvanian (Missourian Series) lower Hoxbar Group (Figure 1.2) (Boyd, 2008). The Medrano interval is overlain by the Wade Sandstone interval followed by the Oolitic Limestone, lithostratigraphic units that are present throughout most of the study area. The Medrano Sandstone is underlain by a thick marine shale on top of the Hedlund Sandstone, and a thin radiogenic "hot shale" above the Hogshooter Limestone locally called the Hogshooter "Marker". These intervals have distinct wireline log signatures and were useful in defining the Medrano interval by providing easily recognized markers for well to well wireline-log correlations across the study area.

Using geological interpretation software (Petra and Geographix) provided by Oklahoma State University and access to approximately 8,000+ public wireline logs, both Petra and Geographix project databases were developed which was used to analyze Medrano Sandstone facies distribution. In order to accurately construct the stratigraphic framework and map the distribution of the Medrano Sandstone, multiple cross sections were constructed that transected the study area (Figure 2.5). A structure map of the Medrano Sandstone was constructed to define the present structural attitude of the area. Using a sea level datum, subsea values were calculated using wireline-log determined drilled depth and kelly bushing (KB) elevation from log headers. Using the previously mentioned markers above and below the Medrano Sandstone, a computer-generated-thickness map of the Medrano interval was constructed to identify thicker and thinner trends and interpret changes in bathymetry and accommodation at the time of deposition of Medrano sediments. Gross and net thickness maps of the Medrano Sandstone were constructed to delineate the distribution of sandstone and demonstrate

thickness of sandstone bodies. These thickness maps were used to select wells to use in cross sections that illustrate the stratigraphic framework of the Medrano interval and individual sandstone bodies. These cross sections were also used to demonstrate Medrano Sandstone electrofacies and spatial relationships between these electrofacies.

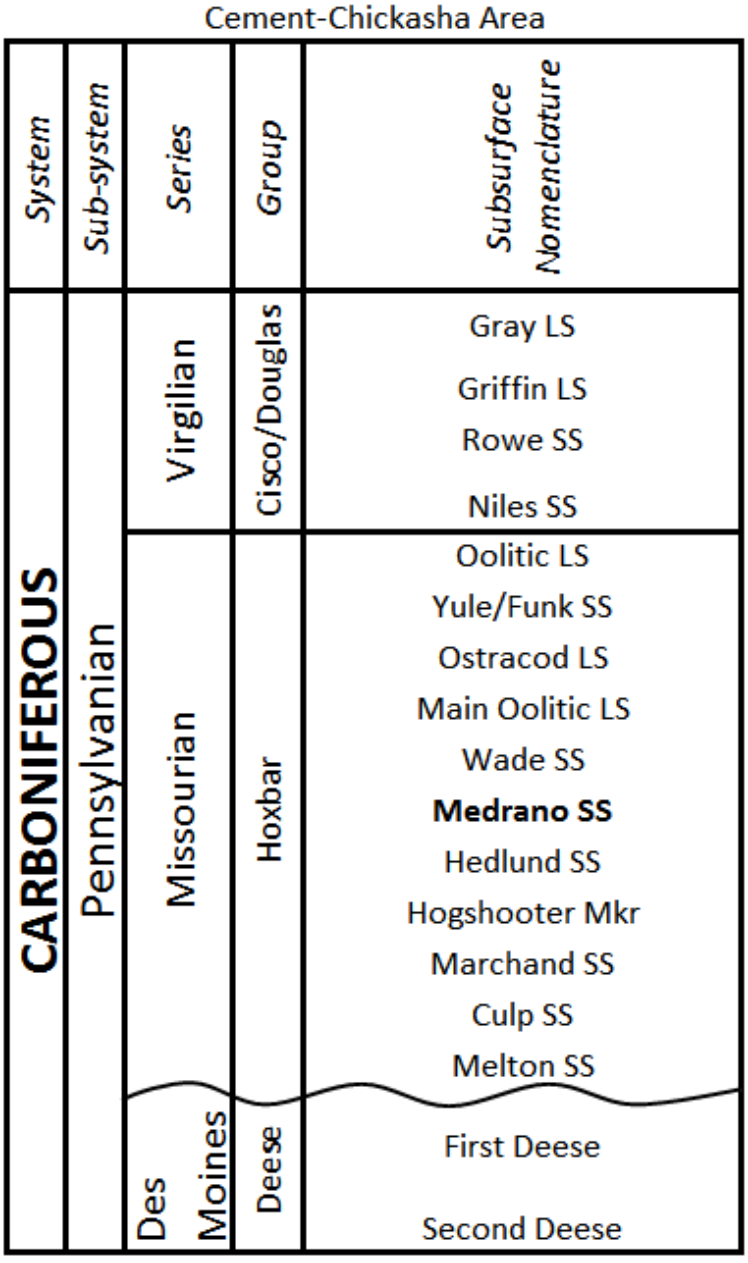

Figure 1.2. Informal stratigraphic nomenclature for Virgilian, Missourian, and Desmoinesian units in the Cement/Chickasha area. (Modified from Lange, 1984)

Two cores were analyzed during this investigation, the Schmidt 16-3H located in Sec. 16, T. 6N., R. 8W, and the Jobe 31-1 located in Sec. 31, T. 6N., R.7W. (Figure 1.3). These cores were examined and described for lithology, sedimentary structures, textures, and biogenic features. Burrowing is abundant and occurs across much of the cored interval. Burrowing intensity (Table 1) was assessed using the guidelines in Taylor and Goldring (1993). Along with hand-sample scale observations from these cores, a petrographic analysis was conducted using thin section microscopy, scanning electron microscopy (SEM) images, and x-ray diffraction (XRD). Petrographic analyses conducted by Weatherford Laboratories in Houston were provided for the investigation by Unit Petroleum Company and EOG Resources. All data were integrated to interpret the origin of the Medrano Sandstone, its distribution and reservoir properties.

Table 1.1. Bioturbation intensity and classification index from Taylor and Goldring (1993).

Bioturbation Index (B.I.)	Percent Bioturbation	Classification
0	0	No bioturbation
1	1-4	Sparse bioturbation, bedding distinct, few discrete traces and/or escape structures
2	5-30	Low bioturbation, bedding distinct, low trace density, common escape structures
3	31-60	Moderate bioturbation, bedding boundaries sharp, traces discrete, rare overlap of traces
4	61-90	High bioturbation, bedding boundaries indistinct, high traces density, common overlap of traces
5	91-99	Intense bioturbation, bedding completely disturbed (just visible), limited reworking, later burrows discrete
6	100	Complete bioturbation, sediment networking due to repeated overprinting

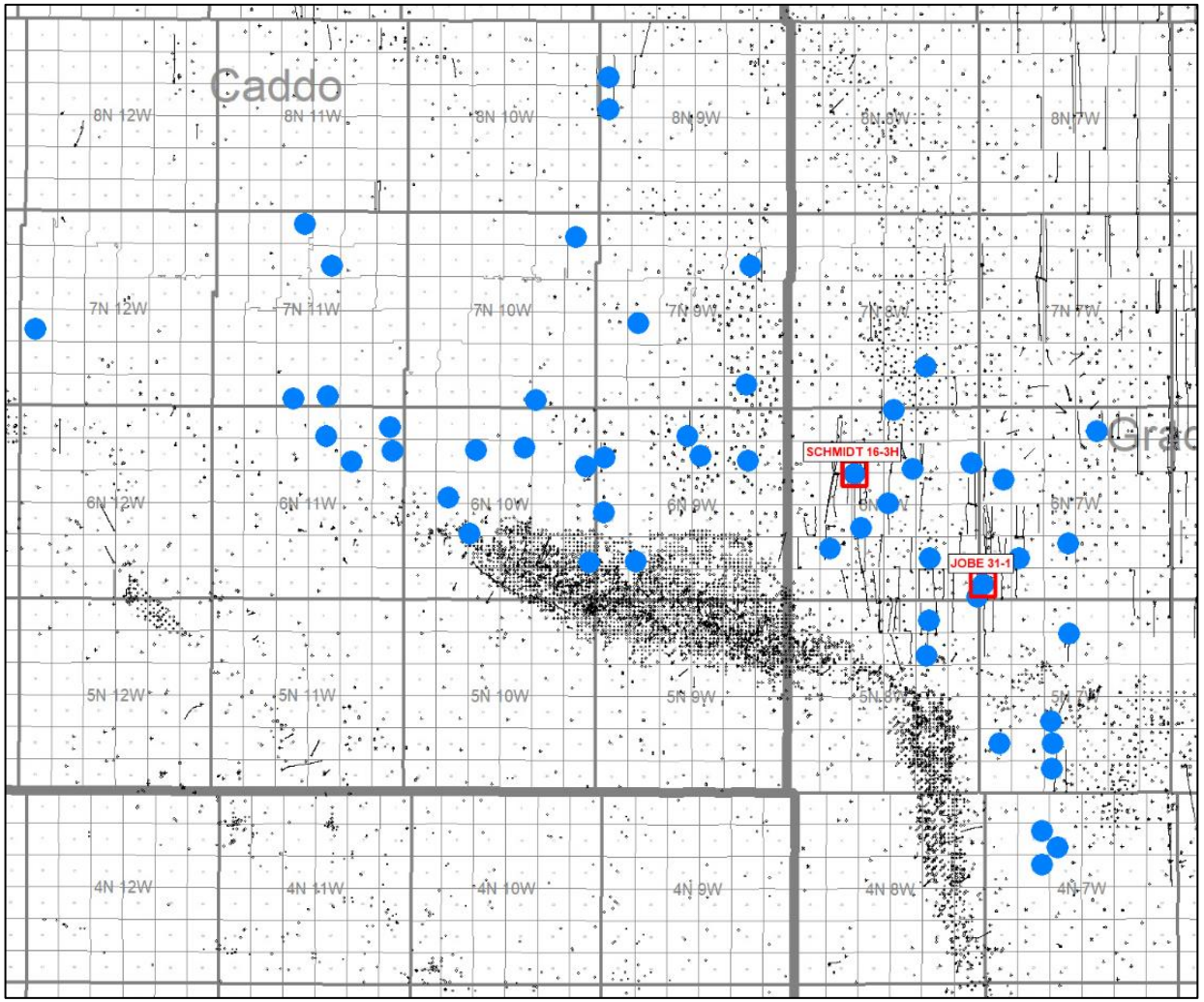

Figure 1.3. Map of study area showing locations of drilled wells and their outcomes. Wells with Nutech logs used for study are indicated with blue circles. Cored wells (Schmidt 16-3H and Jobe 31-1) are highlighted by red box around blue circles.

Previous Investigations

Although the study area has an extensive history with respect to oil and gas activity, the number of studies of the Medrano Sandstone are few and these were parts of broader studies of the Marchand Sandstone unit that is stratigraphically below the Medrano. As previously mentioned, the Medrano Sandstone is one formation in the Hoxbar Group. In contrast to the nomenclature used by the OGS (Boyd, 2008), the United States Geological Survey (USGS) uses Hoxbar Formation (USGS, 2020). Subsurface stratigraphy of the Hoxbar Group uses informal operational names including Hedlund, Medrano, Wade and Oolitic that are accepted by the petroleum industry. Harlton (1960) defined the Hoxbar as the vertical interval from the top of the No-ho-co Formation (Oolitic Limestone) to the base of the Marchand Formation. Lange (1984) defined the Hoxbar Group as extending downward from the Oolitic Limestone to the base of the Melton Sandstone interval (Figure 1.2). White and others (1999) noticed the Hoxbar Group exhibits complex intertonguing relationships of coarse siliciclastics and shale. An abundance of conglomerate within the Hoxbar Group is interpreted as evidence that the area south of the Cement pool was tectonically active during Late Pennsylvanian time (Harlton, 1960). The Medrano Sandstone, originally named in the Cement area, has been divided into "Upper" and "Lower" units, which are separated by shale. The thickness of the Medrano Sandstone ranges from 0 feet to the east where it pinches out stratigraphically, to up to 300 feet to the west in the deeper part of the Anadarko Basin. The Medrano Sandstone is stratigraphically equivalent to the Cottage Grove Sandstone in Canadian County (Boyd, 2008).

Boeckman (1958) concluded that the principal structures that surround the study area strongly influenced the deposition of sand. Sawyerr (1973) and Seale (1982) describe the Medrano sandstone as a tide-dominated deltaic depositional environment, although it has also been described as a fluvial channel to fluvial dominated deltaic environment. Lange (1984) studied the Medrano and its carbonate shelf equivalent, the Belle City Limestone, and proposed

the Lower Medrano represented a significant period of progradation as indicated by the coarsening-upward sequence interpreted from upward-decreasing gamma-ray values evident on numerous well logs. A variety of facies were described within the Lower Medrano unit, but all subunit sandstones were grouped into deltaic (shallow water) and basinal marine (deeper water) facies (Lange, 1984). The Upper Medrano Sandstone is believed to represent a period of transgression, and consists of clastic sands and shales (Lange, 1984). Seale (1982) interpreted the thinner deposits to the east, which grade into the thicker deposits to the west, to represent a transition zone from shelf to basin. Lange (1984) constructed isopach maps of the upper Medrano and suggested thickness was strongly influenced by bathymetric highs in the Lower Medrano topography. Harlton (1960) and Jordan (1957) describe the Medrano Sandstone as mostly very fine to medium-grained sandstone although the uppermost portion of the Medrano is often a chert, sand, and limestone conglomerate. Sawyerr (1973) described the Medrano Sandstone in the Dutton-Verden-Norge field as white to gray, slightly calcareous, with poor to fair sorting and often tightly cemented, characteristics contributing to the lack of oil and gas production in the area at the time. Seale (1982) proposed the facies change from the Belle City Limestone to the east into the Medrano Sandstone toward the west was more evidence that clastic material of the Medrano unit was being transported across the shallow marine shelf into deeper basinal areas.

The only comprehensive petrographic analysis of the Medrano Sandstone is Seale (1982) who used scanning electron microscopy (SEM) to show that clay minerals occur locally as partial coatings on detrital grains, replacing carbonate cement and reducing permeability and porosity. Waller (1994) conducted a similar study on the coeval Cottage Grove Sandstone and found that factors controlling diagenesis in the Cottage Grove Sandstone were closely related to the original depositional processes. These processes produced depositional facies with differing physical and chemical properties that controlled migration of fluids and precipitation of cements.

CHAPTER II

GEOLOGIC SETTING

Regional Structural Setting

The study area is located in the southeastern Anadarko Basin in south-central Oklahoma (Figure 1.1). The Anadarko Basin of western Oklahoma and the Texas Panhandle is among the more prolific petroliferous provinces in North America. The basin is an asymmetrical cratonic basin that extends from south-central Oklahoma to the northwest into the Texas Panhandle, with the axis of the basin adjacent and running parallel to the Amarillo-Wichita Uplift (Adler, 1971). The basin covers an area of roughly 50,000 square miles in western Oklahoma, southwestern Kansas, and the northeastern portion of the Texas Panhandle (Henry and Hester, 1995). The basin contains in excess of 40,000 feet of Paleozoic sedimentary rocks that represent deposition in shallow-water environments (Perry, 1989). The southern boundary of the Anadarko Basin is formed by the frontal fault system of the Amarillo-Wichita Uplift. The basin is bounded to the east by the Nemaha Ridge, and the west and northwest by the Cimarron Arch (Moore, 1979). The northern shelf of the Anadarko Basin extends to the north across Oklahoma and much of western Kansas where it includes the Hugoton Embayment (Figure 2.1).

The structural history of the Anadarko Basin as summarized in Johnson (1988), is divided into four periods: 1) an igneous episode, during Precambrian and Early to Middle Cambrian, when basement rocks were emplaced in the area of the Wichita uplift and the southern part of what would be the Anadarko Basin, 2) an early epeirogenic episode, ranging from Late Cambrian through Mississippian time, when marine sediments were deposited in a broad epicontinental sea referred to as the Oklahoma Basin, 3) an orogenic episode, during the Pennsylvanian, when the

Oklahoma Basin was broken into a series of sharp uplifts and major basins, including the Anadarko Basin and 4) late epeirogenic episode that began in Permian time and has persisted through present day, this episode includes infilling of the basin and uplift associated with the Laramide Orogeny.

The basin assumed its present configuration during the late Mississippian through Pennsylvanian due to compressive stresses associated with movement along the Amarillo-Wichita Mountain frontal fault system. This displacement is characterized by substantial vertical block uplift and regional, left-lateral, strike-slip movement. The component of displacement associated with vertical uplifts exceeds 20,000 feet (Evans, 1979).

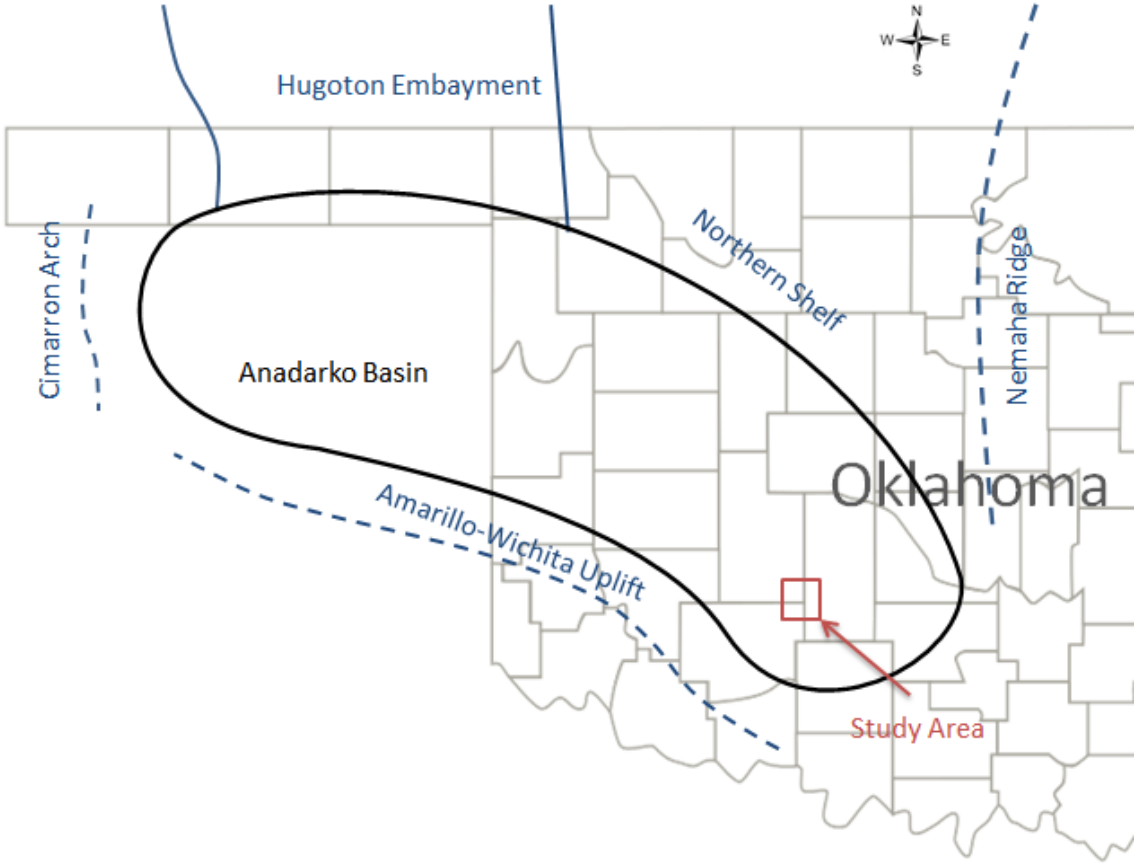

Figure 2.1. Major tectonic provinces of central and western Oklahoma and the Texas Panhandle. The deep Anadarko basin is outlined and location of study indicated by red box on map.

A majority of sediment deposited in eastern Oklahoma and the eastern Anadarko Basin during the Late Pennsylvanian (Missourian and Virgilian) series was sourced from the Ouachita Mountains (Cain, 2018; Krumme and Visher, 1972). This Ouachita source was also noted by Rasco and Adler (1983) by the evidence of increasing sediment in an easterly direction and progression from marine to marginal-marine environments to the east (Figure 2.2).

Local Tectonism and Structural Geology

Two major structural features dominate the study area. These are the Cement anticline in the south-central portion of the study area, and the Chickasha anticline in the southeastern portion (Figure 2.3). The Cement anticline, discovered in 1916, consists of the East and West Cement structures, asymmetrical, west-northwesterly trending anticlines. The Chickasha anticline, which is located 5 miles southeast of the town of Cement, Oklahoma, trends north-northwest, (Herrmann, 1961). The present structural configuration is evident on a computer-generated structure map contoured on the Medrano Sandstone. The Medrano structural contour map shows an elongated northwest-southeast trending, bowl shaped syncline to the north of the Cement and Chickasha anticlines. Structural strike in the eastern part of the study area is south-southeast to north-northwest, whereas dip is to the southwest toward the tectonically low area in the syncline immediately north of the Cement-Chickasha anticlines.

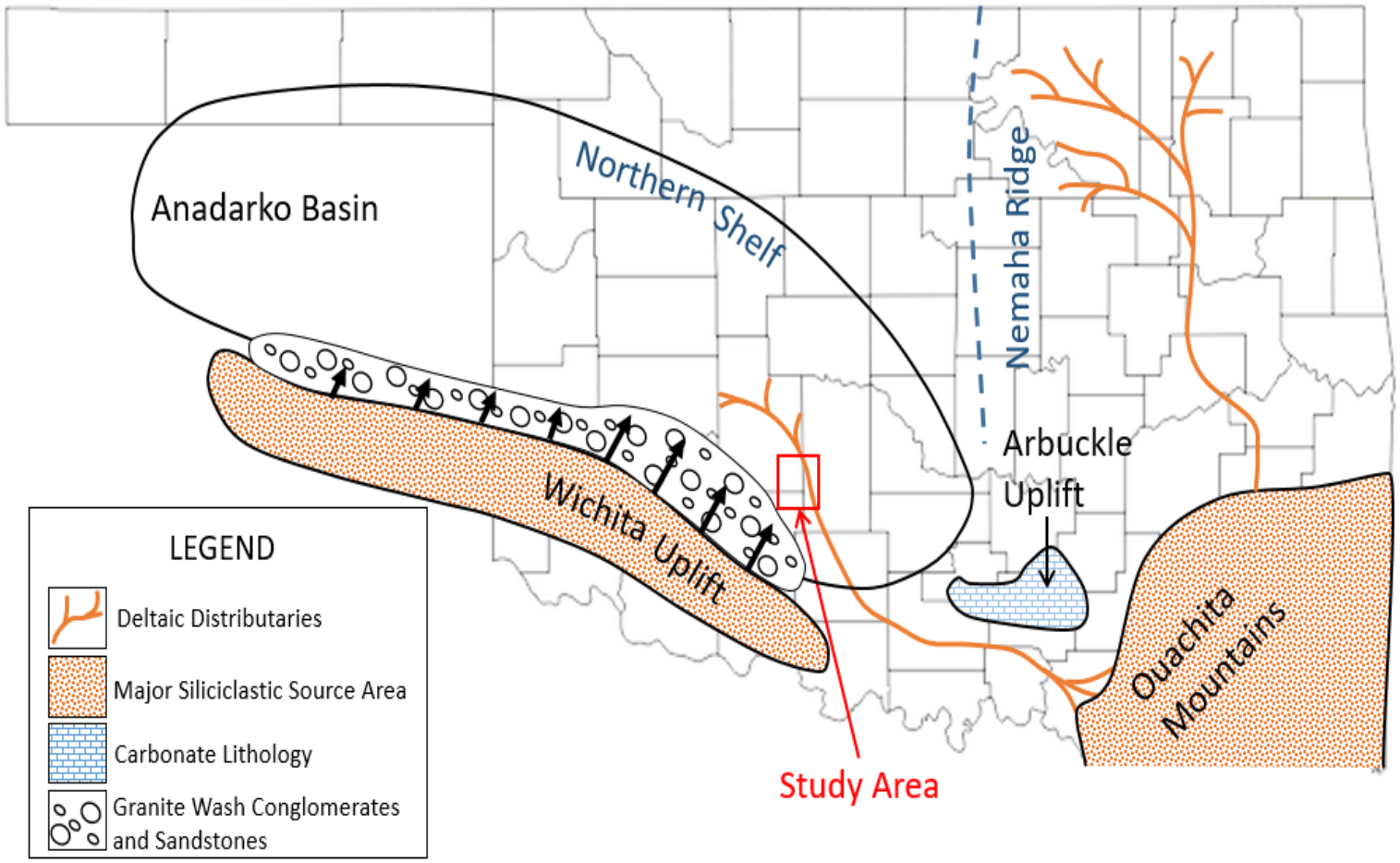

Figure 2.2. Major paleogeographic features of the Mid-continent during Missourian time. Interpretation of the Medrano Sandstone depositional environment is inferred by the deltaic distributary pattern from Rascoe and Adler (1983).

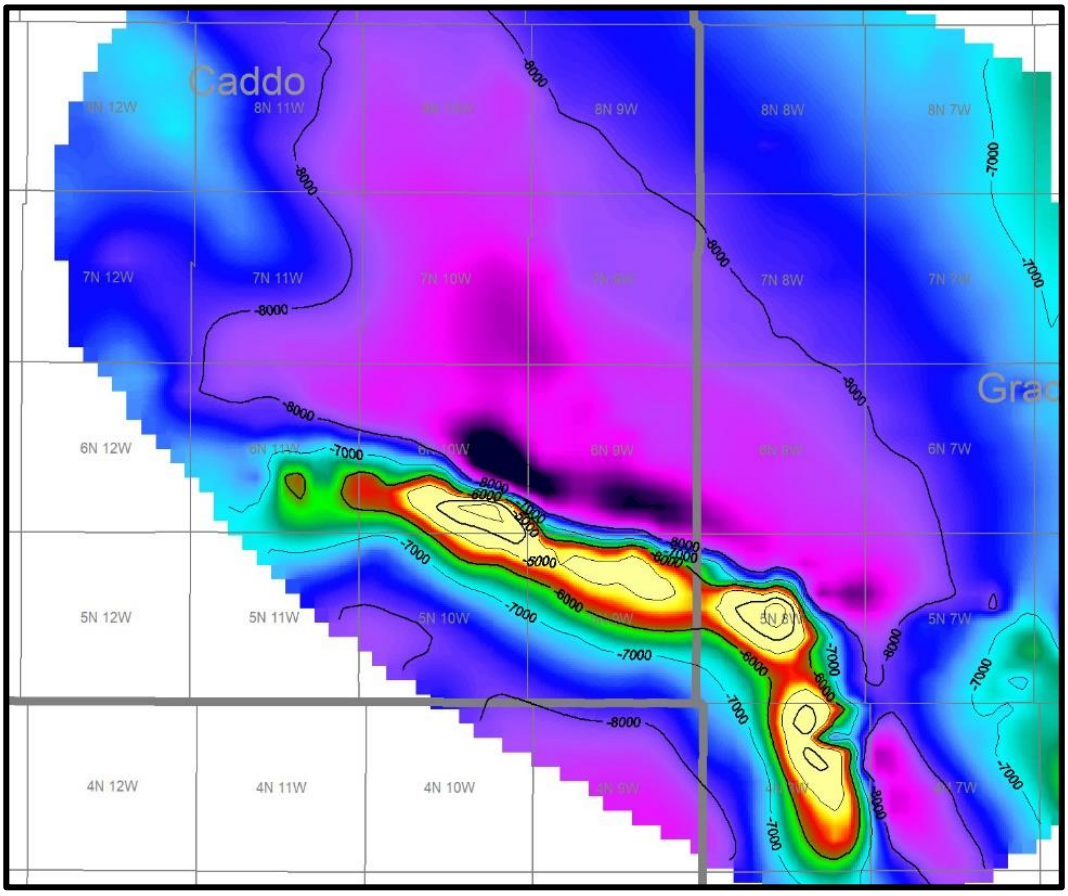

Figure 2.3. Relief map highlighting major structures (Cement and Chickasha anticlines) located within study area. Cement anticline has 4000 feet of relief above adjacent basin.

Stratigraphic Framework

The Pennsylvanian Medrano Sandstone is an operational formation in the Missourian Hoxbar Group. The Medrano interval is a siliciclastic-dominated, basinward-thickening, succession of shale and sandstone depositional cycles dominated by progradation and transgression. Five (5) significant coarsening-upward progradational sandstone bodies occur between the base of the group below the Hedlund Sandstone to the top at the Oolitic Limestone (Figure 1.2; Figure 2.4).

The Hoxbar Group represents roughly 3,000 feet of sedimentary rocks in the study area, and can be divided into an Upper and Lower Hoxbar interval. The Lower Hoxbar subgroup in the study area includes in descending order the Wade Sandstone, Medrano Sandstone, Hedlund Sandstone, Marchand Sandstone, Culp Sandstone, and the Melton Sandstone. Within the study area, a number of shale markers below the Medrano Sandstone facilitated correlation in local areas, but none were correlatable throughout the study area. The Medrano Sandstone is directly overlain by a thick (roughly 600 feet) interval of dark gray to black marine shale. This shale extends from the base of the overlying Wade Sandstone to the top of the Medrano Sandstone. This shale, in combination with the thickness and lateral continuity of the Medrano Sandstone, made the Medrano Sandstone relatively easy to recognize on wireline-log curves. The gamma-ray log response for the Medrano Sandstone is typically a cleaning upward signature with a gamma-ray curve response that decreases in value from 100-120 American Petroleum Institute (API) units at the base to 30-50 API units at the top of the sandstone. The induction wireline log response showed an average deep/true resistivity (R_t) value of approximately 70-90 ohm-m near the top of the Medrano Sandstone. Induction resistivity values gradually increased upward in conjunction with decreasing gamma-ray values as the facies changed from shale-rich at the base to sandstone-rich at the top. The Medrano Sandstone was divided into an Upper Medrano unit and a Lower Medrano unit, which can typically be differentiated on logs by a shale rich interval (Figure 2.4). Moving down the stratigraphic column, the Medrano fines into another shale that overlies the Hedlund Sandstone. A nearly identical cycle of sedimentation occurs above the Marchand sandstone, which lies roughly 400 feet below the Medrano Sandstone (Harlton, 1960). Directly above the Marchand unit is a radiogenic “hot shale” marker coined the “Hogshooter Shale Marker” that was used to facilitate correlation in the study area. The marker is easy to recognize because it is a radiogenic shale with gamma-ray curve response on wireline logs that ranges from 130 to >250 API units.

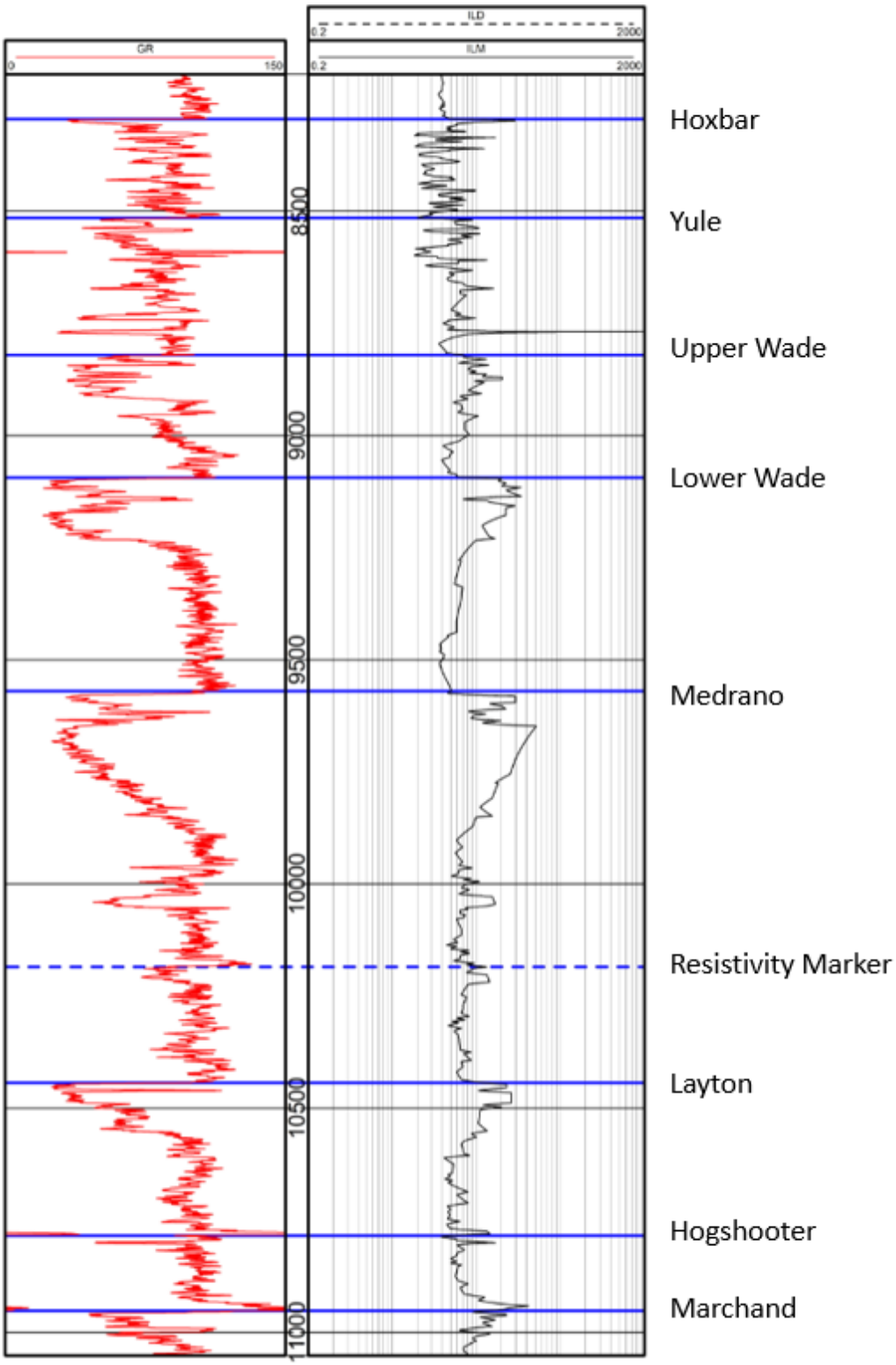

Figure 2.4. Type log showing wireline characterization of a portion of the Hoxbar interval that is dominated by shale and cleaning-upward sandstones recognized by upward increasing resistivity and upward decreasing gamma-ray values, respectively. Representative partial wireline log is the Pritchett Trust 1-22 located in Sec. 22, T.6N., R.8W.

Cross Section Network

A network of five cross sections was constructed to understand the spatial relationship between the formal and informal operational stratigraphic units that make up the Hoxbar Group. Two sections were oriented south-north and three east-west (Figure 2.5). The orientations of cross sections were chosen to be strike-oriented and dip-oriented relative to paleobasin bathymetry as based on the thickness of the interval between the top of the Medrano Sandstone and the Hogshooter Marker (Figure 2.6). Cross sections were critical to visualizing stratigraphy and interpreting the distribution of the Medrano Sandstone. Additionally, cross sections were essential to ensure reliable correlation across the study area, establishing wireline log character of lithofacies that make up the Medrano Sandstone and developing electrofacies necessary for mapping sandstone distribution.

It should be noted that correlations of the Medrano unit in the southeastern, northeastern, and northwestern areas were achieved with more confidence than correlations in the south-central portion of the study area. This is the result of structural complexity in the Cement-Chickasha area and difficulty in recognizing correlatable units on wireline logs from wells in the southwestern portion of the study area (Figure 2.3).

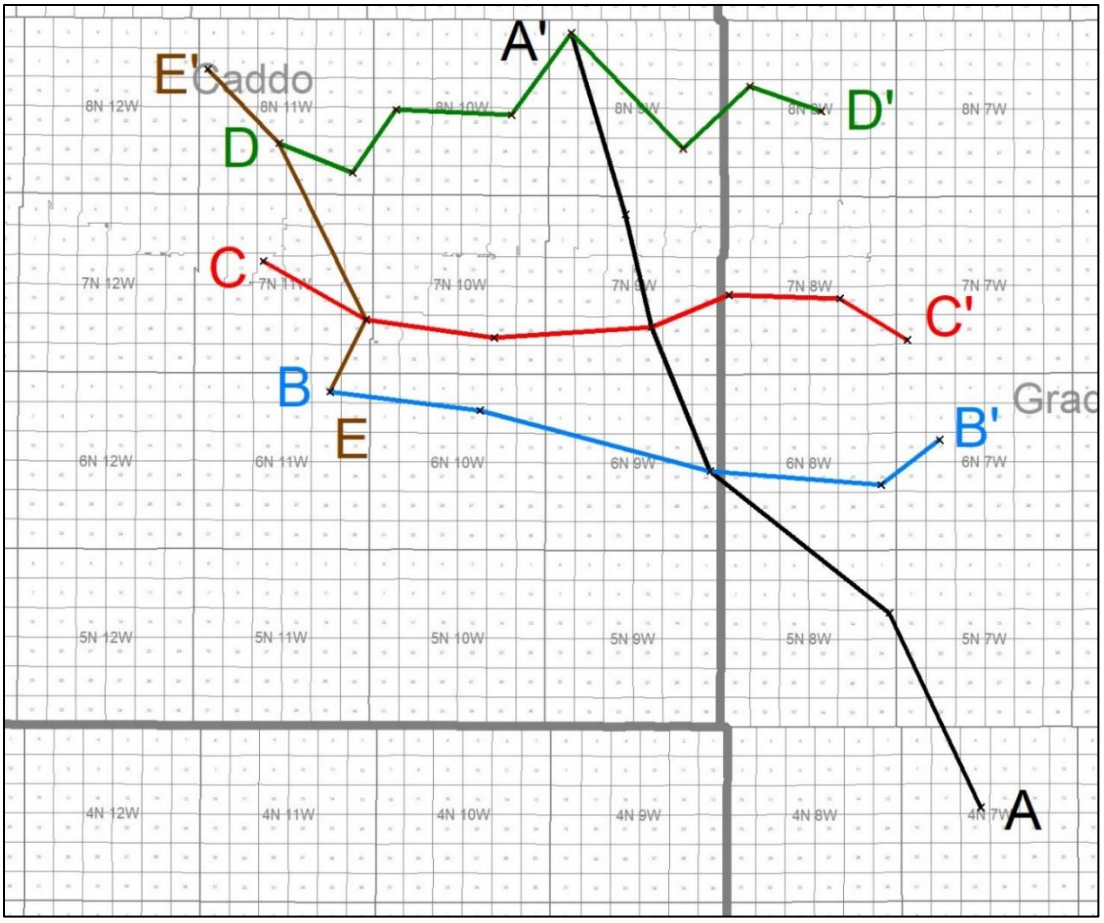

Figure 2.5. Map of study area showing cross sectional network used to establish stratigraphic framework of the Medrano Sandstone

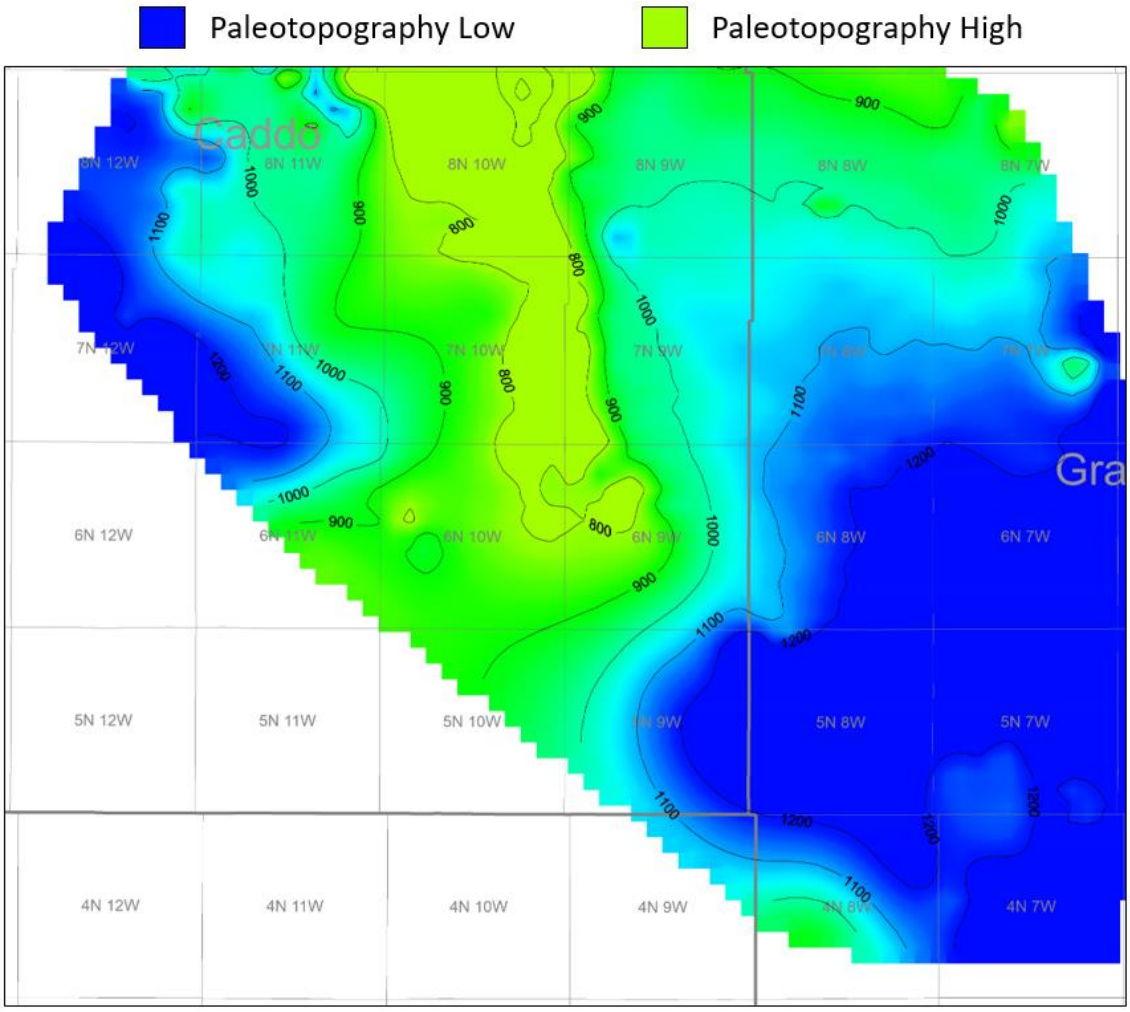

Figure 2.6. Map showing thickness of the Medrano-Hogshooter interval, representing basin paleobathymetry that influenced Medrano deposition.

CHAPTER III

RESULTS

A principal goal of this project was to determine depositional environments of the Medrano Sandstone. To achieve this goal, three objectives essential to establishing the evidence to interpret depositional processes that influenced Medrano interval deposition were proposed: 1) infer the geometry of sandstone bodies from core-calibrated wireline log curves, 2) establish the distribution of these sandstone bodies using well to well wireline log correlation of the Medrano unit, and 3) identify sedimentary features, biogenic structures and body fossils in cores and thin sections.

Core Descriptions

Two cores of the Medrano Sandstone graciously provided by Unit Petroleum Company and EOG Resources were available. The first core was the EOG Resources, the Schmidt 16-3H is located in Sec. 16, T.6N., R.8W. The second core was the EOG Resources Jobe 31-1 located in Sec. 31, T.6N., R.7W. (Figure 3.9). Both cores were examined and described, and sampled for thin sections, scanning electron microscopy, and x-ray diffraction. Additional porosity/permeability and fluid saturation core tests were conducted by Weatherford Laboratories and used with the permission of Unit Petroleum Company and EOG Resources.

Jobe 31-1 Core Summary

The EOG Resources, Jobe 31-1 was drilled in February 2013, with the Medrano Sandstone being cored from a depth of 9,430 – 9,634.3 feet. This interval includes in ascending order, the underlying shale through the entire Medrano Sandstone to the overlying

shale (Figure 3.1). The cored interval is represented by decreasing gamma-ray from 9,634 feet (50 API units) to 9,530 feet (18 API units), followed by another thin cleaning-upward interval from 9,540 to 9,530 feet that (22 to 18 API units) is followed by an interval of increasing gamma-ray values from 9,520 feet (15 API units) to 9,465 feet (36 API units) with a more radiogenic peak at 9,475 feet that reaches 75 API units.

From 9,634 feet through 9,600 feet, lithology was dominated by gray sandstone with abundant shale stringers and shale wisps. The interval is highly bioturbated with small (5 mm) to large (25 mm) scale burrows (Figure 3.2). Core depth 9600 feet marks the start of a transition to decreasing shale stringers/wisps and increasing more massive sandstone facies dominated by highly burrowed, light gray sandstone with lenticular bedding, and clay wisps. Siderized clay and shale laminae and one (1) inch (25 – 26 mm) thick beds of dark gray to brown sandstone become common within the interval (Figure 3.3). At 9,561 feet, facies change within the cleaning upward sequence (Figure 3.1) is observed as the gray sandstone with frequent clay wisps and shale stringers becomes gray sandstone with frequent brown to tan sandstone intervals. Siderite nodules and burrowing are common deeper in the interval from 9,561 – 9,502 feet. Horizontal laminae of sandstone and siltstone with color change from white to tan occur, cross-bedding is common in the section, and mud/clay drapes are prevalent throughout the massive sandstone with the fine grained drapes becoming more prevalent deeper in the sequence. Small scale vertical fractures occur across the interval (Figure 3.4).

From 9,502 feet through the top of the cored interval marks the transition from a coarsening upward sequence to a fining upward sequence (Figure 3.1). Cross bedding, ripple laminations, planar bedding, and burrowing are frequent from 9,502 – 9,465 feet. Individual siderite nodules and layers are found throughout the interval. Depth 9,464.5 feet marks the top of the Upper Medrano interval and is recognized by facies change from white sandstone with millimeter thick siltstone laminae with shale clasts throughout, to the overlying shale (Figure 3.5). The top of the Medrano Sandstone is overlain by a dark gray to black shale that is characterized

by an interval that is heavily bioturbated. The overlying shale continues fining upward to a dark-gray to black shale (Figure 3.6) with sub-millimeter scale mineralized fractures.

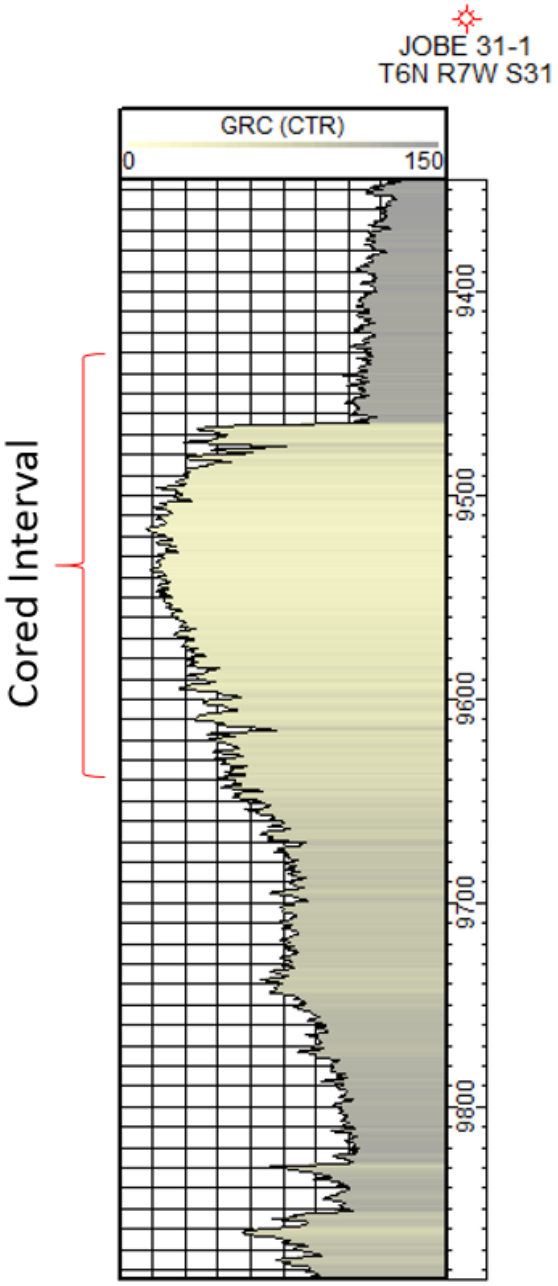

Figure 3.1. Gamma-ray curve across part of the Hoxbar Group, EOG, Jobe 31-1. The cored interval marked is marked by red bracket and depth is in feet.

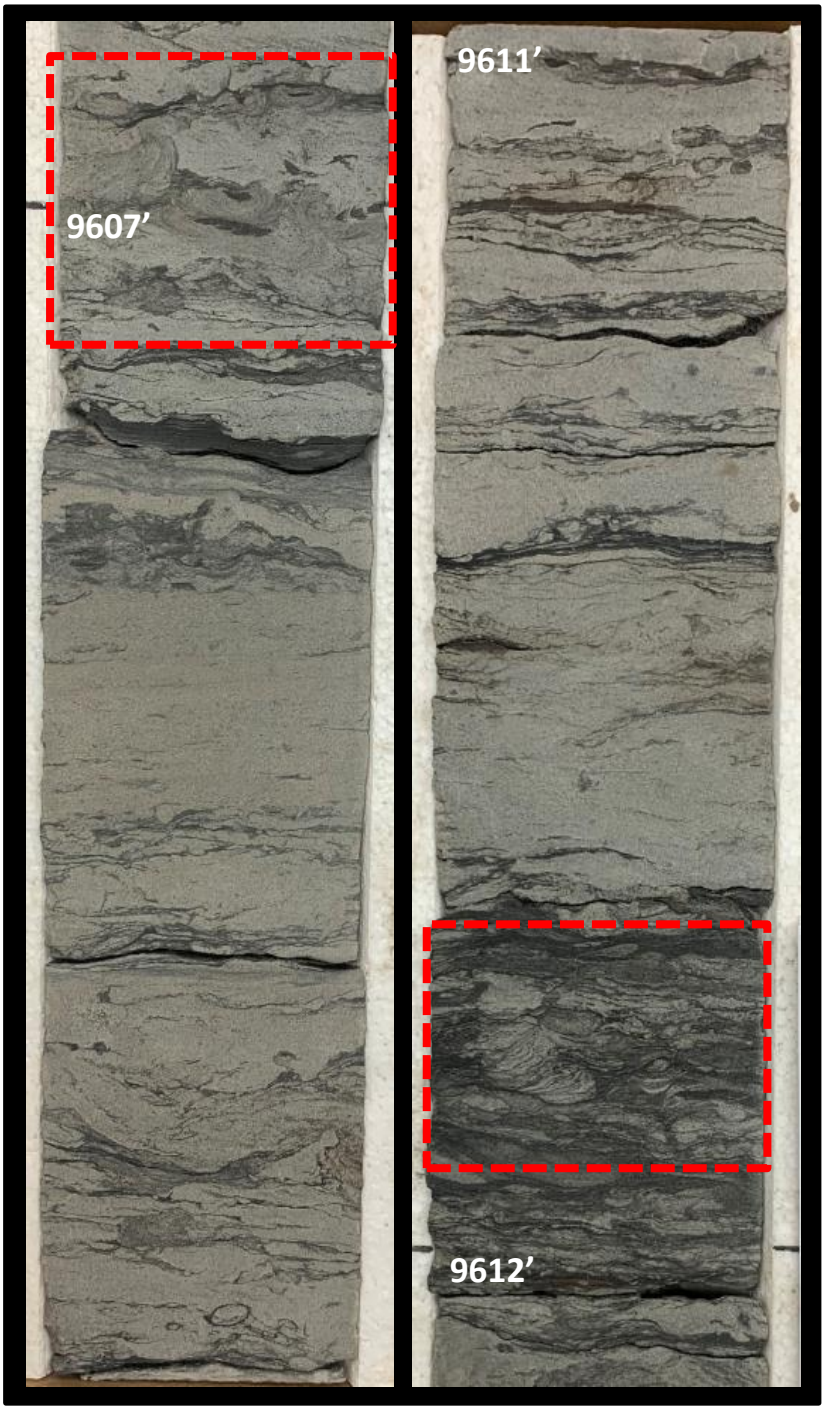

Figure 3.2. Jobe 31-1 core showing thin shale and clay wisps. Shale stringer is present at the base of 9611 feet with burrow containing spreite (indicated with red box). Burrow without spreite at 9607 feet (indicated by red box).

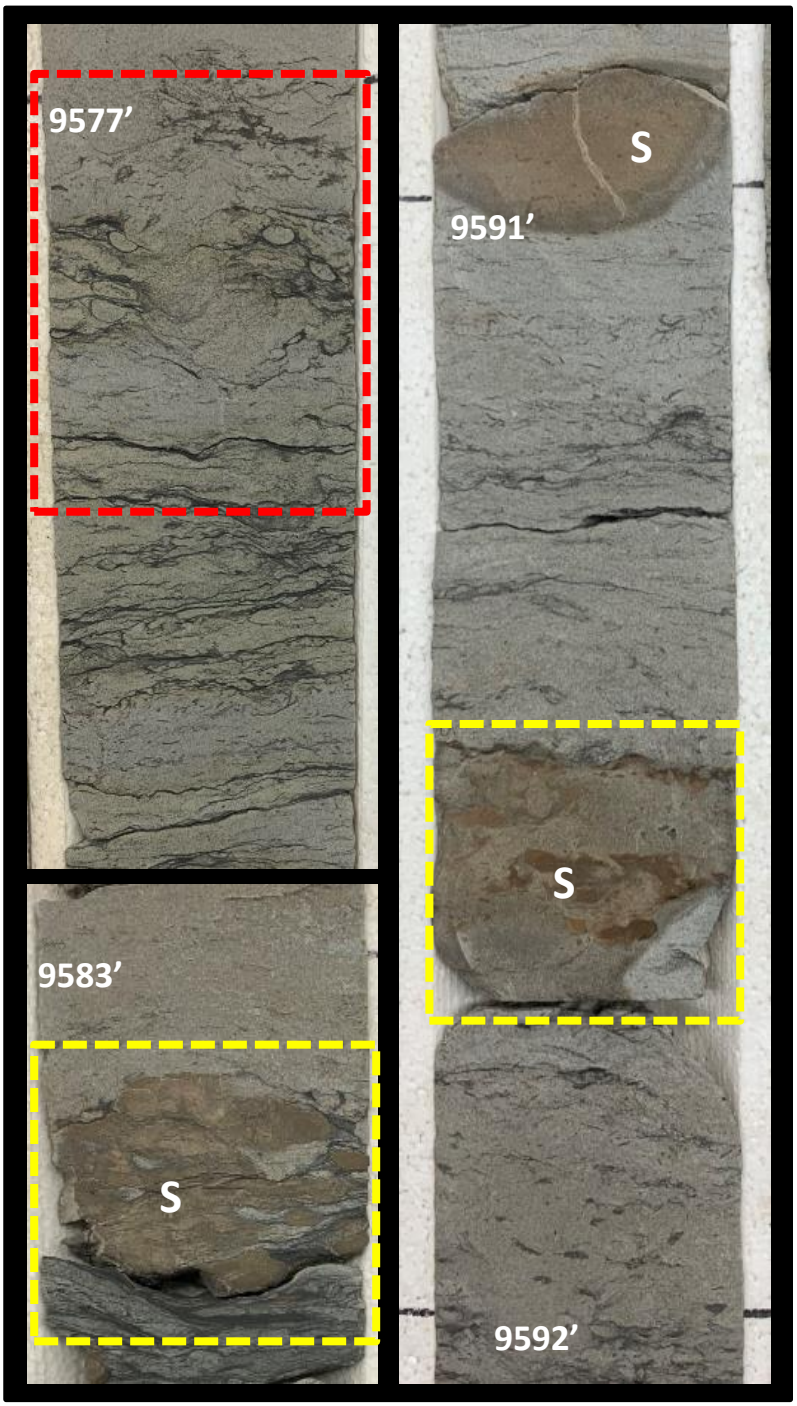

Figure 3.3. Jobe 31-1 core showing large scale burrow located at 9577 feet that disrupts bedding containing smaller circular burrows. Depth 9591 feet marks sandstone interval with color change from gray to brown accompanied by increase in vertical fractures. Yellow boxes highlight interval where clay and sandstone intervals were chemically altered by precipitation of siderite.

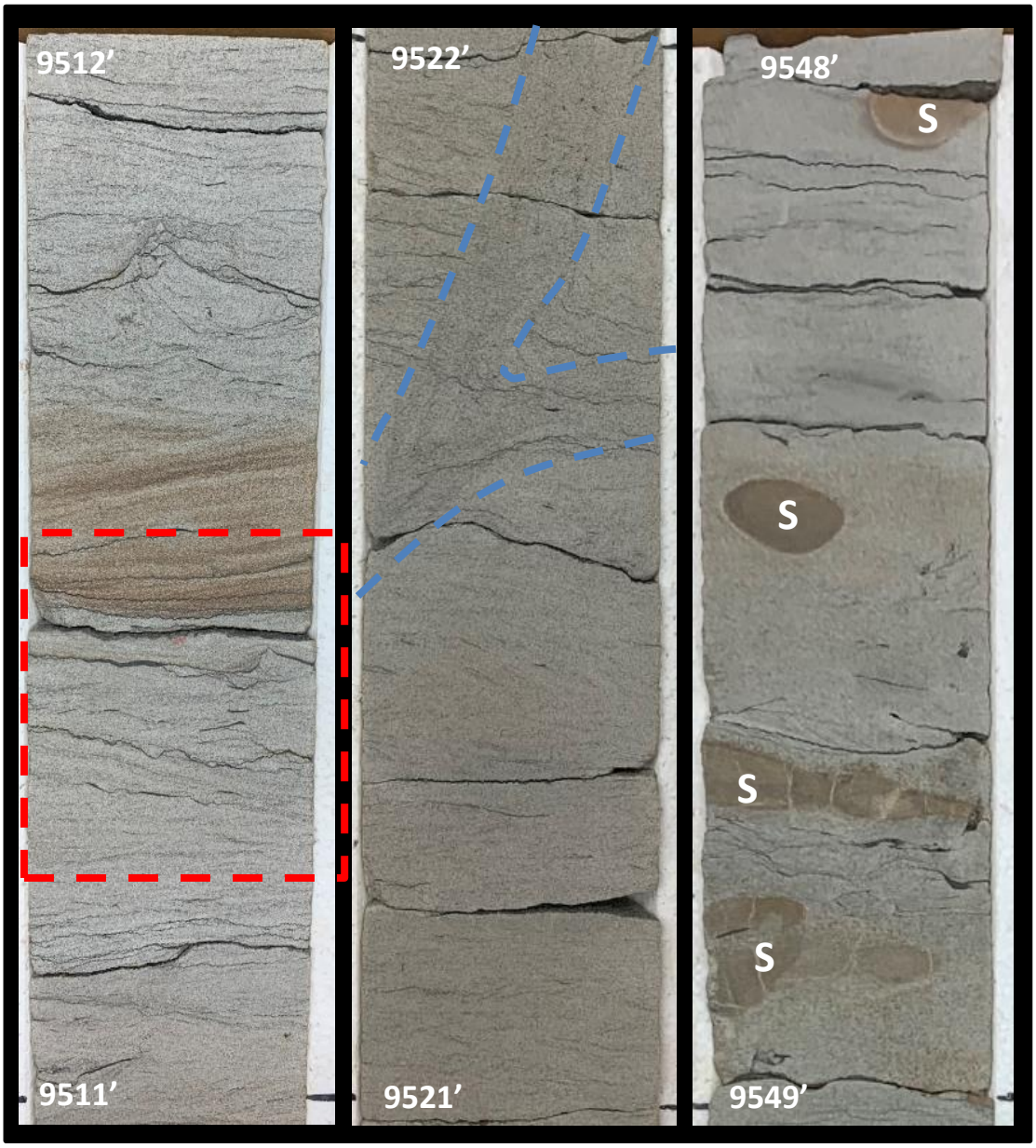

Figure 3.4. Jobe 31-1 core showing large scale cross bedding (red box) at 9512 feet, overlain by possible bioturbation or soft-sediment deformation. Immediately below the red box is subtle bidirectional cross stratification. Depth 9522 feet shows large scale burrow (blue line). Depth 9548 feet shows bedded to nodular siderite with vertical fracturing.

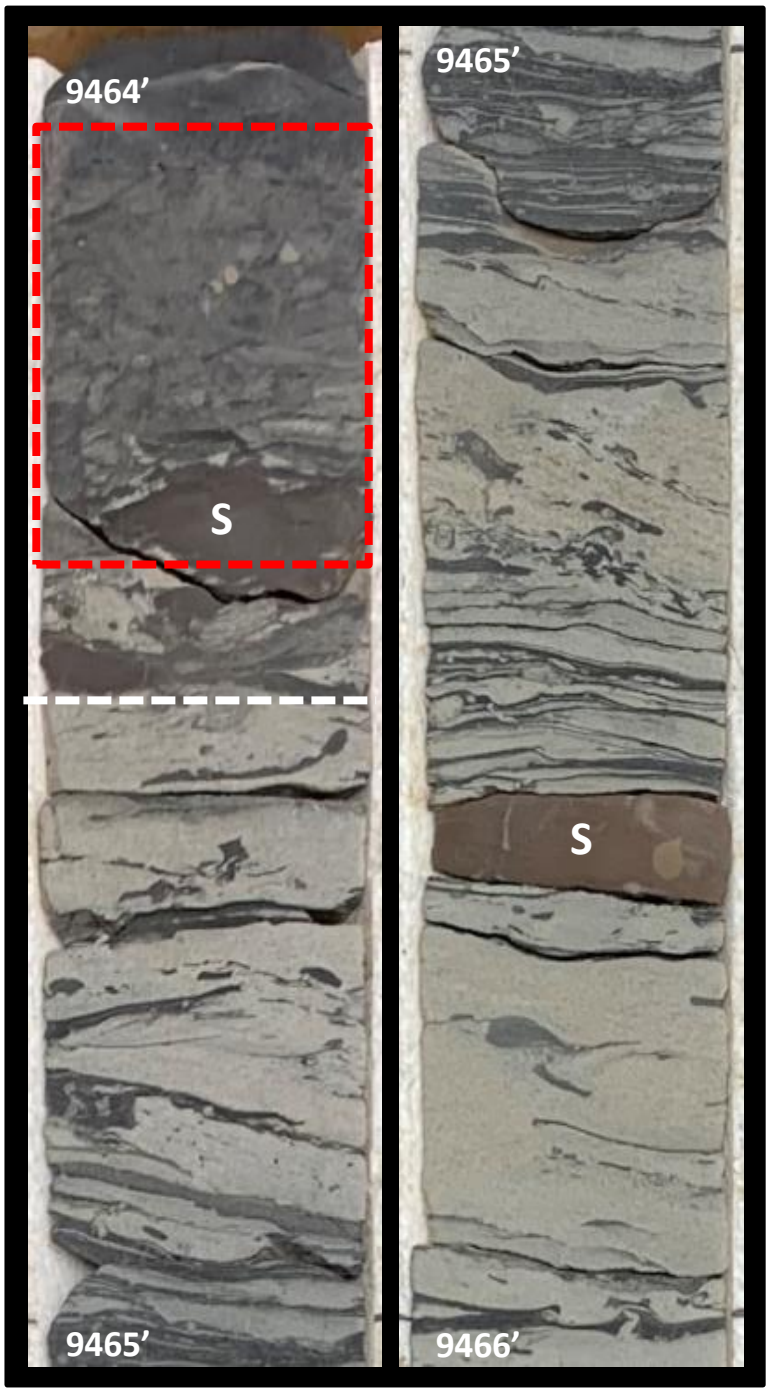

Figure 3.5. Jobe 31-1 core showing the top of the Medrano Sandstone at 9464.5 feet (white line). Red box highlights 5-inch (12.5 cm) interval that is highly bioturbated (B.I. = 5, Taylor and Goldring, 1993), which obliterated all sedimentary structure. Sedimentary structures found near the top of the Medrano sandstone include shale clasts, large siderite nodule, as well as shale/clay wisps.

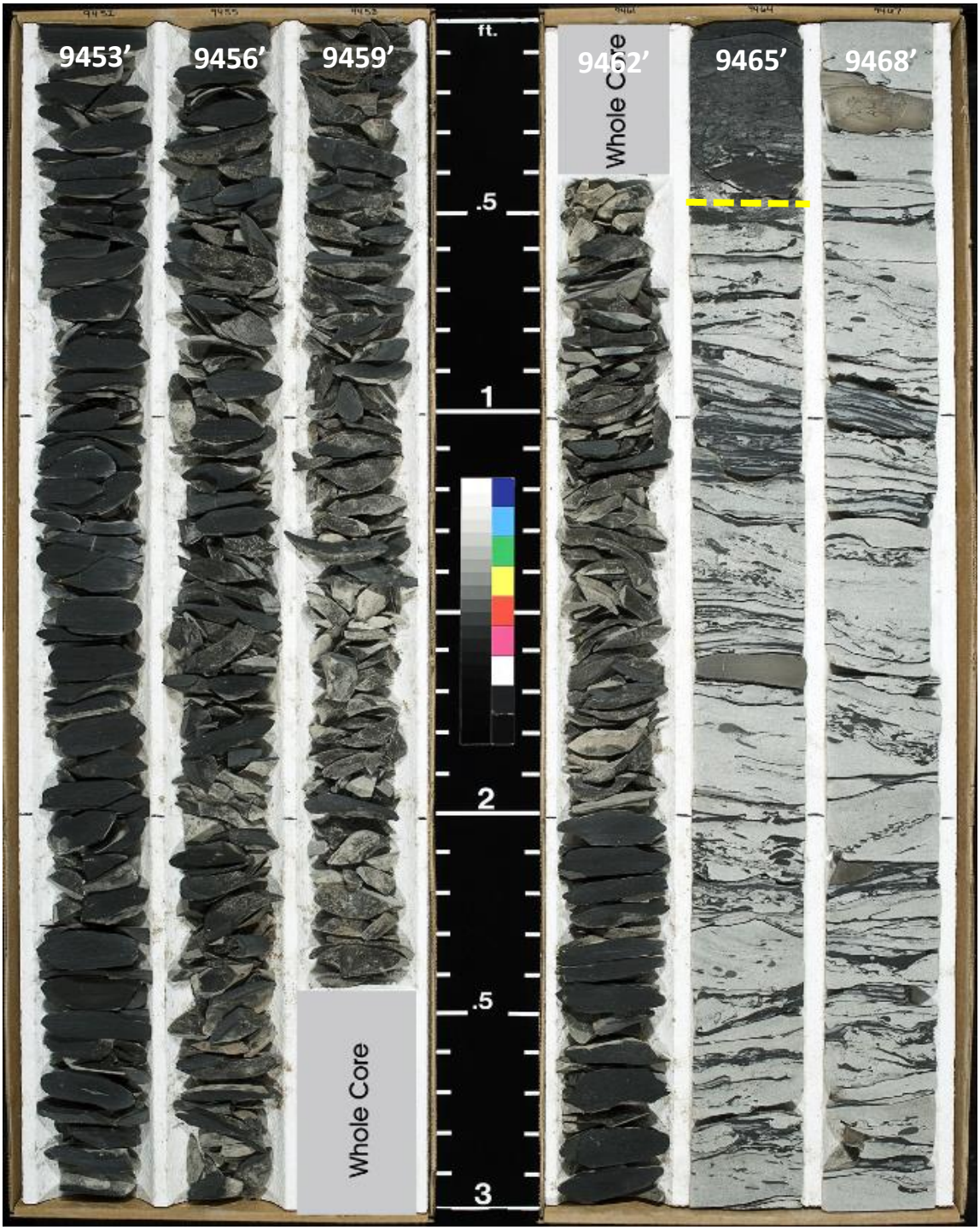

Figure 3.6. Jobe 31-1 box core photo showing transition of light gray Medrano sandstone to the overlying shale. Yellow line marks the top of the Medrano Sandstone at 9465.5’

Schmidt 16-3H Core Summary

The EOG Resources, Schmidt 16-3H was drilled in October 2014, and cored the Medrano Sandstone interval 9,608' to 9,774.25 feet (Figure 3.7). This interval includes approximately eighty-five (85) feet of the Lower Medrano Sandstone reservoir, the entire Upper Medrano interval and roughly nine (9) feet of overlying dark gray marine shale. As previously mentioned, the base of the cored interval falls in the middle of the Lower Medrano sandstone reservoir that is classified in a very generalized sense as massive light gray to gray sandstone.

The interval from 9,774.5 to 9,681 feet (Figure 3.7) shows an approximately one-half chart division decrease in gamma-ray value (7-8 API units) from base to top. Below cored interval the gamma-ray curve decreases from approximately 55 API units at 9,880 feet to 30 API units at 9,775 feet. From 9,681 to 9,660 feet the gamma-ray curve increases to an average value of 90 API unit with a peak at approximately 9,663 feet of 105 API units. This shale-rich section separates the Lower Medrano Sandstone from the Upper Medrano Sandstone. The gamma-ray decreases immediately above 9,660 feet to about 60 API units, which corresponds to the base of the Upper Medrano Sandstone. For the next thirty-seven feet (9,660 to 9,623 feet), the gamma-ray curve decreases from 60 API unit to about 30 API units at 9,623 feet (Figure 3.7). From 9,623 feet to the top of the core at 9,608 feet, the gamma-ray averages a consistent 110 API units (Figure 3.7).

Lithology of the Lower Medrano is dominated by light gray to gray sandstone, isolated centimeter-scale clay clasts (often sideritized), dark gray to gray clay wisps and clasts, soft-sediment distortion of bedding, horizontal laminations, and high angle laminations of siltstone and sandstone. Dipping laminae occur throughout the interval and cross-bedding was very common. A dark gray to black fossiliferous (marine fauna) shale facies is present from 9741.75 – 9740 feet. The sandstone above

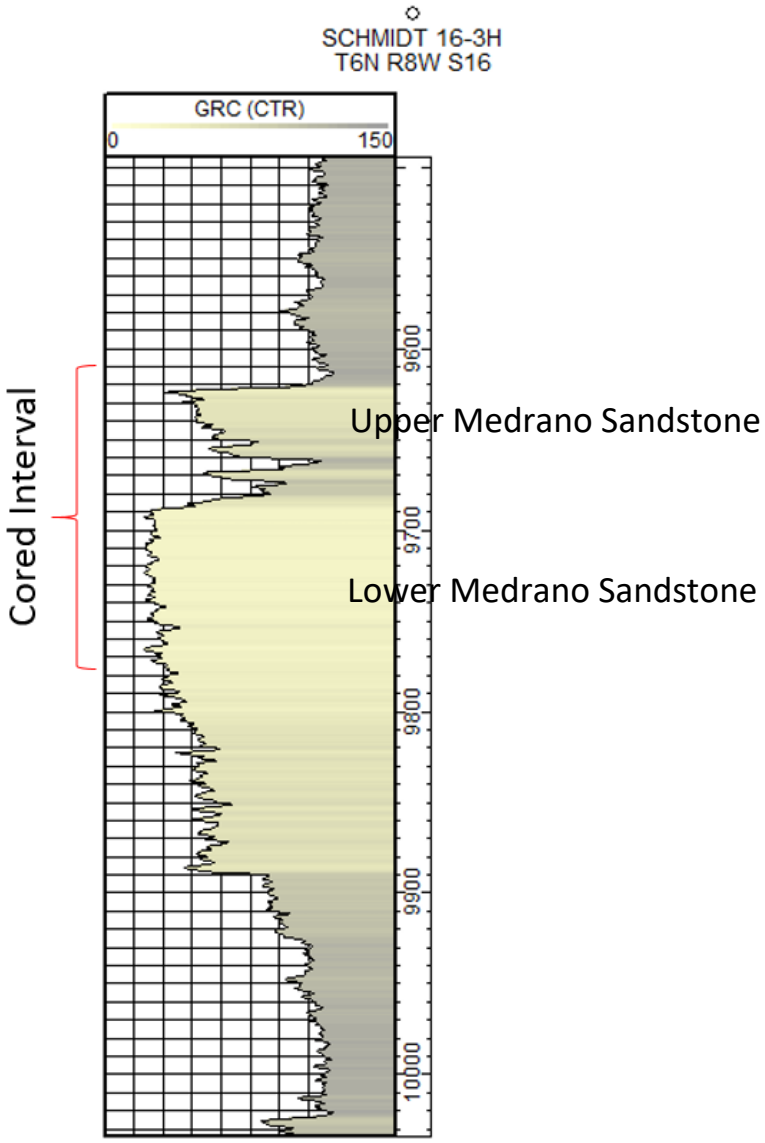

Figure 3.7. Gamma-ray wireline log of the Schmidt 16-3H with cored interval of well indicated on the left.

9736 ft. has vertical fractures, an abundance of stylolites, burrows, and possible herringbone cross-bedding (Figure 3.8). The upper portion of the Lower Medrano interval is characterized by a massive sandstone interval where clay wisps, herringbone cross-bedding, and mineralized vertical fractures are common. Lenticular bedding, burrowing, clay drapes, clay wisps, angular to rounded rip-up clasts of black shale, and small typically rounded sideritized brown clay clasts were found throughout the Lower Medrano (Figure 3.8).

From 9,680 to 9,659 feet, the core is dark gray siltstone that fines to dark gray shale. In the operational industry stratigraphy, this interval separates the Lower Medrano Sandstone unit below from the Upper Medrano Sandstone interval above. This interval is highly burrowed silty to sandy shale (Figure 3.9). Silt dominated thin wavy and lenticular bedding of gray and dark gray silt laminations are preserved in some sections of the interval. The top of the interval is dominated by a dark gray to black shale with dark gray clay wisps.

From 9,658 to 9,620 feet is the Upper Medrano Sandstone. The wireline gamma-ray signature for this interval begins with an average of approximate 60 API units at 9,658 ft., which decreases upward to approximately 45 API units at 9,623 ft. This second cleaning-upward sequence makes up the entire Upper Medrano Sandstone. The Upper Medrano interval grades from a black to dark gray shale at the base to a light gray conglomeratic sandstone and sandy conglomerate at the top. From 9,658 to 9,647 feet horizontal laminations of shale and siltstone occur, but most of the sedimentary structures were homogenized due to the high amount of bioturbation or distorted by soft-sediment deformation. Beginning at 9,647 feet the dominate lithology changes to a light gray sandstone that continues to a depth of 9,622 feet, this interval contains abundant sideritized clay clasts. Sedimentary features consist of parallel laminations to dipping laminae with clay drapes, rip-up clasts of dark shale, ripple laminae and wavy to distorted bedding due to soft-sediment deformation. Pebble-sized siderite nodules are common throughout, but are more prevalent towards the top of the interval (Figure 3.10). The interval contains abundant horizontal burrows that tend to mix clay-rich laminae and the adjacent sandstone. From 9,621 feet to 9,619.5 feet, the sandstone grades into a conglomerate with fine-sand to pebble-sized grains. This conglomerate is considered the top of the Upper Medrano Sandstone (Figure 3.11). The conglomerate occurs in two beds, the upper approximately 1.4 feet thick and the lower <0.4 feet thick. The intervening sandstone contains clay drapes, rip up clasts of shale, and horizontal to dipping clay/shale laminae Starting at 9,619.5 feet is a change in lithology from conglomerate with a sandstone

matrix to medium gray, bioturbated argillaceous siltstone to sandstone that marks the transition zone between the Upper Medrano sandstone to the overlying dark shale with marine invertebrate fossils (Figure 3.12). The dark gray to black shale from 9,617 to 9,608 feet contains calcite-cemented vertical fractures, sand grains and brachiopod fragments toward the base.

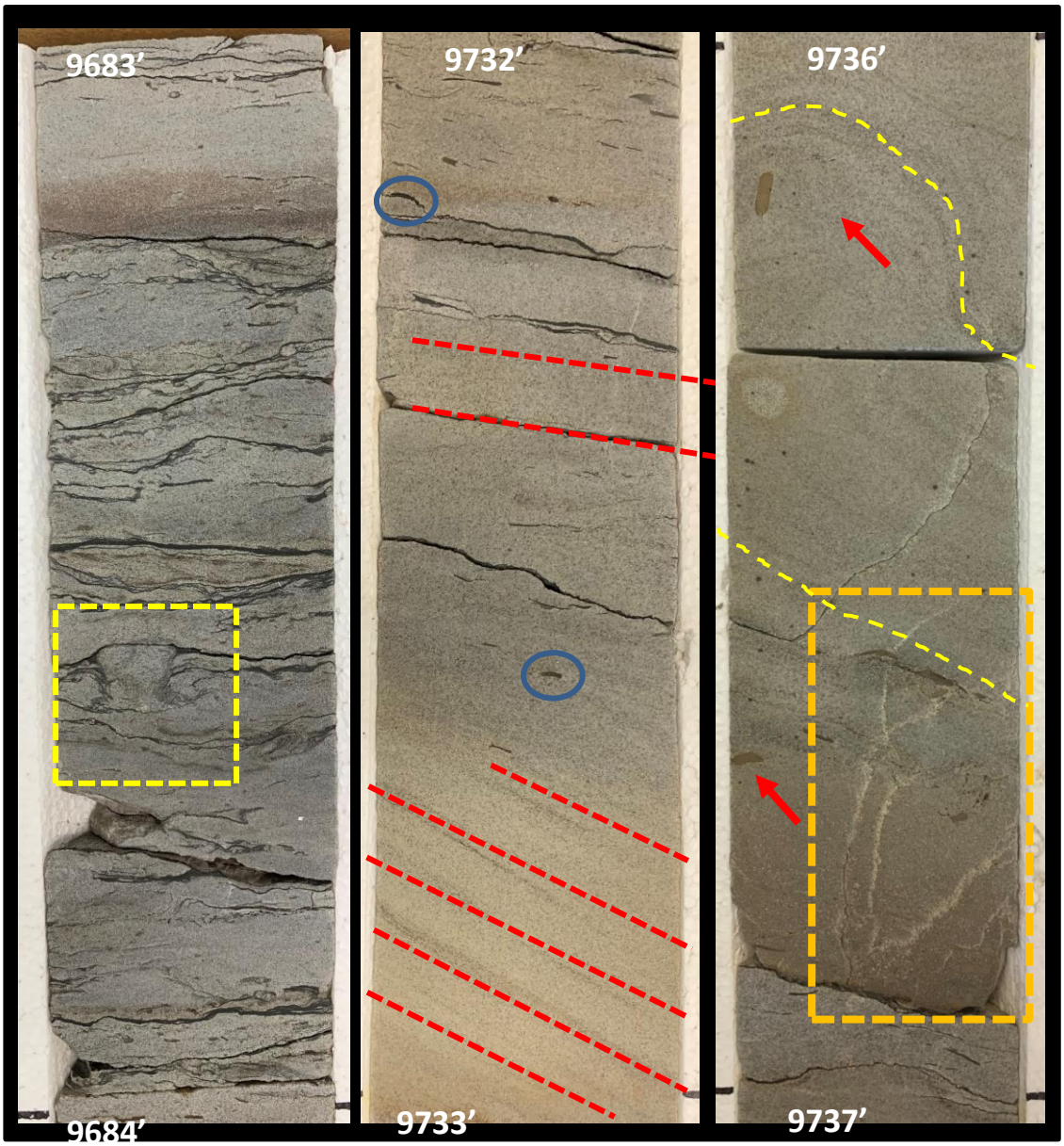

Figure 3.8. Schmidt 16 3H core – Mushroom shaped burrow (yellow box) in highly burrowed sandstone with lenticular bedding, clay drapes, laminae and wisps 9683 to 9684 feet (left). Inclined planar cross stratification below nearly flat bed (red dashed lines) and dark shale clasts (blue circles) 9732-9733 feet (middle). Rounded sideritized clay clasts indicated by red arrows, soft-sediment deformation with bedding traced by yellow dashed line and mineralized fractures outlined by orange box, 9736-9737 feet (right). Bedding planes appear stylolitized

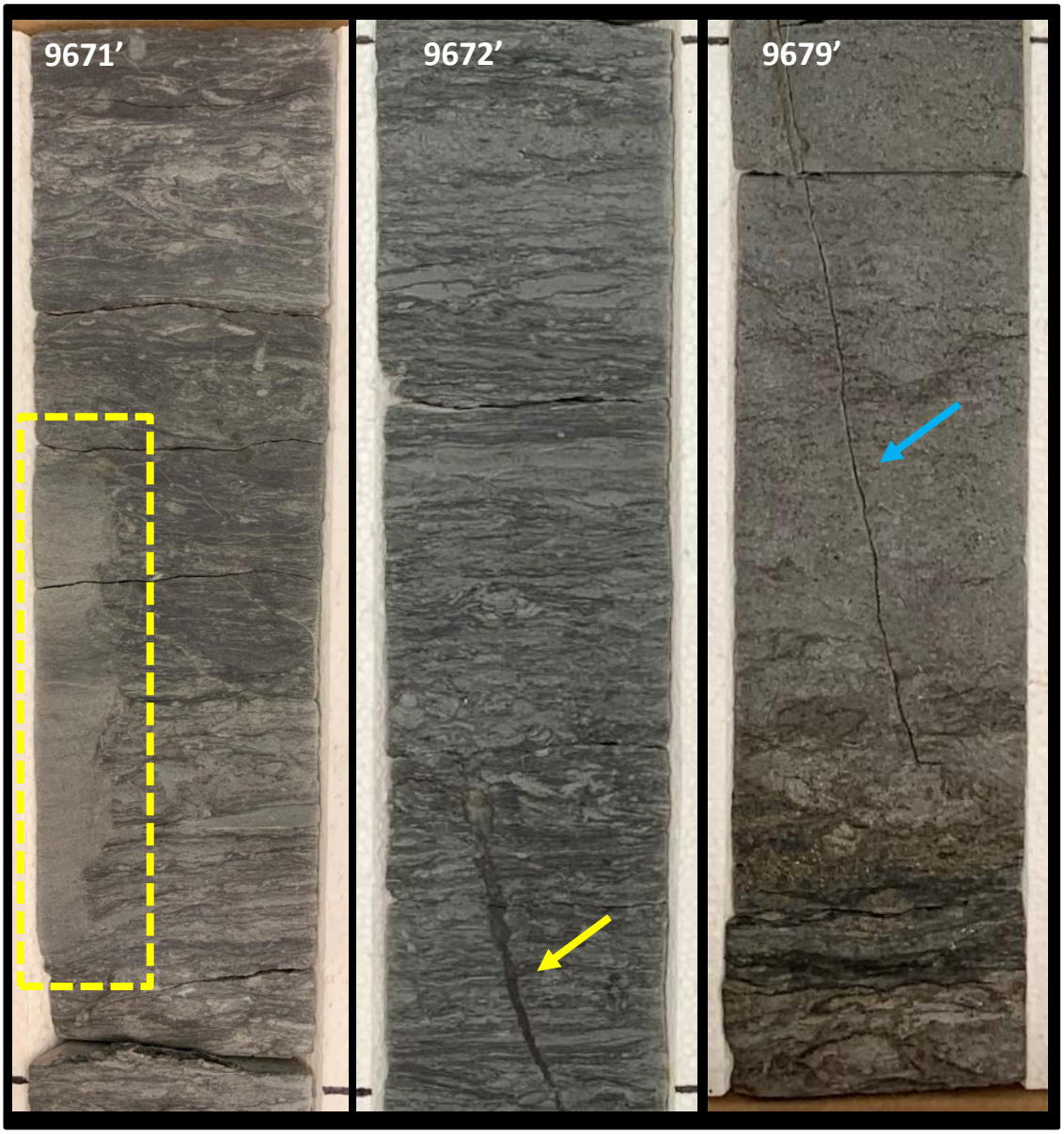

Figure 3.9. Schmidt 16 3H core – Large and small scale burrowing. Complete bioturbation (B.I. 5) has obliterated original sedimentary features from 9679 to 9679.9 ft. Fracture indicate by blue arrow. Mostly horizontal burrows 9672 to 9673 feet (B.I 3) with clay-filled vertical feature (yellow arrow). Large vertical burrow (yellow box) cross cutting interval with smaller burrows (B.I. 3) at depth 9671.4 to 9671.9 feet.

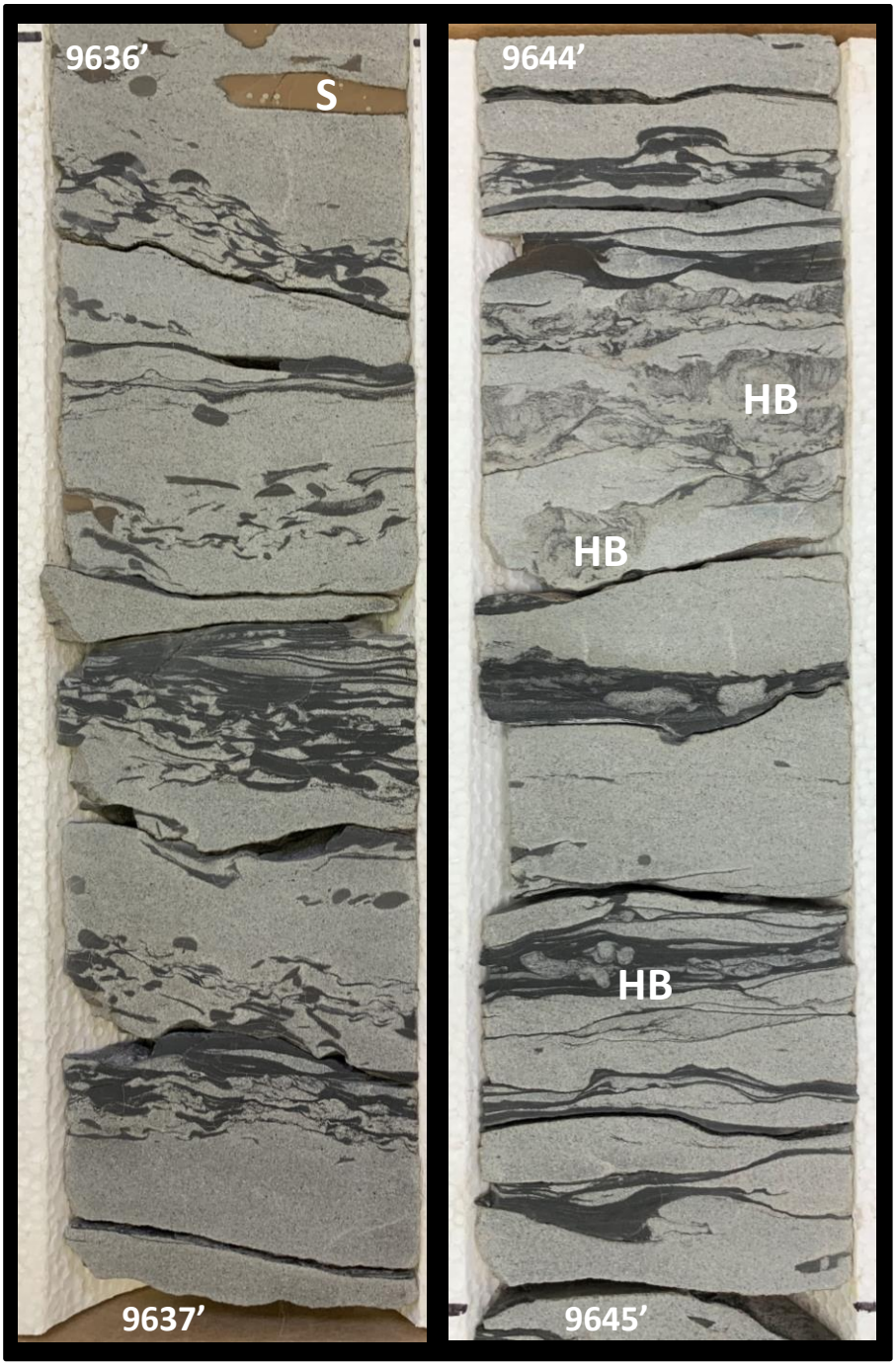

Figure 3.10. Schmidt 16 3H cored interval showing sideritized clay clasts (S), horizontal burrows (HB) (B.I. 1-2), dark-colored, rounded to sub-angular clay/shale wisps (rip ups), and dark gray clay/shale laminae. Soft-sediment deformation distorts original fabric, but near horizontal to gently inclined dip inferred.

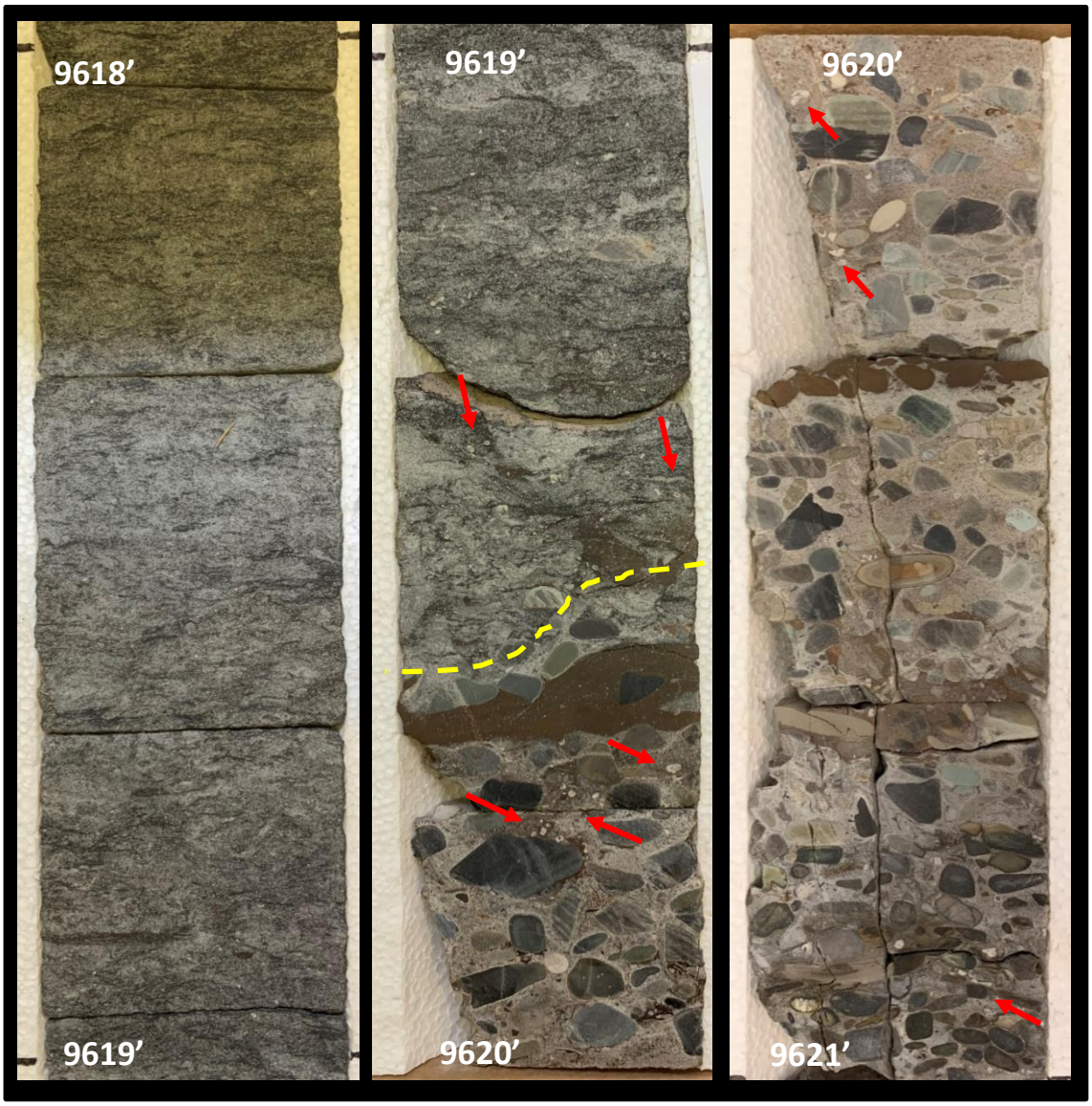

Figure 3.11. Schmidt 16 3H cored interval showing contact (yellow dashed line) at 9619.6 feet between conglomerate of the Upper Medrano interval and overlying bioturbated argillaceous sandstone of the Wade interval. The conglomerate lacks burrowing, whereas bedding is obliterated in the sandstone. Red arrow points to marine invertebrate bioclasts, mostly crinoids. Depth 9618 to 9621 feet.

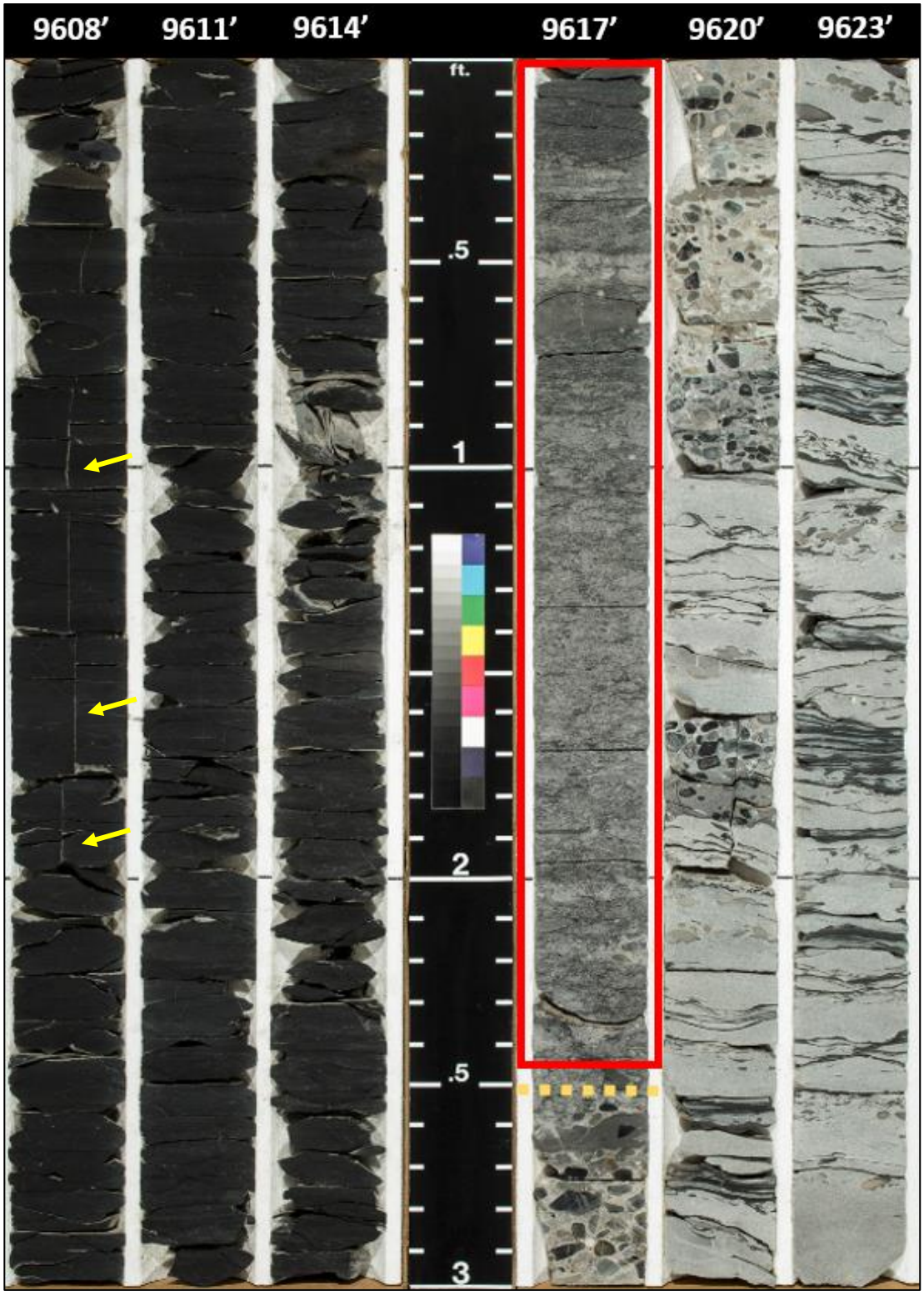

Figure 3.12. Schmidt 16 3H cored interval showing top of the Upper Medrano Sandstone (yellow dashed line). Immediately above the fossiliferous sandy conglomerate is bioturbated argillaceous fossiliferous sandstone (see Figure 3.11) outlined by red box. Medium to dark gray shale is fossiliferous and contains mineralized fracture (yellow arrows).

Inferred Geometry, Electrofacies and Distribution of Medrano Sandstone

Many previous studies have identified the relationship between electrofacies signatures and depositional environments, including studies from Moore (1979) and Shelton (1973) among others, which will be used as analogs for this section of the investigation. Within the study area, the Medrano Sandstone exhibits multiple wireline log curve patterns that are similar to those used in in other studies to infer sandstone geometry and depositional environment. Of the available log curves, the gamma-ray curve provided the most reliable patterns as it is unaffected by drilling fluid properties. Gamma-ray curves for wireline logs across the Medrano Sandstone interval repeated four (4) generalized patterns: (1) cleaning-upward signature (CUS) (funnel shaped) in which gamma-ray values decrease with shallower depth, (2) blocky signature (cylinder shape) with relatively constant gamma-ray values of 20-30 API units, (3) fining-upward signature (FUS) (bell shape) in which gamma-ray values decrease upward, and (4) shale pattern with no significant change from an average around 100 API units.

The most abundant gamma-ray pattern across the Lower Medrano Sandstone interval was the cleaning-upward signature (CUS), which is found across most of the eastern one-half and north-central part of the mapping area (Figure 3.13). The blocky signature occurred in the same approximate area as the cleaning-upward signature, but was confined to northwest to southeast trends (Figure 3.13). The fining-upward signature (FUS) was the least common of the electrofacies signatures found and occurred mostly in the southeast and north-central parts of the study area. The shale pattern occurs mostly along the western edge of the study area in the north-central part (Figure 3.13). The Hoxbar Group is not recognized in the southwest corner of the study (white on Figure 3.13), where Middle and Late Pennsylvanian is dominated by “Granite Wash” and the shale and sandstone intervals used to define the Hoxbar Group cannot be discerned using wireline log signatures. Multiple electrofacies signature maps using the gamma-ray curve were generated to delineate the distribution of each of the three distinct gamma-ray

signatures, as well as the distribution of electrofacies differentiated between the upper and lower Medrano intervals. Figure 3.13 shows the distribution of electrofacies for the lower Medrano interval. The map shows the cleaning-upward sequence was seen to be present throughout of most of the study area in which the lower Medrano was deposited. The second most prevalent pattern was the blocky signature, which shows a southeast to northwest trend. The fining-upward sequence was the least common signature seen for the lower Medrano and was contained mostly to the southeast and central part of the lower Medrano depositional area. The no sandstone or shale pattern signature is more apparent within the lower Medrano interval in the northwest part of the study area. Figure 3.14 shows the distribution of electrofacies of the upper Medrano interval. The most prevalent signature found in the upper Medrano is the CUS. Small patches of FUS occur along the eastern edge of the study area and trend mostly south to north. Three blocky trends are apparent in the central study area and trend to the north to northwest. Two shale pattern areas located in the upper Medrano depositional area, one in the central part of the study area and the second along the western edge of the Medrano sandstone deposition and study area.

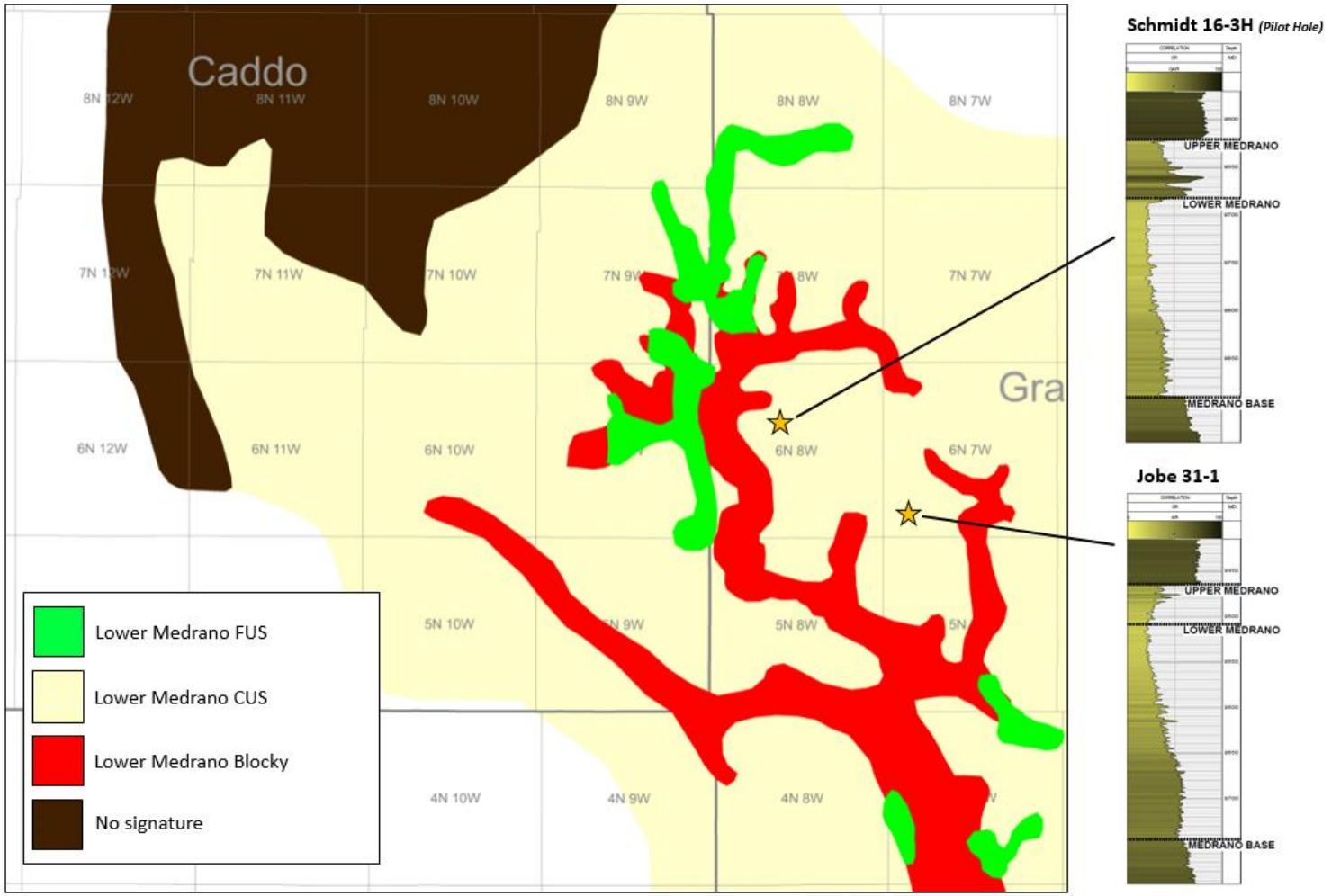

Figure 3.13. Map showing lower Medrano electrofacies distribution. Cylindrical/blocky signature is shown in red. Cleaning-upward signature is shown by light yellow, light green represents the FUS. The location of the two cored wells are displayed as well as their associated gamma-ray character.

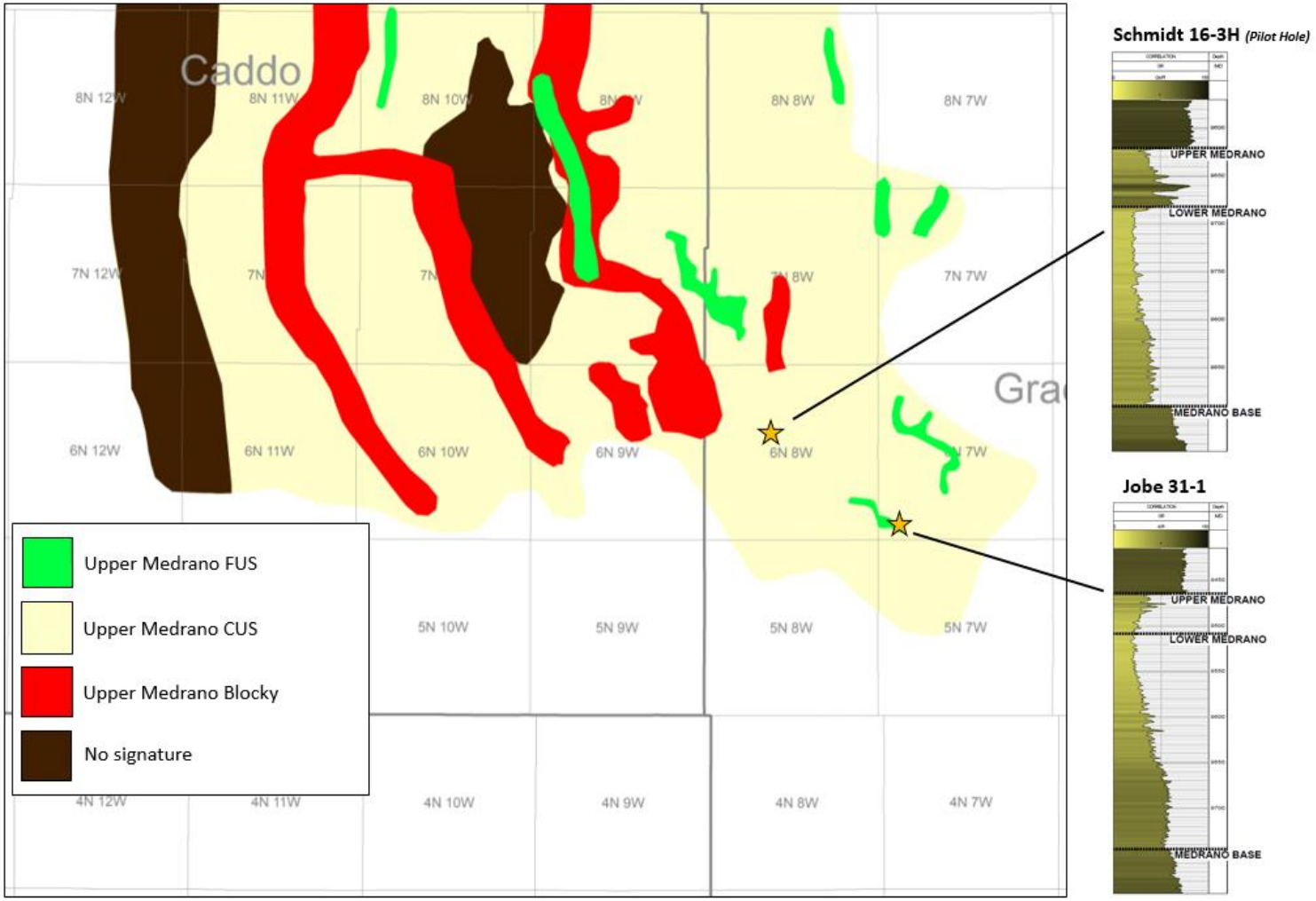

Figure 3.14. Upper Medrano electrofacies distribution map. Cylindrical/blocky signature is shown in yellow. Cleaning-upward signature is shown by magenta, green represents the FUS. The location of the two cored wells are displayed as well as their associated gamma-ray character.

Distribution of the Medrano Sandstone

Throughout the course of the investigation several maps were generated to understand and demonstrate the distribution of the Medrano Sandstone. Along with structure maps, a net sandstone thickness map for the Medrano Sandstone was generated using gamma-ray curves with a shale volume (V_{shale}) cutoff of 33%. Shale volume was calculated using a modified V_{shale} equation of Asquith and Krygowski (2006), which is based on a linear response and suggested for a first order estimate of shale volume ($V_{shale} = (GR_{log}-GR_{min})/(GR_{max}-GR_{min})$). The components of this equation were determined by identifying a normal marine shale (not radiogenic of "hot" like the Hogshooter Marker) whose gamma-ray value was assigned the baseline value gamma-ray maximum (GR_{max}). The gamma-ray minimum value (GR_{min}) was measured in the cleanest (lowest API unit value) part of a thick (>50 feet) Medrano sandstone. The gamma-ray log value (GR_{log}) was the average for each ten (10) feet of sandstone. A cutoff value was chosen based on a petroleum industry value of 33% shale used for Pennsylvanian sandstone in the study area. The following revised equation was used to determine net sandstone, which is >67% sandstone and <33% shale: 33% $V_{shale}=((GR_{max}-GR_{min})*0.33)+GR_{min}$. For the Schmidt 16 3H well log, the cutoff calculation ≥67% sandstone and the cutoff line plotted on the gamma-ray curve are shown in Figure 3.15. The Schmidt 16 3H calculated approximately 130 feet of net Lower Medrano Sandstone and <10 feet of net Upper Medrano Sandstone.

This shale volume equation was used to create net thickness maps for the Lower Medrano Sandstone (Figure 3.16), the Upper Medrano Sandstone (Figure 3.17) and a combined net thickness (Figure 3.18). To understand the net thickness trends, an additional thickness map of the Medrano to the Hogshooter Marker was generated (Figure 2.6). This map is designed to show the total thickness of the Medrano Sandstone to Hogshooter "hot shale" marker interval and support inferences regarding paleobathymetry, accommodation and paleotopography during Medrano deposition.

The distribution of net Lower Medrano Sandstone, as defined by the net sandstone thickness map (Figure 3.16) is along a generalized southeast to northwest trend. Maximum thickness is centered

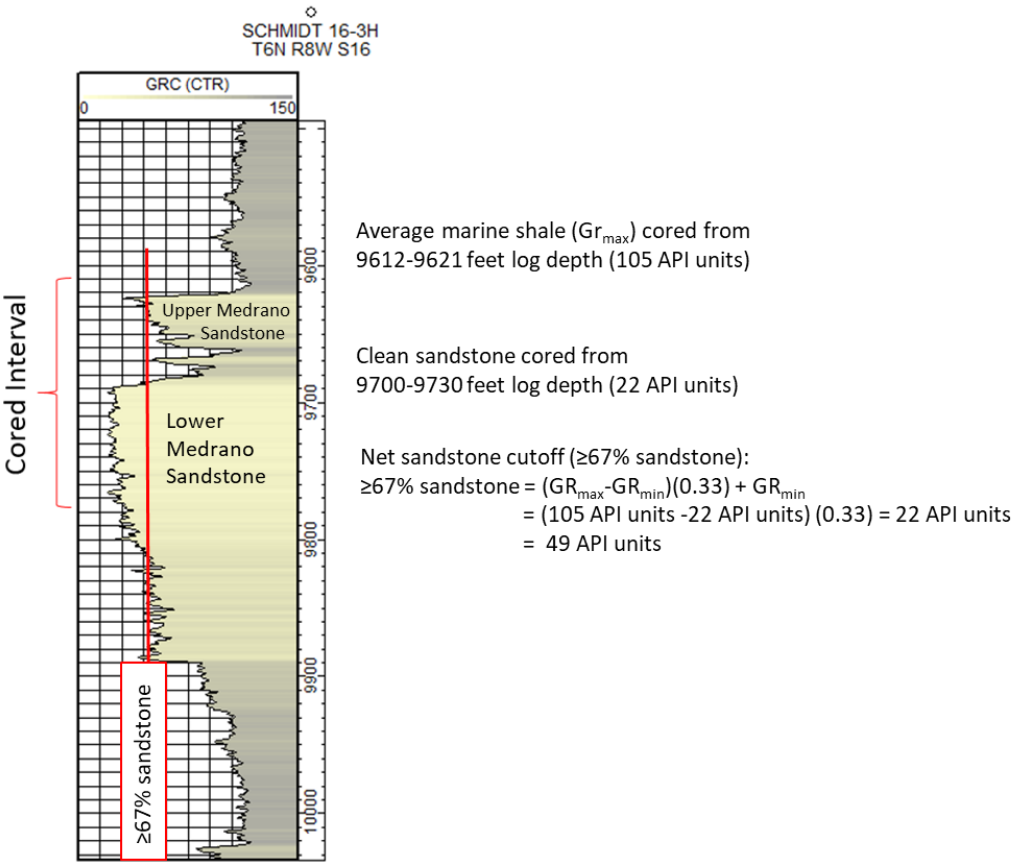

Figure 3.15 Calculation of ≥67% sandstone (≤33% shale) cutoff using the gamma-ray curve for the EOG Schmidt 16 3H well. Gamma-ray maximum (GR_{max}) and gamma-ray minimum (GR_{min}) values based on gamma-ray curve were confirmed by core examination.

in Sections 30 and 31, T.6N., R.8W. and Section 6, T.5N., R.8W. where values exceed 200 feet (Figure 3.16). The dominant thickness trend is north to south trend across T.6N. and T.7N., R.8W., becomes northwest-southeast across T.5N., R.8W. and remains the same to the center T.4N., R.7W., where again it becomes north-south and extends to the edge of the mapping area. A secondary thickness trend extends east to west across the south one-half of T.5N., R.9W. before trending northwest across the east one-half of T.5N., R.10W. and into south one-half of T.6N., R.11W. (Figure 3.16). The dominant trend of Lower Medrano Sandstone appears to cross

the Chickasha anticline and east end of the Cement anticline. The secondary trend crosses the west end of the Cement anticline.

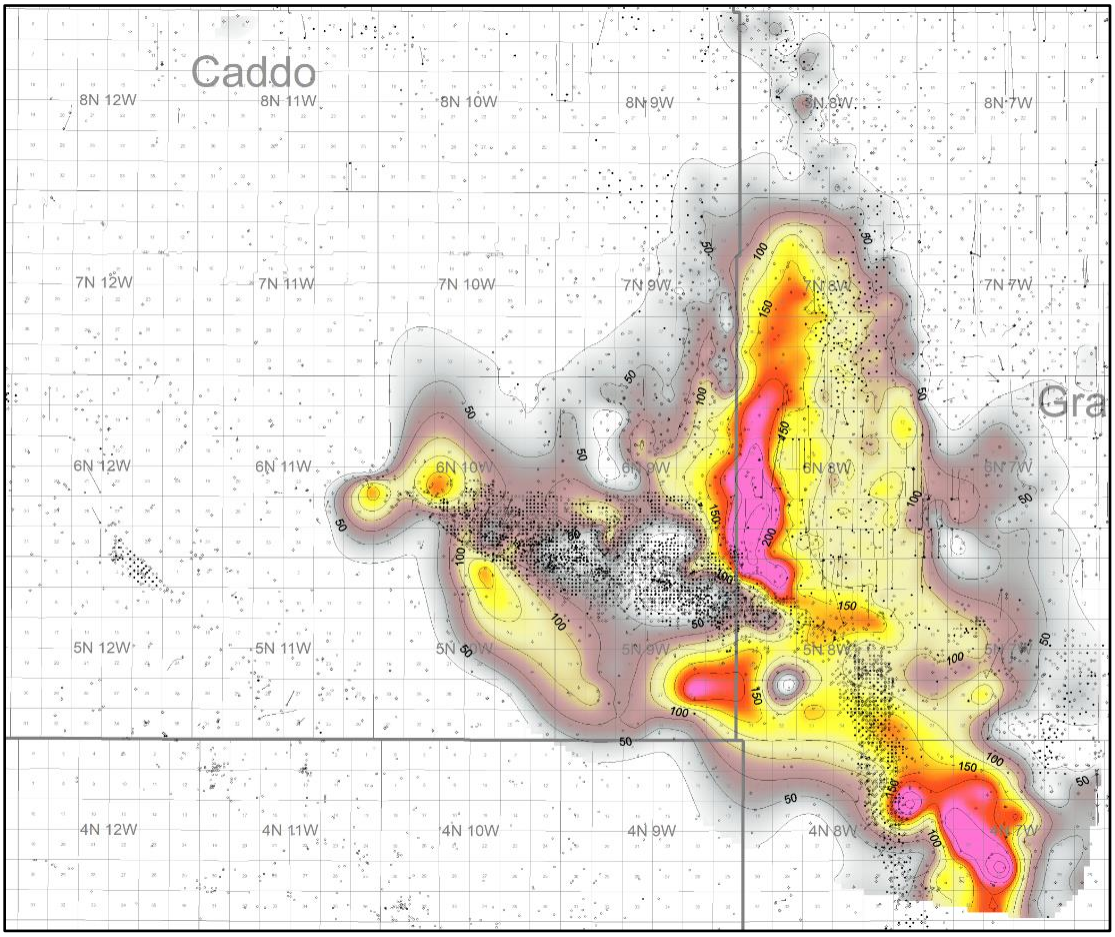

Figure 3.16. Thickness of net Lower Medrano Sandstone (C.I. = 25 feet) using a sandstone cutoff of ≥67% (shale volume cutoff of ≤33%). Maximum thickness is ≥225 feet (pink domain). Two prominent thickness trends cross the Chickasha anticline (concentration of black wells, T.4N., R.8W. and T.5N., R.8W.) and the east and west ends of the Cement anticline represented by concentration of oil wells (black) near center of map.

The distribution of net Upper Medrano Sandstone is different than distribution of the Lower Medrano Sandstone. The thickest net Upper Medrano Sandstone is in the northern part of the study area, immediately north of the Lower Medrano accumulation (Figure 3.17). The trends of thicker

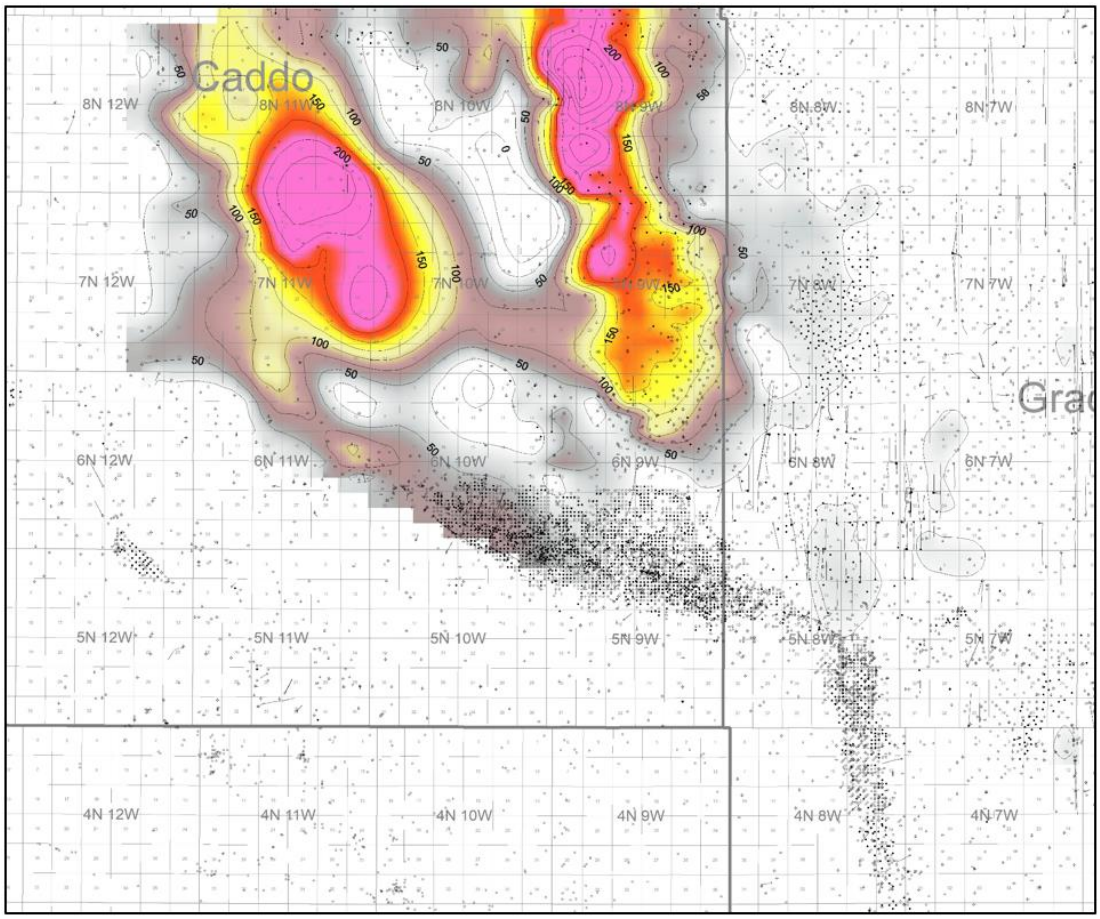

Figure 3.17. Thickness of net Upper Medrano Sandstone using a sandstone cutoff of ≥67% (shale volume cutoff of ≤33%). Maximum thickness is ≥225 feet (pink domain) and contour interval is 25 feet. Two prominent thicker trends are north of Cement anticline represented by concentration of oil wells (black) near center of map.

upper Medrano Sandstone are an east accumulation that extends from the northern one-third of T.6N., R.9W. through T.7N., R.9W and T.8N., R9W. and a west accumulation centered in T.7N., R.11W. and including the southwestern corner of T.8N., R.10W. and southeastern T.8N., R.11W. (Figure 3.17). These thicker areas are connected by a thinner distribution of Upper Medrano Sandstone trend that extends west-northwest to the north of Cement anticline (Figure 3.17). The combined thickness of net Lower and Upper Medrano sandstones is shown in Figure 3.18. The combined thickness accentuates the northwest to southeast trend of Medrano sandstone and the relationship of Medrano thickness to the present Cement and Chickasha anticlines. The combined thickness pattern shows a single trend in the southeast corner of the study area in T.4N., R.7W.

that appears to bifurcate in T.5N., R.8W. to form the prominent trends in the northern study area. It is noteworthy that the trends continue to both the north and south beyond the study area.

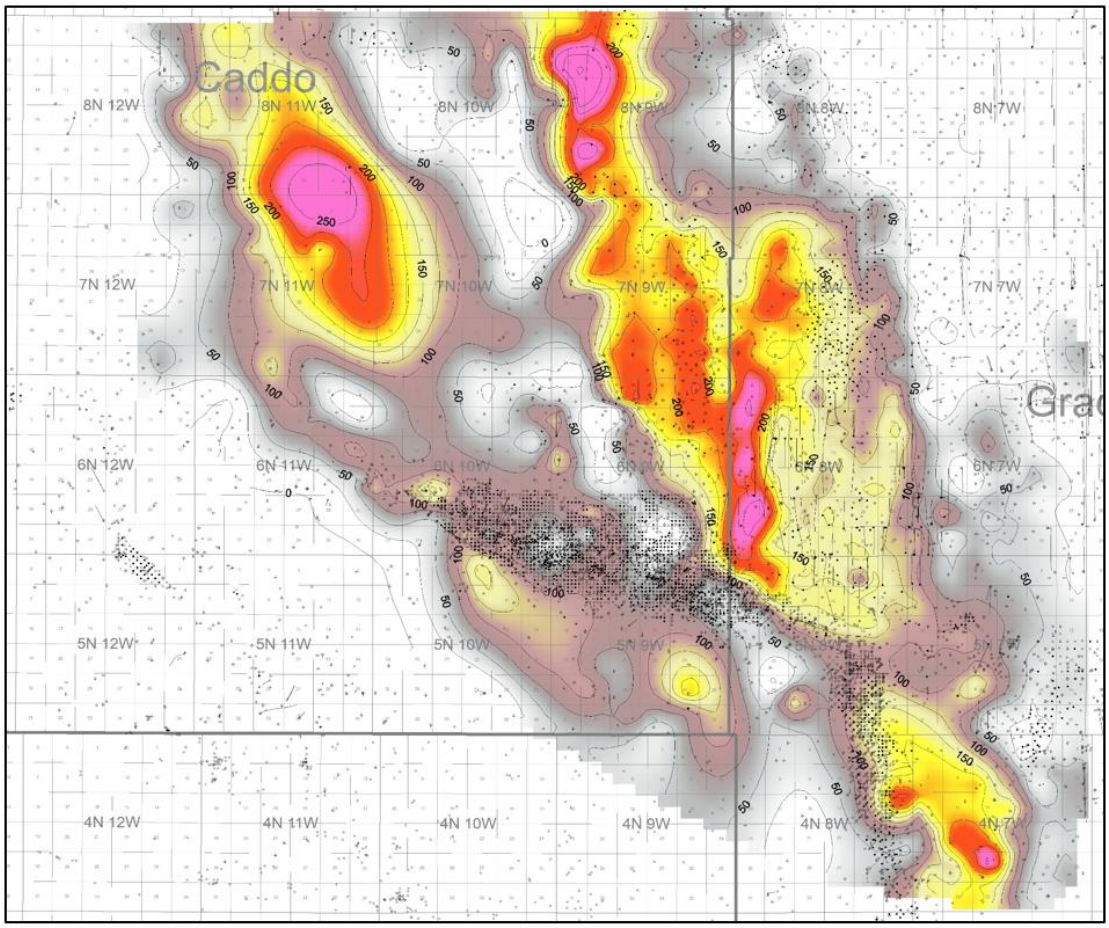

Figure 3.18. Map of combined thickness of net Upper and Lower Medrano Sandstone using a sandstone cutoff of ≥67% (shale volume cutoff of ≤33%). Maximum thickness is ≥225 feet (pink domain) and contour interval is 25 feet. A single trend of combined Medrano Sandstone in T.4N., R.7W. appears to bifurcate in T.5N., R.7W. to form the two prominent thicker trends that extend to the northern edge of the map.

The relationship between Lower Medrano Sandstone and Upper Medrano Sandstone is illustrated in a regional cross section extending from T.4N., R.7W. in the southeast corner of the study to T.8N., R.9W. along the northern edge. This cross section, which is called cross-section A-A'

(Figure 3.19) extends some 30 miles beginning in the area of a single trend and continuing along the east thickness branch following bifurcation in T.5N., R.8W. (Figure 3.19 inset map).

Cross-section A-A' is a stratigraphic cross section that uses the top of the Lower Wade Sandstone as datum (Figure 3.19). While log curves cannot be discerned with confidence because of scale issues, the Lower Medrano Sandstone is colored light brown, whereas the Upper Medrano Sandstone in colored light green. Color is applied irrespective of electrofacies and is solely intended to show changes in net sandstone thickness and the vertical spatial relationship between the Lower Medrano Sandstone and Upper Medrano Sandstone. The two sandstone bodies are separated using the shale interval evident on the gamma-ray curve (Figure 3.15) and confirmed in core from the EOG Schmidt 16 3H well. The Lower Medrano Sandstone is thicker in the southeastern corner of the mapping area in the vicinity of wells numbered 1, 2 and 3, cross-section A-A'. Starting with cross section well number 4 and moving northward, the Lower Medrano gradually thins until it is no longer mappable near cross-section well number 13 in T.8N., R.9W. (Figure 3.19; Figure 3.16).

The thickness of the Upper Medrano Sandstone complements the thickness of the Lower Medrano Sandstone and as the Lower Medrano Sandstone thins, the Upper Medrano Sandstone thickens. The Upper Medrano Sandstone is <20 feet thick in wells in the southeastern corner of the study area in cross section wells 1, 2 and 3 is too thin to represent on cross-section A-A'. From cross section well number 4 northward, the Upper Medrano Sandstone thickens gradually and reaches maximum thickness in the vicinity of cross section wells numbered 13 and 14 in T.8N., R.9W.

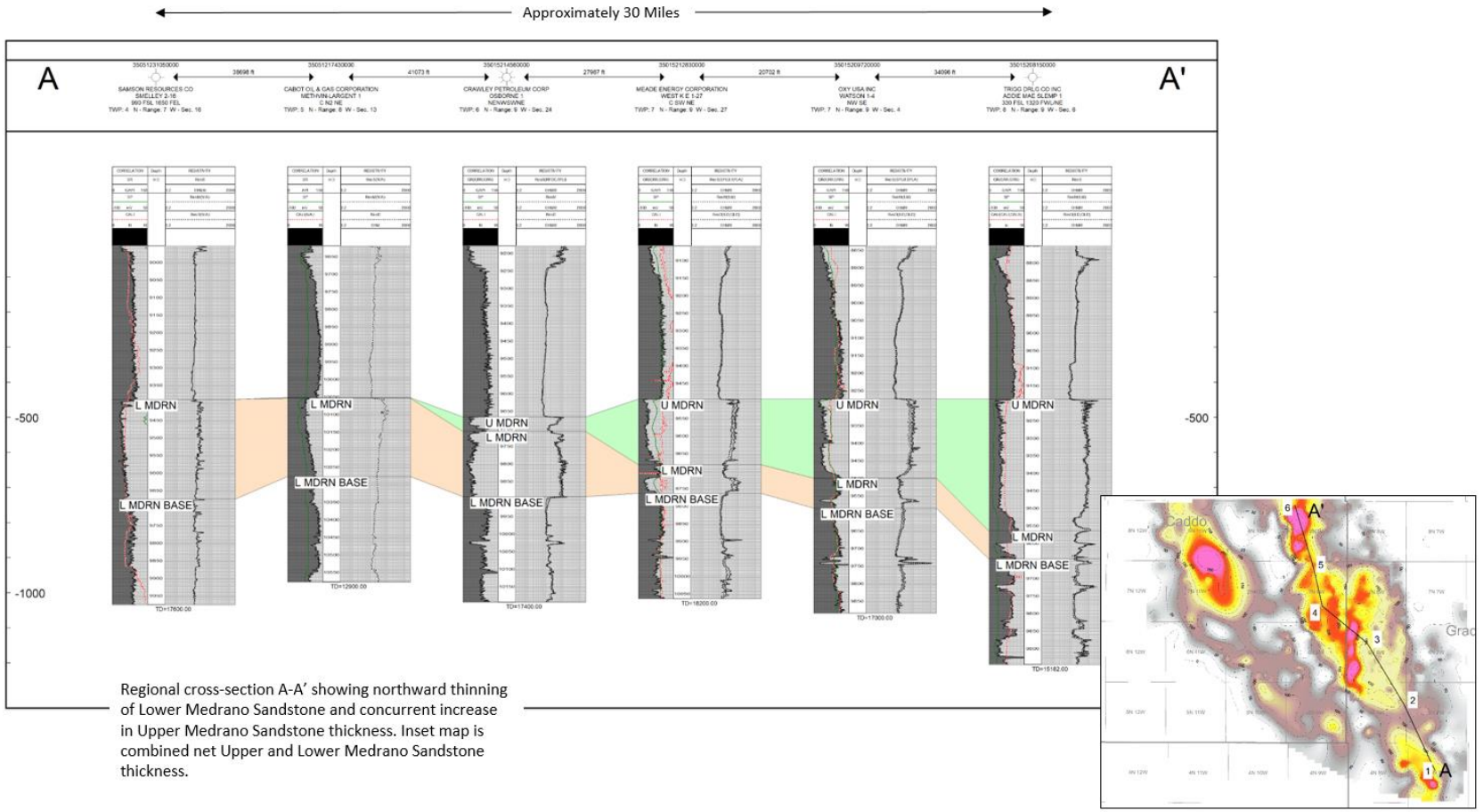

Figure 3.19. Generalized depositional relationship between Lower Medrano Sandstone thickness and Upper Medrano Sandstone thickness. Cross section is flattened on top of Hoxbar Group datum. Inset map is combined Lower and Upper Medrano thickness (Figure 3.17)

Local basin configuration and paleotopography at the time of sediment deposition can be inferred interval thicknesses. To better understand paleotopograghy and potential accommodation during Medrano sediment deposition, a thickness map of the interval between the top of the Medrano interval/base of Wade interval and the Hogshooter shale marker bed was constructed. The top of the Medrano Formation is picked at the base of dark gray shale at the base of the Wade Sandstone interval (Figure 2.4). This contact is distinct and recognizable across the study area. To facilitate confidence in picking the base of Medrano interval, the top of the radiogenic Hogshooter shale or Hogshooter marker bed was chosen as the interval base (Figure 2.4). To reduce the wordiness, the phrase Medrano-Hogshooter will be used to describe the interval of interest.

The thickness of the Medrano-Hogshooter interval is greatest the southeast and west-central parts of the study. The southeastern thick area is centered on T.5N., R.7W., where the Medrano-Hogshooter interval exceeds 1200 feet. The second thicker area is centered on the common corner of sections 6 and 7, T.6N., R.11W. and sections 1 and 12, T.6N., R.12W. A prominent trend of thin Medrano-Hogshooter interval extends north-south from T.8N., R.10W. to the common border of T.5N., R.9W. and T.5N., R.10W. This thinner area transects the Cement anticline without disruption. Cross-section C-C' (Figure 3.21) shows this thinning of the Medrano-Hogshooter interval and corresponding thinner Medrano Sandstone in the same area that includes cross section well number 3. This same cross section shows a generalized thickening of the Medrano-Hogshooter interval to the east of cross section well 4, but thinning of the Medrano Sandstone in the same direction. Thickening of the Medrano-Hogshooter interval with corresponding thinning of the Medrano Sandstone is illustrated by cross section well 1 (Figure 3.21). Increasing Medrano-Hogshooter thickness to the west is expected as that represents moving toward the axis of the Anadarko Basin.

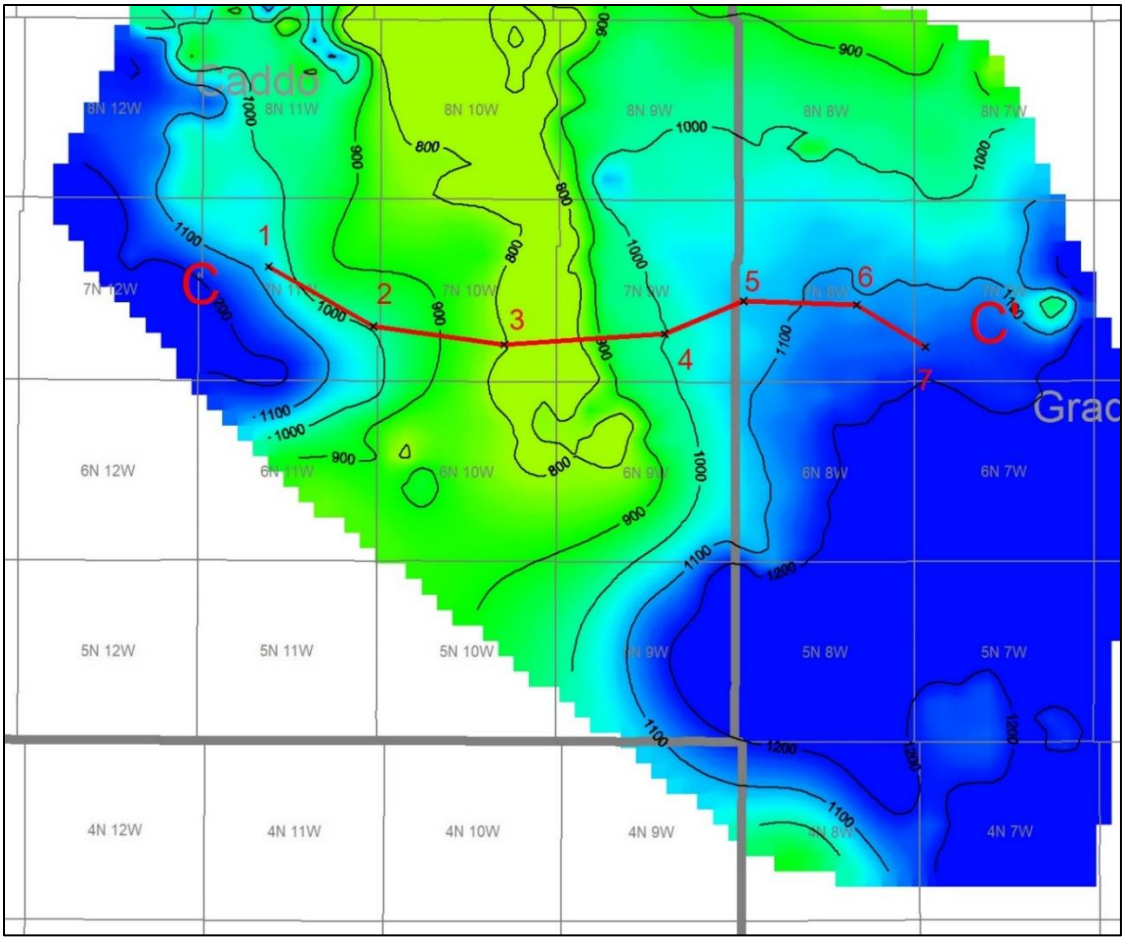

Figure 3.20. Map showing thickness of the Medrano-Hogshooter interval (C.I. = 100 feet). Thickest interval (blue) exceeds 1200 feet. Thinner interval shown by green colors and are < 800 feet in T.8N., R.10W. The trend of thinner Medrano-Hogshooter interval extends north-south across Cement anticline. Cross-section A-A' is Figure 3.21.

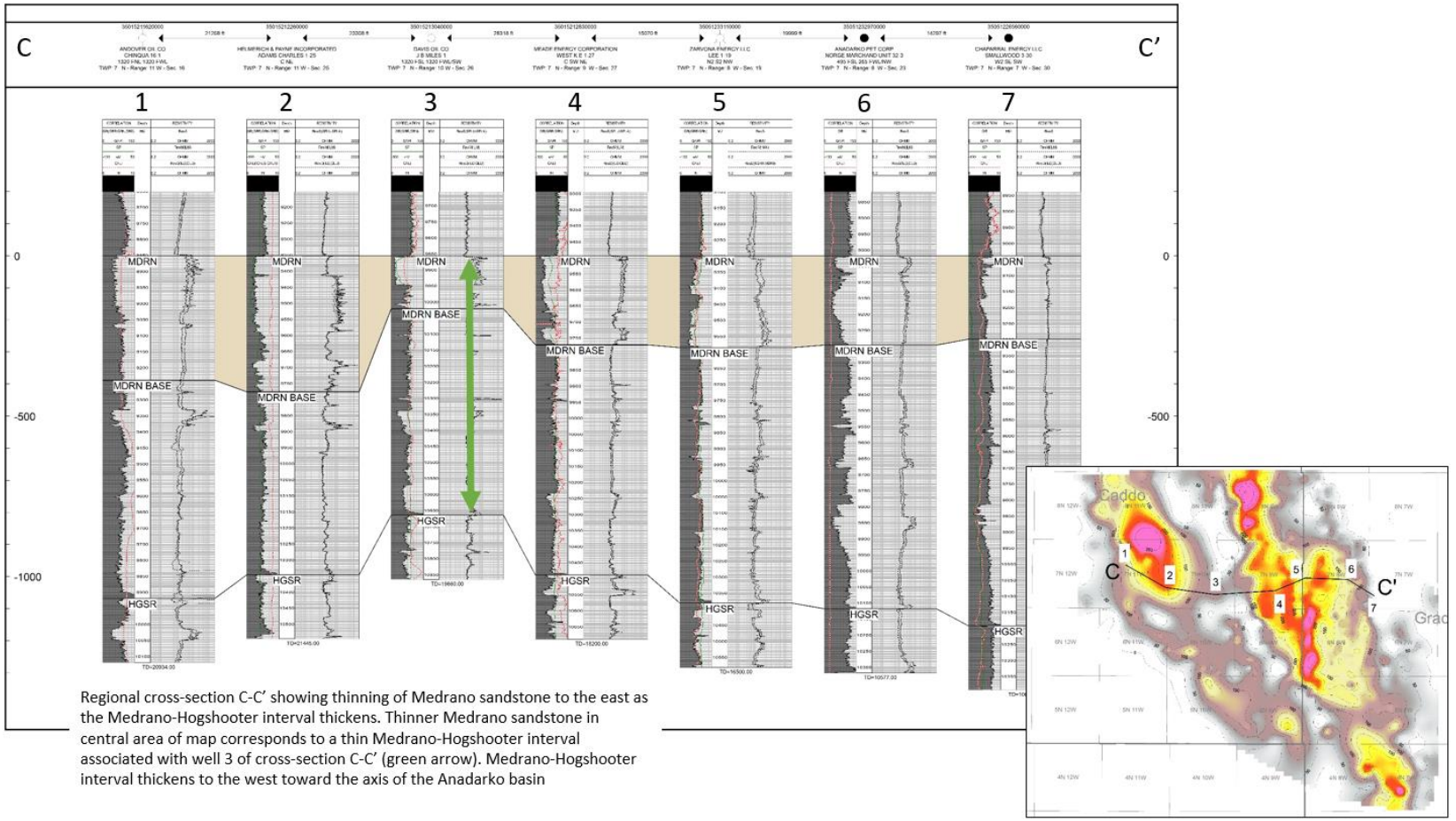

Regional cross-section C-C' showing thinning of Medrano sandstone to the east as the Medrano-Hogshooter interval thickens. Thinner Medrano sandstone in central area of map corresponds to a thin Medrano-Hogshooter interval associated with well 3 of cross-section C-C' (green arrow). Medrano-Hogshooter interval thickens to the west toward the axis of the Anadarko basin

Figure 3.21. Cross-section A-A' showing thickness changes of Medrano-Hogshooter interval and corresponding thickness changes for the Medrano Sandstone. Inset map is Figure 3.16, total net Medrano Sandstone. Location of cross section A-A' is also shown on Figure 3.19, the Medrano-Hogshooter thickness map.

Petrology

The Jobe 31-1 and Schmidt 16 3H cores provided for this study were slabbed library sets consisting of approximately one-third core diameter. The remaining two-thirds or butt portion was not available. Consequently, only thin sections and Scanning Electron Microscope (SEM) images provided by EOG Resources and Unit Petroleum were available for the petrologic analysis of the Medrano Sandstone reservoir. Five thin sections were provided for the Jobe 31-1 core. These thin sections sampled depths of 9,490, 9,500, 9,520, 9,530, and 9,545 feet. The SEM images provided for the Jobe 31-1 were taken at the same depths as thin sections. Four thin sections were prepared for the Schmidt 16 3H at depths of 9,617, 9,620, 9,692, and 9,717.5 feet, whereas SEM images provided for the Schmidt 16 3H were taken at depths of 9,615, 9,697, and 9,749 feet. Sample analysis and photomicrographs conducted by Weatherford Labs were provided by Unit Petroleum and EOG Resources. The Medrano Sandstone is dominantly quartz arenite and sublitharenite according to the Folk (1974) classification based on nomalized percentages of quartz (Q), feldspar (F) and rock fragments (F) for sandstones containing less than 15% matrix (Figure 3.22). As a result of chert clast content, the conglomeratic zone in the Schmidt 16 3H core classified as litharenite. Classification was based on four hundred points for each thin section.

Jobe 31-1

Depth: 9,490 feet. Detrital grains making up the majority of the sample are monocrystalline quartz grains, chert, argillaceous sedimentary rock fragments, plagioclase feldspar, and microcline. Cementation occurs as quartz overgrowths, trace authigenic chlorite coating detrital grains, minor kaolinite occluding pores and trace carbonates as calcite and ferroan dolomite. Suture-seam microstylolites and pseudomatrix of deformed argillaceous rock fragments are common (Figure 3.23). Minor secondary intragranular pores are associated with partially dissolved grains; micropores are associated with partially leached grains and authigenic clay (Figures 3.23 and 3.24).

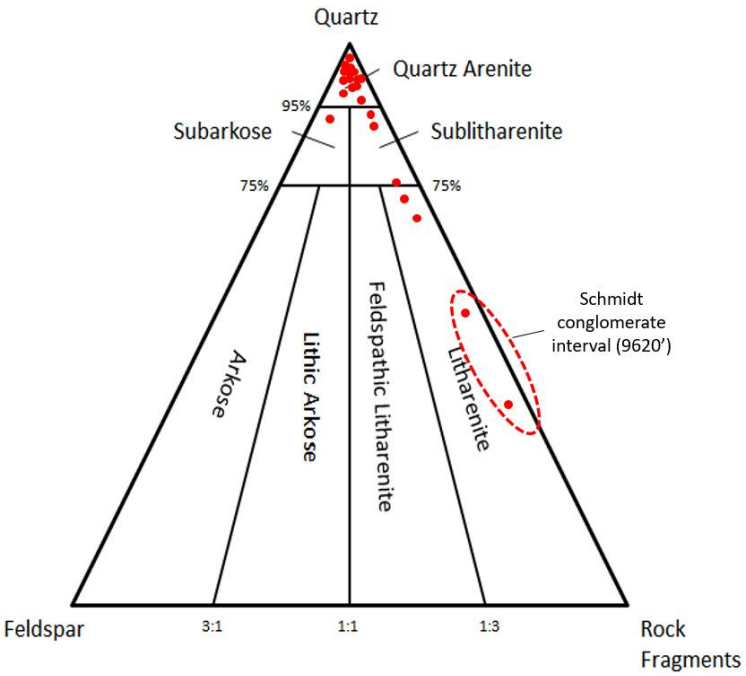

Figure 3.22. Folk (1974) classification of the Medrano Sandstone based on normalized percentages of detrital quartz (Q), feldspar (F) and rock fragments (R) for sandstone with less than 15% matrix. Plot contains point count data from cores.

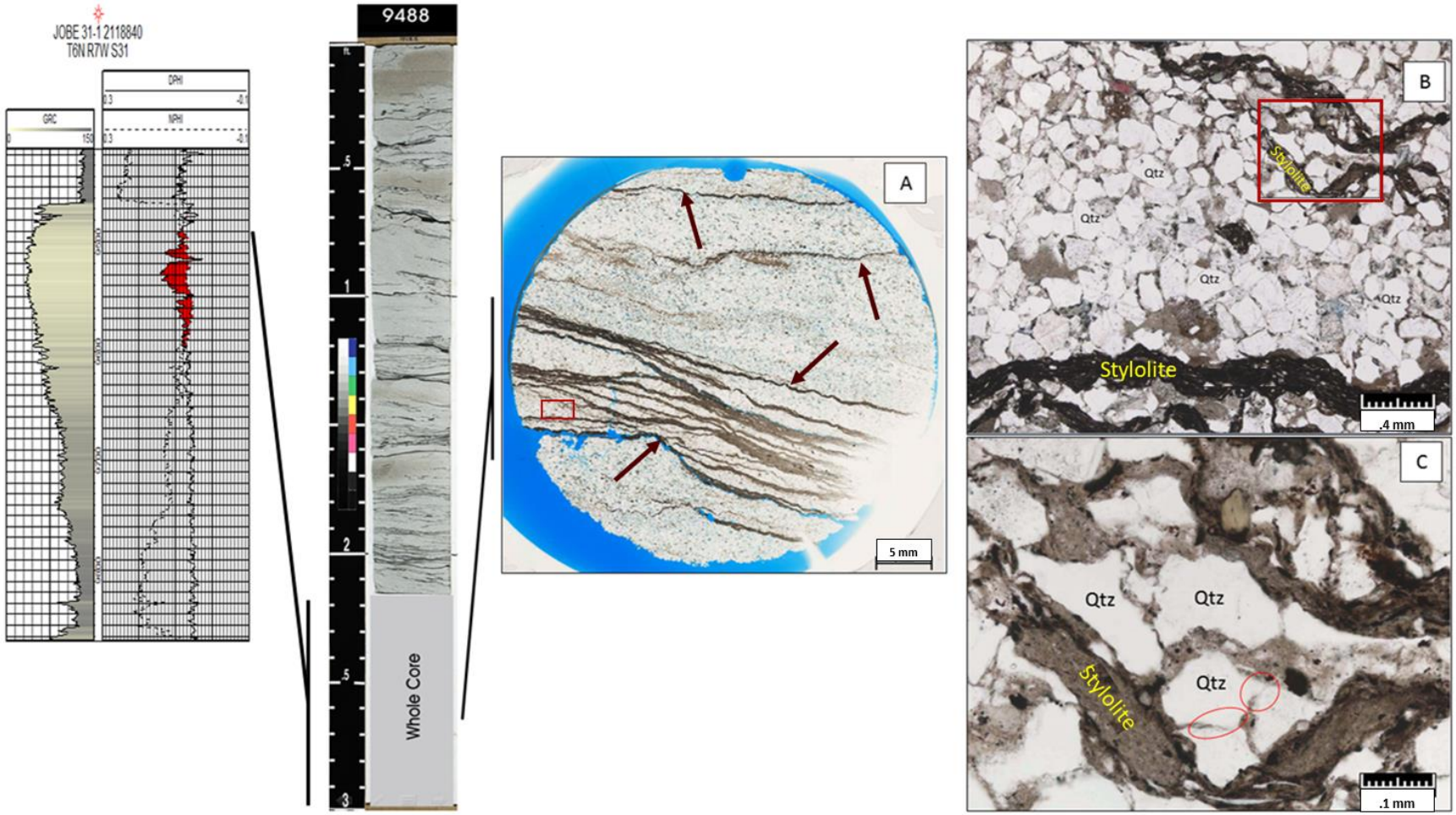

Figure 3.23. Photomicrographs: A) Sandstone fabric with argillaceous/organic-rich laminations and solution-seam low-amplitude microstylolites. Red box is location of image B. Scale bar is 5 mm. B) Quartz (Qtz) is dominant detrital grain. Microstylolites of detriral clay and insolubles (red box shows location of picture C). Scale bar is 0.4 mm. C) Sutured grain contacts (red) associated with stylolite formation. Scale bar is 0.1 mm. All images plane-polarized light. Jobe 31-1, depth 9490 feet.

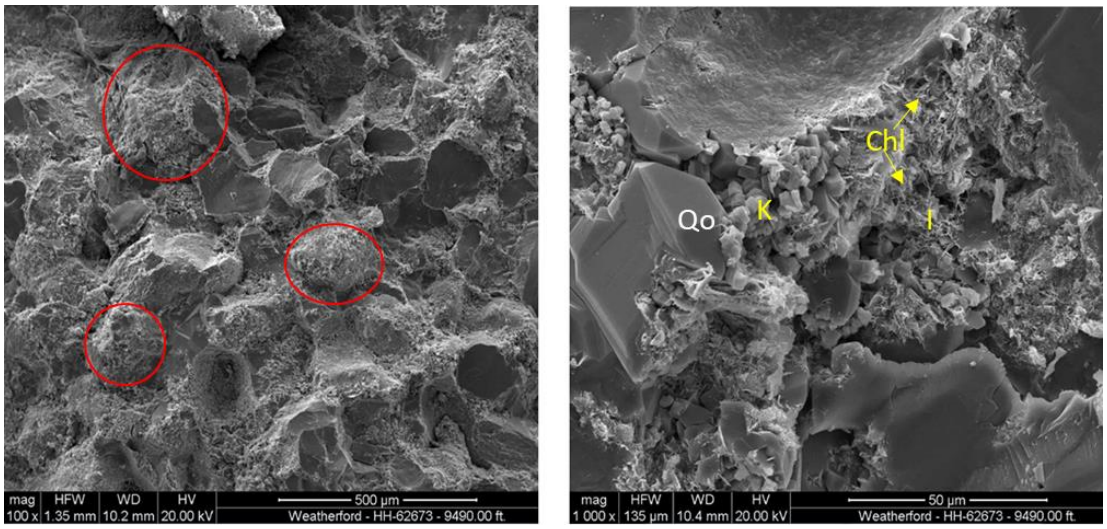

Figure 3.24. SEM images of Medrano Sandstone sampled at 9,460 feet. Left image showing quartz grains coated (red) with clay minerals. Right: Syntaxial quartz overgrowth (Qo), authigenic pore-bridging illite (I), kaolinite (K) partially filling pores and chlorite (Chl) coating grains. Microporosity develops between authigenic clay minerals. Smooth concave area toward top of right image is imprint of ooid removed during sample preparation.

Depth: 9,500 feet. Monocrystalline quartz is the major detrital grain in this sample, while minor constituents include ooids, coated grains, sedimentary rock fragments argillaceous siltstone and mudstone, plagioclase feldspar, and k-feldspar. Detrital clay matrix is minimal; pseudomatrix results from the compaction of argillaceous rock fragments. Abundant calcite occurs as pore-filling cement, with minor replacement/recrystallization of allochems and quartz grains. Ooids are commonly replaced by ferroan dolomite and siderite. Pyrite partially replaces grains and carbonate cement. Minor secondary intragranular porosity is associated with partially dissolved grains, and micropores occur in partially leached grains and authigenic clay (Figure 3.25).

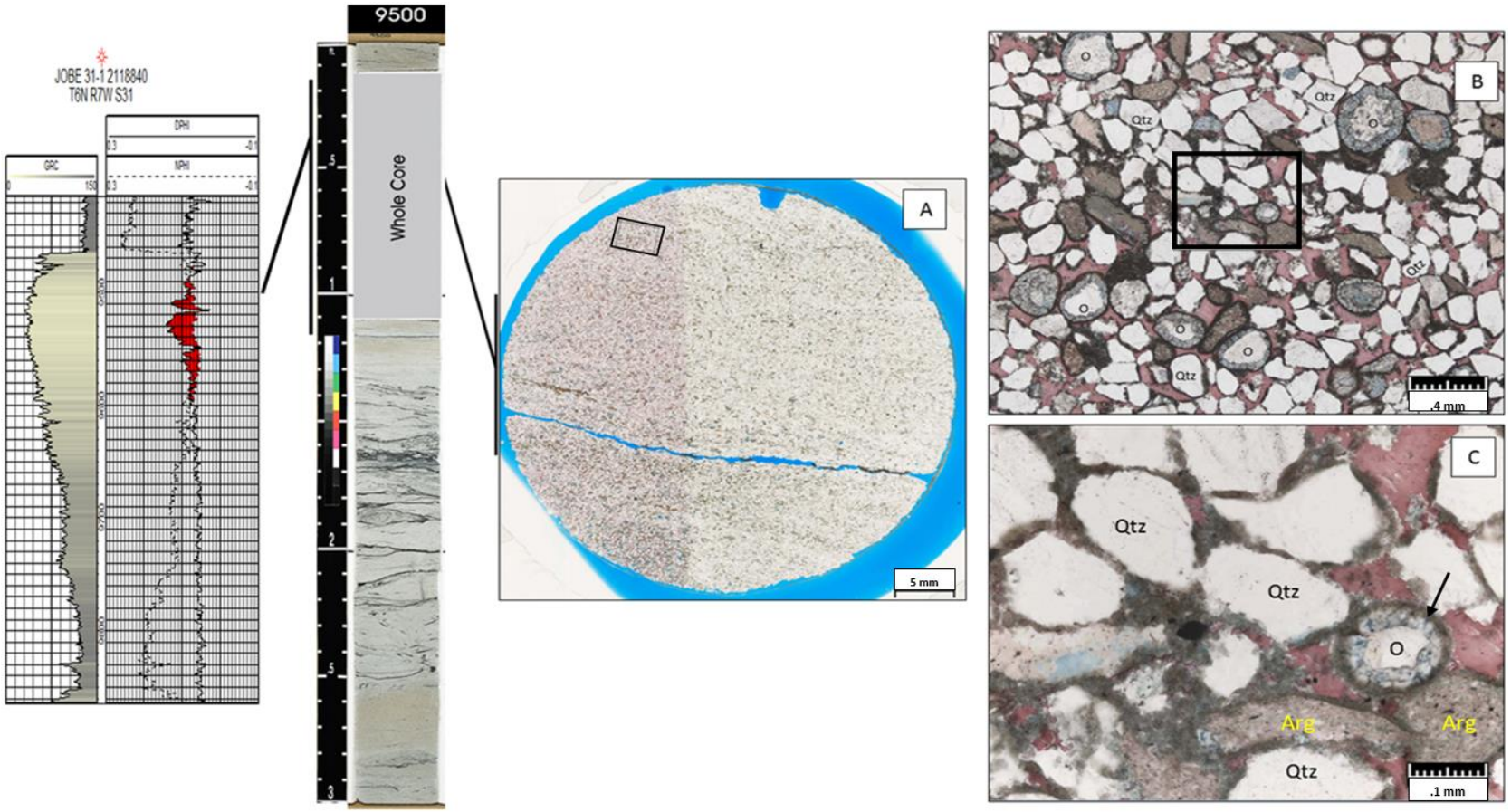

Figure 3.25. Photomicrographs: A) Calcareous sandstone with separation in core plug along clay seam. Left side of slide is stained with alizarin red to identify carbonate minerals; abundant calcite present (pink). Black box in upper left represents photo B. Scale bar is 5 mm B) Abundant detrital quartz (Qtz), ooids (O) and calcite cement (pink). Ooids are partially recrystallized with clay coating and nucleated on quartz, siltstone, and chert grains. Intergranular porosity is occluded by the abundant calcite cement. Scale bar is 0.4 mm. Black box shows location of picture C. C) Quartz, argillaceous rock fragments (Arg) and ooids coated by dominantly chlorite (green-gray) rims (arrow) and cemented by calcite (pink). Opaque near center of image is pyrite. Scale bar is approximately 0.1 mm. Images both plane-polarized light. Depth 9500 feet, Jobe 31-1.

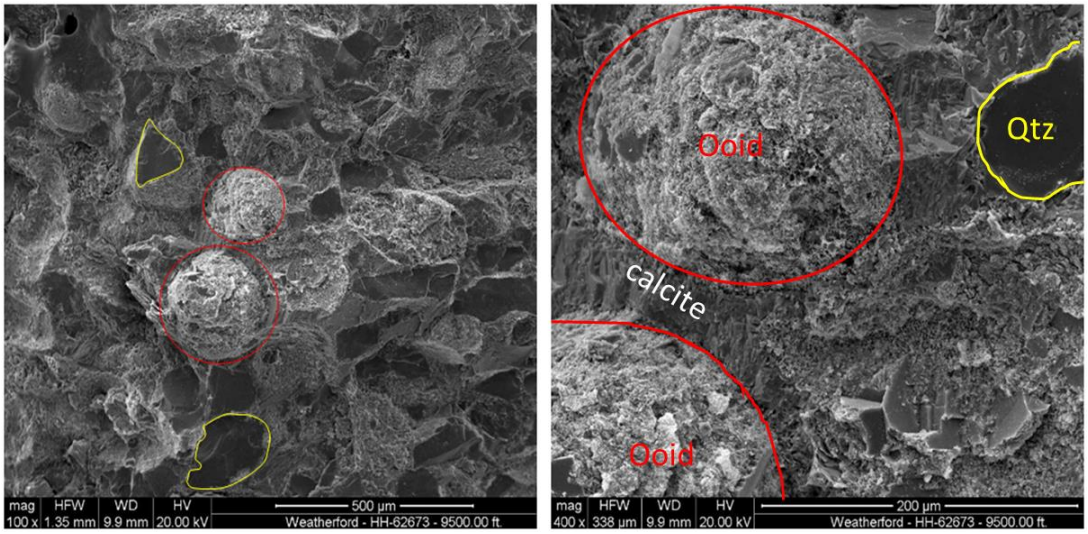

Figure 3.26. SEM images from 9,500 feet sample. Left shows quartz grains (yellow) and coated ooids (red). Right is close up of clay-coated ooids cemented by calcite. Coatings are dominantly detrital illitic/chloritic clays, ferroan dolomite, and siderite. Detrital coating provided substrate for later precipitation of authigenic illite and chlorite. Scale bars on individual images.

Depth 9,520, 9,530, & 9,545 feet: The major detrital grain in these thin sections is monocrystalline quartz with minor constituents including argillaceous rock fragments, plagioclase feldspar, K-feldspar. Quartz overgrowth is common to abundant and the principal cement. Trace to minor amounts of clay include chlorite-dominated coatings of detrital grains. Pseudomatrix formed by the compaction of argillaceous sedimentary rock fragments is common as are microstylolites in samples from 9,530 and 9,545 feet (Figure 3.29). Porosity is dominantly secondary and forms from the partial dissolution of labile grains including feldspar and sedimentary rock fragments. Moldic pores are common and include remnants of partially dissolved grains and clay coatings. Micropores occur within masses of authigenic clays. Minor amounts of primary intergranular porosity are preserved as triangular-shaped pores lined by euhedral faces of syntaxial quartz overgrowths (Figure 3.28).

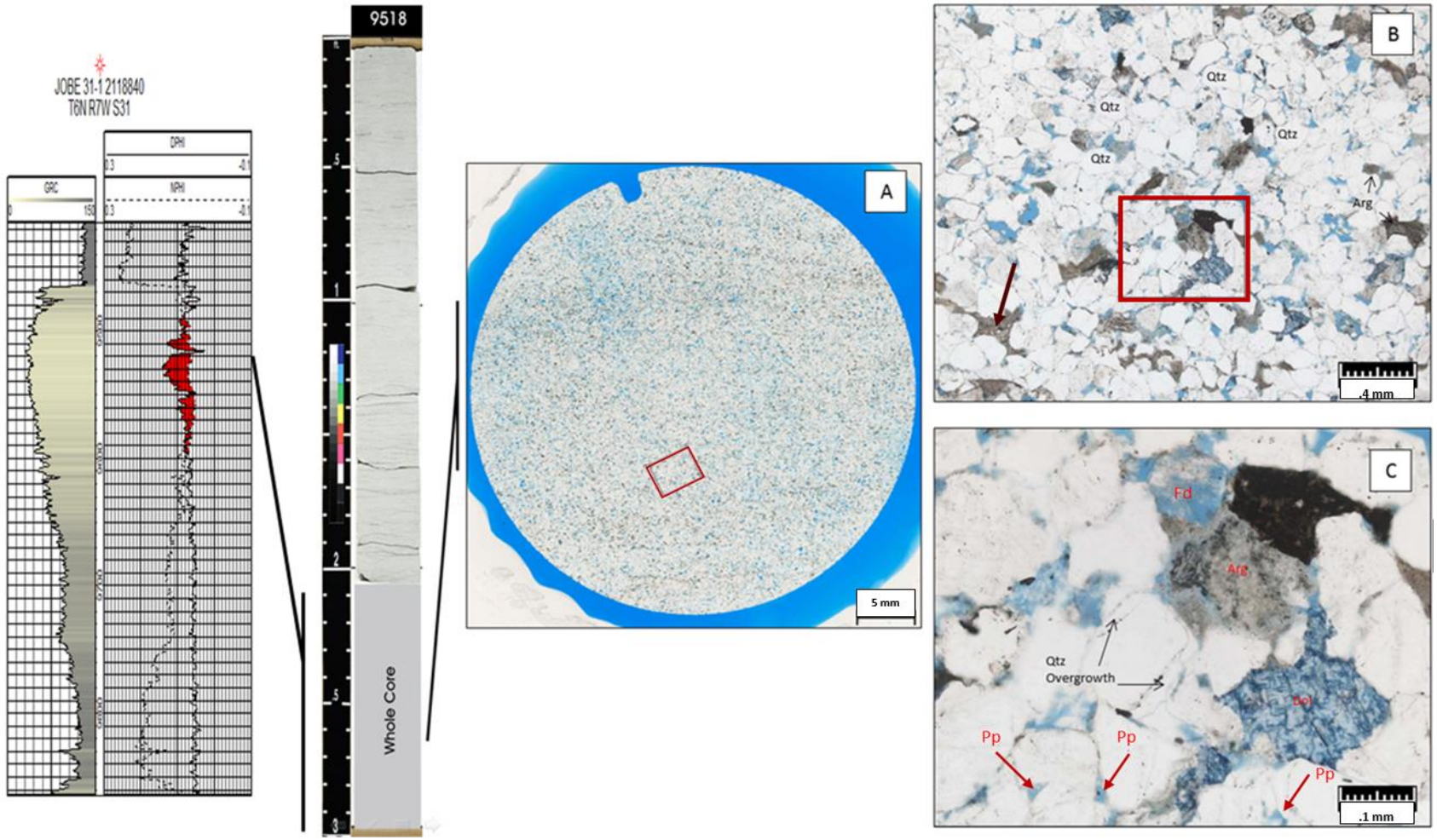

Figure 3.27. Photomicrographs: A) Sandstone with porosity (blue) and cemented areas (white). Red box indicates location of photo B. Scale bar is 5 mm. B) Detrital quartz (Qtz) and argillaceous (Arg) sedimentary rock fragments. Red box shows location of image C. Scale bar is 04 mm. C) Quartz overgrowth, dark deformed grain (mudstone) forming pseudomatrix, syntaxial quartz overgrowth, primary porosity (Pp), and partially dissolved feldspar (Fd). Dolomite (stained blue) replacing detrital quartz and cement. . Scale bar is 04 mm. Plane-polarized light. Jobe 31-1, depth 9520 feet.

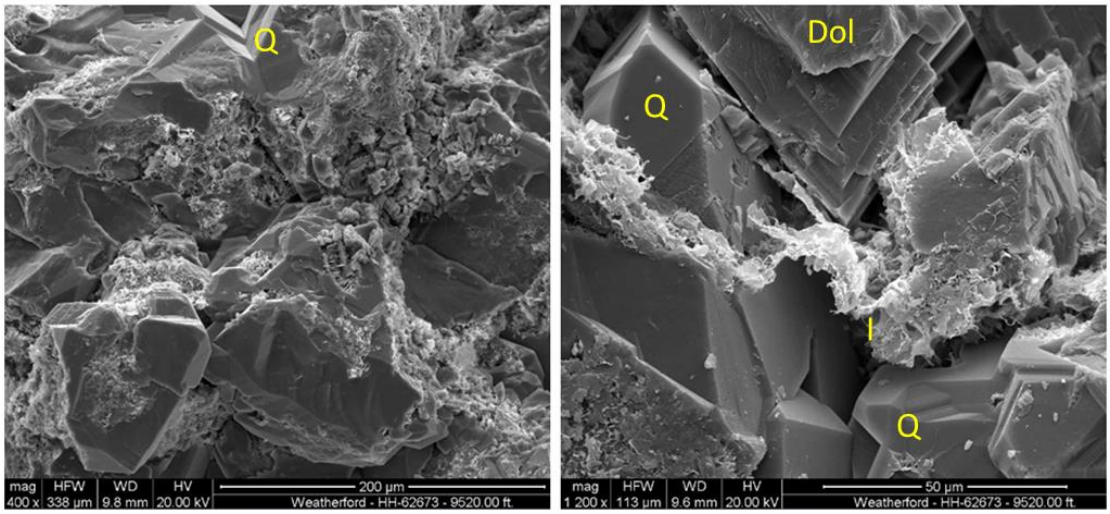

Figure 3.28. SEM images of Medrano sandstone, depth 9,520 feet. Left: quartz overgrowth (Q) and partial clay mineral coatings of detrital quartz grains. Right: authigenic clays including pore bridging illite (I), euhedral syntaxial quarts cement (Q) and euhedral pore-filling dolomite (Dol). Scale bars on respective images.

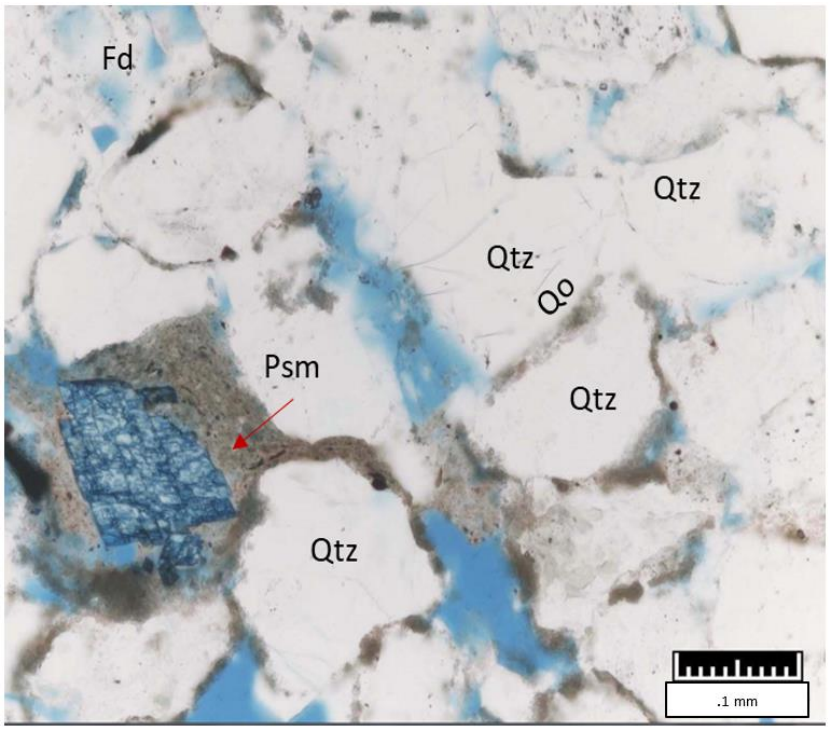

Figure 3.29. Photomicrograph showing dolomite (blue grain) in pseudomatrix (Psm) generated by deformed argillaceous sedimentary rock fragment. Other features include quartz (Qtz) with syntaxial overgrowth (Qo) and partially dissolved feldspar (Fd). Scale bar is 0.1 mm. Plane-polarized light (PPL). Depth 9,530 feet, Jobe 31-1.

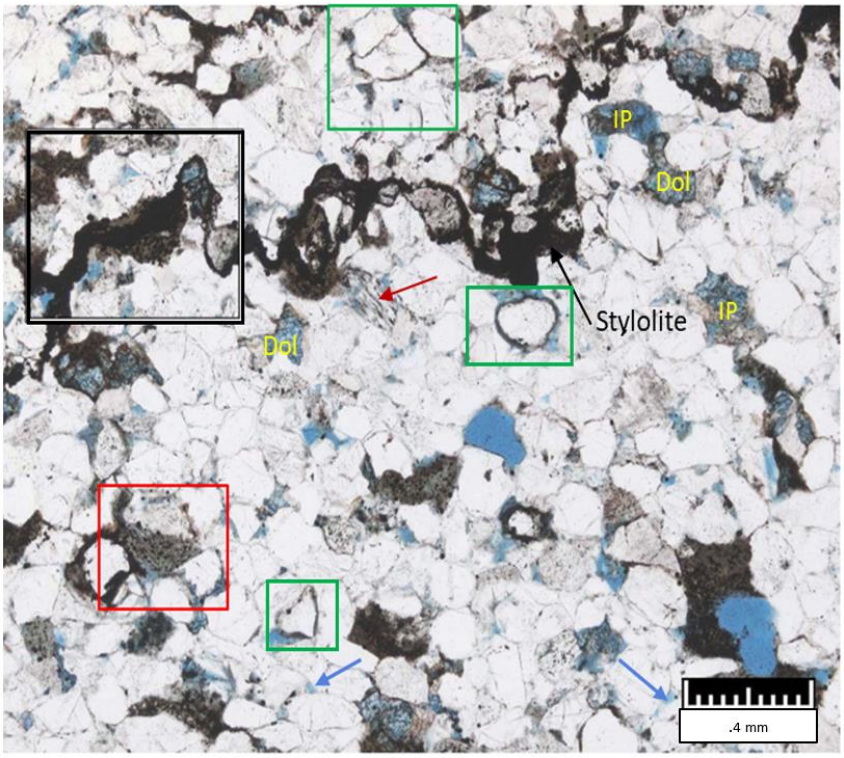

Figure 3.30. Photomicrograph showing white detrital quartz grains with clay coated grains outlined by green boxes. Horizontal microstylolite with accumulation of clay, organic material and unidentified insolubles. Black box shows amplitude of stylolite. Pseudomatrix is common and formed by the compaction of argillaceous sedimentary rock fragments (red box). Red arrow is micaceous foliated grain. Porosity (blue) is mostly secondary moldic and intraparticle (IP); trace primary porosity remains as small triangular pores between euhedral quartz cement (blue arrows). Dolomite (Dol) is important pore-filling cement. Jobe 31-1, depth 9,545 feet. PPL. Scale bar is 0.4 mm.

Schmidt 16 3H: Depth 9,692 feet: The Lower Medrano Sanstone is predominantly sublitharenite. Monocrystalline quartz as the dominant detrital grain with lesser amounts of plagioclase feldspar and sedimentary rock fragments (Figure 3.31). Silica cement in the form of syntaxial quartz overgrowth (Figure 3.31) is common as is pore-filling calcite. Dolomite is less common and occurs as euhedral crystals that partially fill pores. Porosity is mostly secondary and includes moldic porosity formed by dissolution of feldspar and sedimentary rock fragments. Partially dissolved feldspar and sedimentary rock fragments contain intragranular porosity. Minor primary porosity is retained between quartz overgrowths (Figure 3.31).

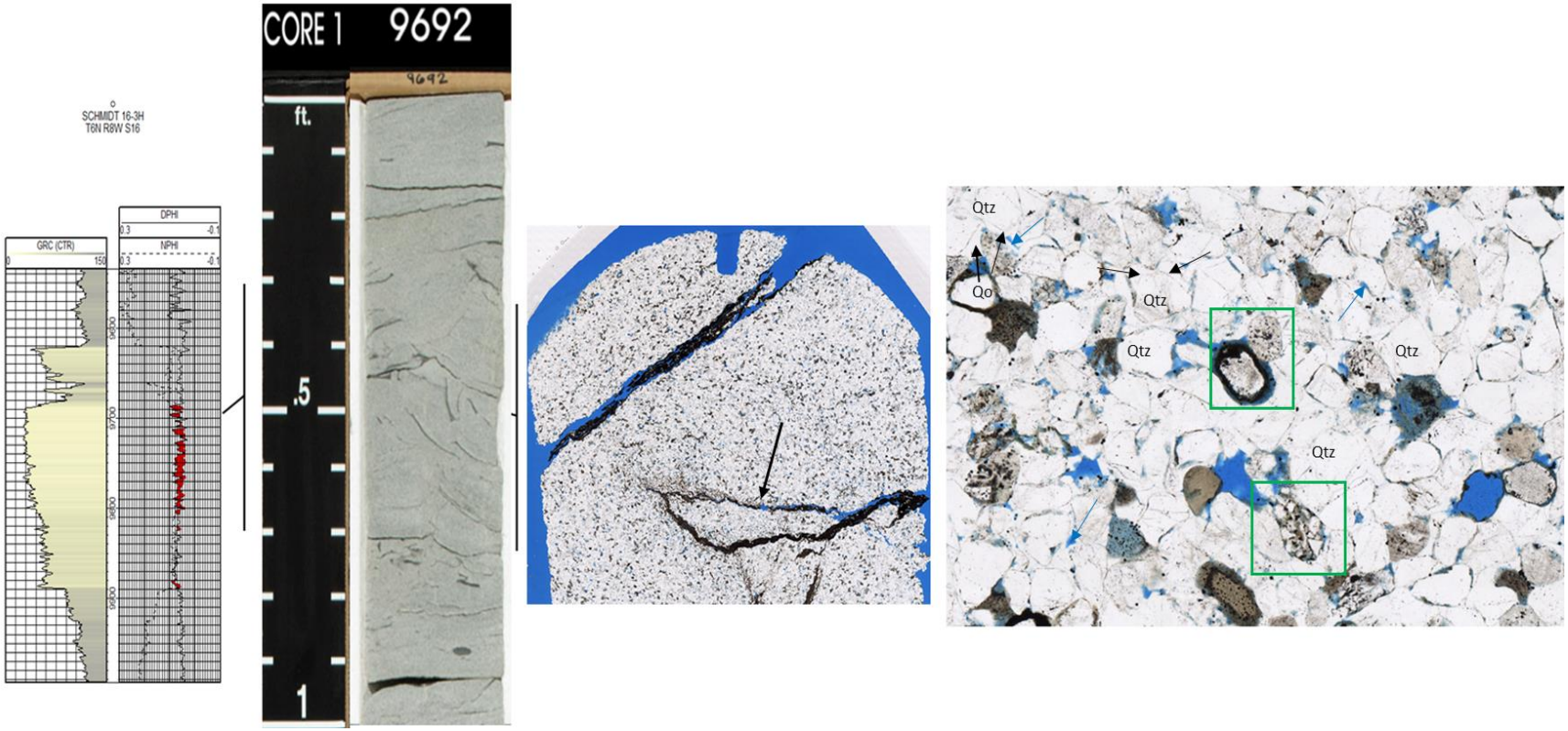

Figure 3.31. Core photograph and photomicrographs, Lower Medrano Sandstone. Core photograph shows disruption of originally horizontal clay laminae by soft-sediment deformation. Middle core plug image shows dipping and horizontal laminae that are dissolution fronts that form sutured seam stylolites (arrow). Scale bar is 5 mm. Photomicrograph on right shows dominance of quartz (Qtz) detrital grains and sedimentary rock fragments (green boxes). Silica cement as quartz overgrowths (Qo) is prevalent. Porosity is secondary in the form of moldic pores (blue) formed mostly by dissolution of feldspar and sedimentary rock fragments. Primary porosity (blue arrows) is minor and is identified by planar margins formed by euhedral quartz overgrowths. Scale bar is .04 mm. PPL. Schmidt 16 3H, depth 9,692 feet.

Depth 9,620': Major detrital grains ared pebble-sized chert, granule-sized sedimentary rock fragments and crinoid and bryozoan skeletal fragments (Figure 3.32). Smaller detrital grains include abundant monocrystalline quartz grains and less-abundant ooids and plagioclase feldspar (Figure 3.32). Trace amounts of clay coat detrital grains. Pseudomatrix was formed in some areas due to the compaction of detrital grains. Primary intergranular porosity was occluded by pervasive calcite cement that is stained with alizarin red. Dolomitization is evident and replaces calcite cement (Figure 3.32; 3.33). No igneous rock fragments such as granophere and microperthite that indicate Wichita Mountain provenance are evident.

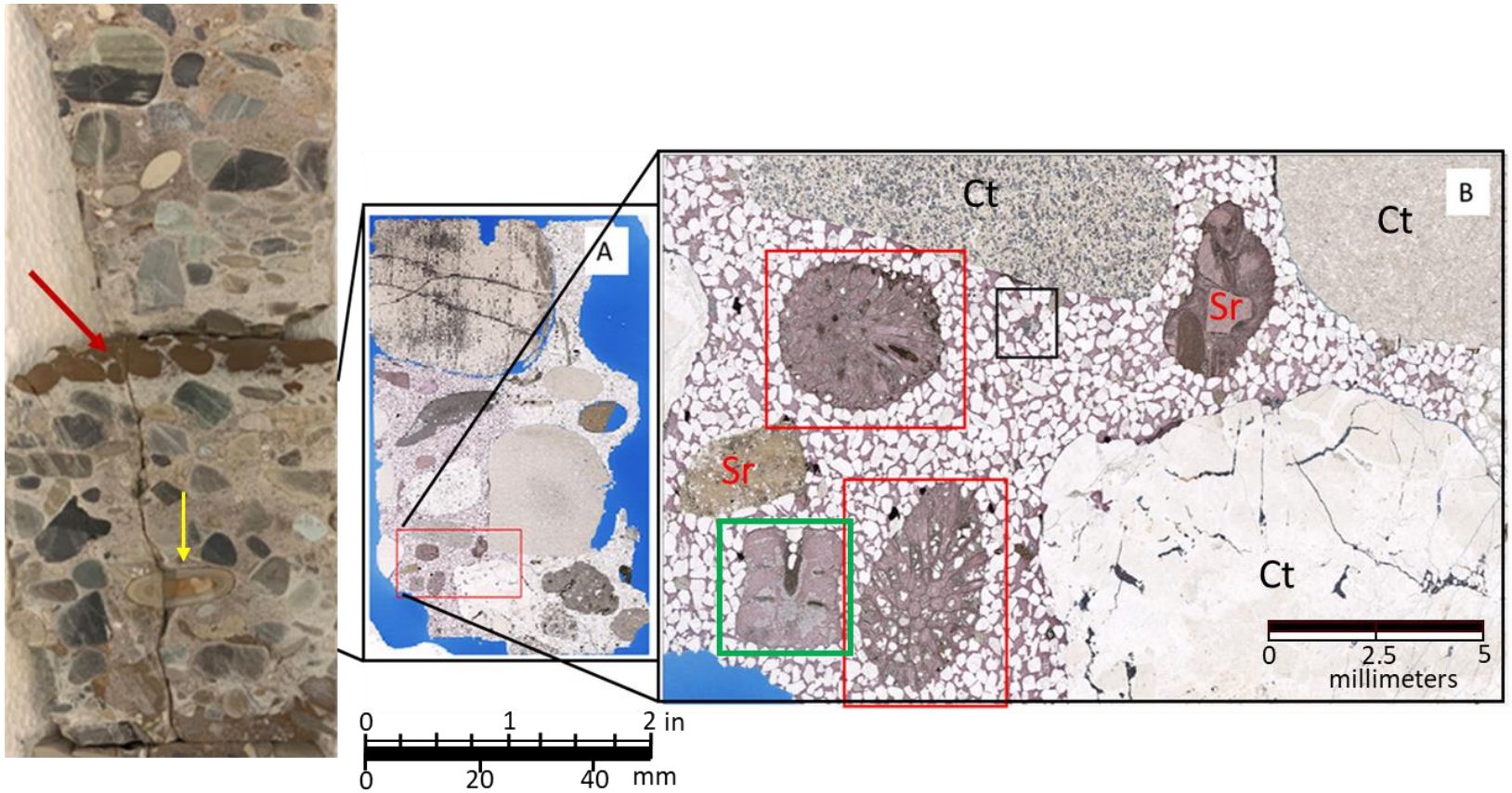

Figure 3.32. Core photograph and photomicrograph of the Upper Medrano Sandstone. Core photograph shows chert pebble conglomerate in sand-sized matrix. Some chert clasts are fractured, others have well developed weathering rind (yellow arrow). Accumulation of sideritized clay clasts (red arrow) separates chert-dominated beds. A) photomicrograph showing larger pebble-sized detrital clasts and finer detrital quartz sand matrix. Sample was stained with alizarin red to identify calcite cementation. Location of photomicrograph is indicated by red box. B) Photomicrograph showing bryozoan (red boxes) and echinoderm (green box) bioclasts as well as other sedimentary rock fragments (Sr). Black box outlines dolomite cement replacing calcite cement. PPL. Schmidt 16 3H, depth 9,620 feet.

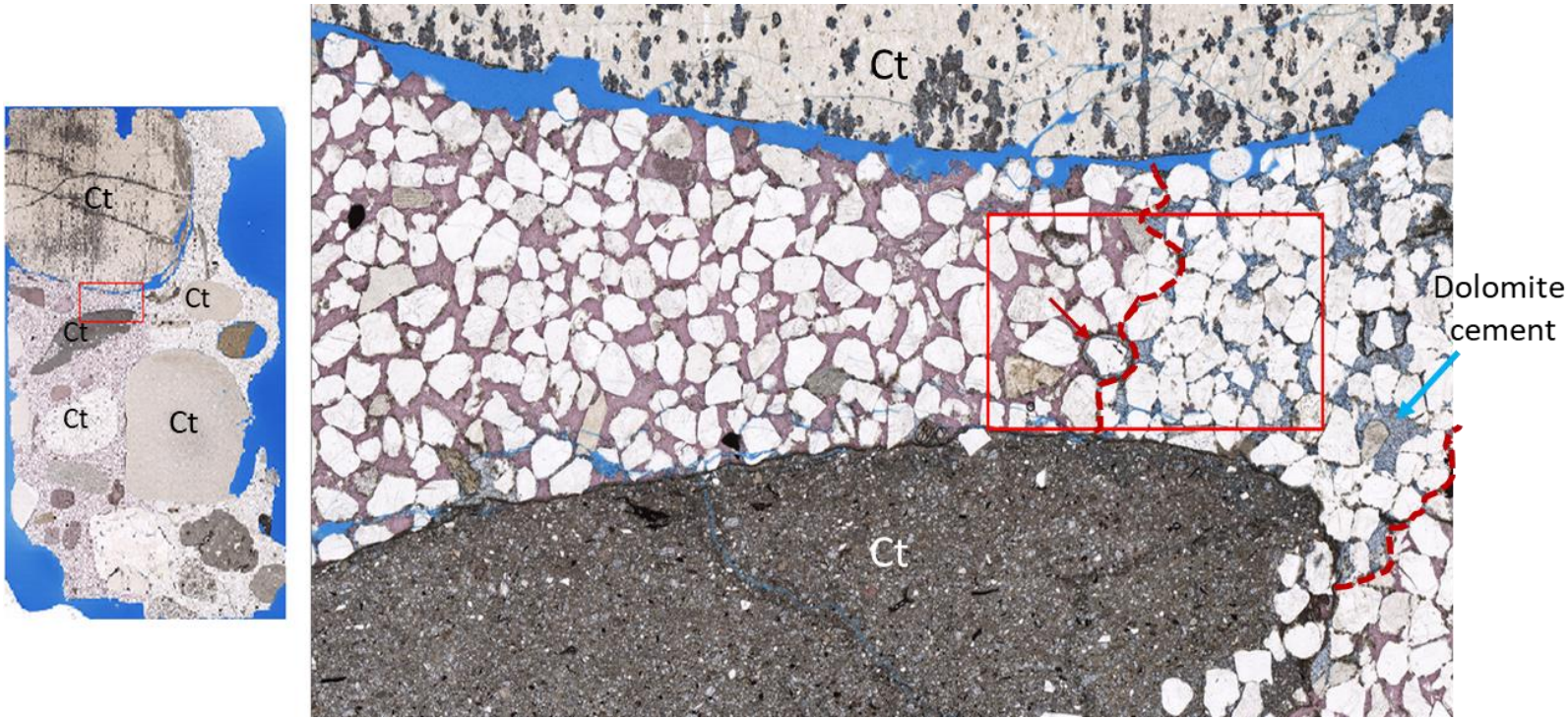

Figure 3.33. Photomicrographs of the Upper Medrano Sandstone, Schmidt 16 3H, depth 9,620 feet. Left photomicrograph shows chert (Ct) pebbles in sand matrix. Red box shows location of figure on right. Right photomicrograph shows chert (Ct) pebbles, mostly quartz sand grain matrix, partially dolomitized ooid (red arrow) and carbonate cement. Calcite cement is pink as a result of alizarin red staining. Dolomite cement is blue as a result of potassium-ferricyanide staining. Red dashed lines delineate the area of dolomitization. Both calcite and dolomite partially replace quartz forming corroded grain to cement contacts.

Depth 9,617 feet: The bioturbated interval immediately overlying the Upper Medrano conglomerate and conglomeratic sandstone is a mix of dark gray to mudrock (shale) to dark to medium gray interlaminated clay and silt-sized detrital quartz. The more massive dark gray to mudrock contains suspended quartz grains and skeletal material including complete benthic uniserial foramanifera (Figure 30). These homogenized zones lack bedding on a microscale, but are part of the upper an interval with weakly defined lighter gray-colored sand- silt-rich zones that alternate with darker more clay-rich zones at the core hand specimen scale (Figure 3.34).

Porosity

Porosity in the lower and upper Medrano sandstones is both primary and secondary. Primary porosity occurs in minimal amounts, due to burial compaction and resulting cementation. Secondary porosity is more prevalent and occurs mostly as molds where grains are completely removed and as intragranular porosity in partially dissolved detrital grains such as feldspars and sedimentary rock fragments. Fracture porosity is evident in core, but was not captured in thin section. Microporosity occurs within partially dissolved detrital grains and between clay mineral crystals. Occlusion of intergranular porosity is mostly the result of silica cement that occurs as syntaxial quartz overgrowths. The number of thin sections was too few to make a meaningful comparison between wireline log measured porosity and thin section point count porosity.

To determine if a relationship exists between porosity and sandstone distribution, net porosity thickness maps were constructed using a cutoff of >6% density porosity at a grain density of 2.68 g/cc. Maps were constructed for the Lower Medrano Sandstone, Upper Medrano Sandstone and for the combined Medrano sandstone.

The distribution of net porosity in the Lower Medrano Sandstone (Figure 3.36) was similar to the distribution of the net Lower Medrano Sandstone in that two distinct trends develop.

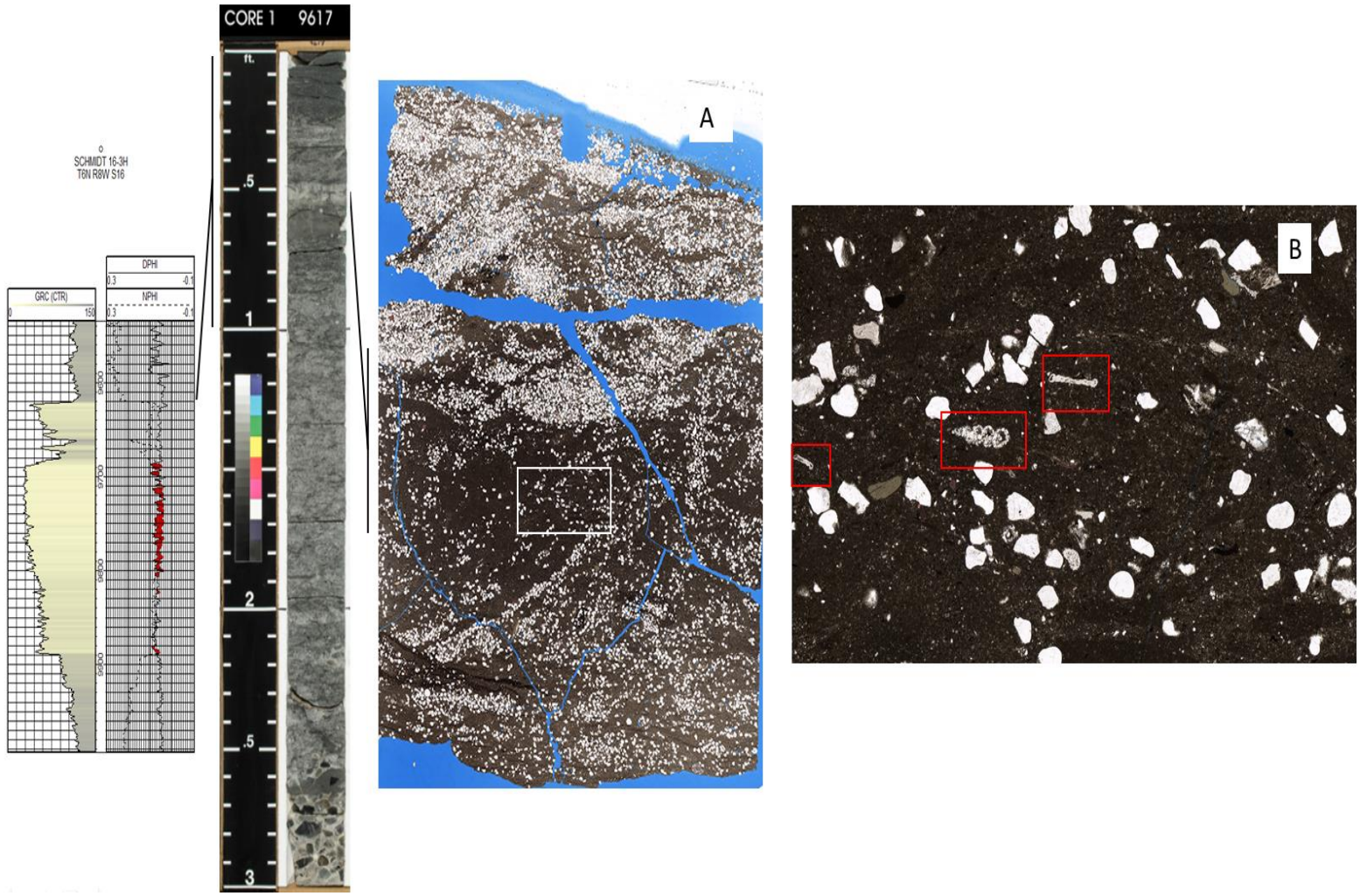

Figure 3.34. Core photo and photomicrographs of the bioturbated clay-rich interval immediately above the Upper Medrano Sandstone in the Schmidt 16 3H. A) Fabric of dark gray claystone with suspended silt and sand grains (white). White box indicates location of photo B. B) Photomicrograph of mudstone showing remains complete benthic uniserial foraminifera and unidentified skeletal remains (indicated in red boxes). Depth 9,617 feet, PPL.

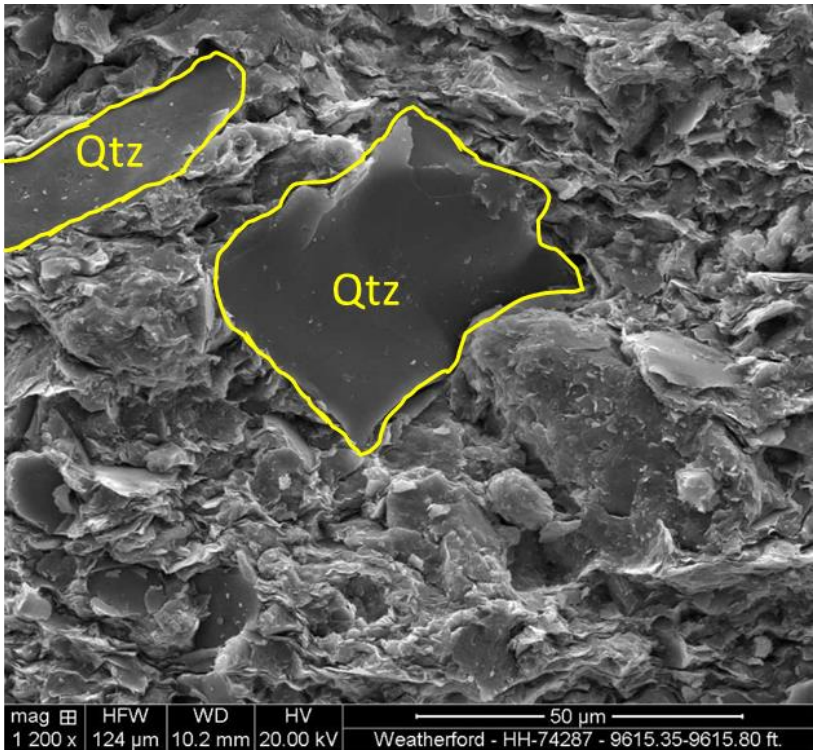

Figure 3.35. SEM image of mudstone with detrital quartz grains (Qtz) engulfed in detrital clays. Schmidt 16 3H, depth 9,615 feet. Scale is shown on image.

The eastern trend extends north-south through T.7N., R.8W., T.6N., R.8W., E/2 of T.5N., R.8W. and T.4N., R.7W. A second trend extends northwest-southeast in T.5N., R.8W. and T.5N., R.9W. (Figure 3.35). The thickest values in the porosity trend are in T.4N., R.7W. and T.6N., R.8W., where cumulative thickness exceeds 120 feet. The area of greater than eighty (80) feet of porosity ≥6% includes more than 11 square miles in T.4N., R.7W. and more than 24 square miles in T.6N., R.8W. (Figure 3.36).

The porosity thickness map for the Upper Medrano Sandstone (Figure 3.37) shows a distribution pattern that complements the distribution of porosity in the Lower Medrano Sandstone. The parameters used to define net porosity are ≥ 6% density porosity using a 2.68 g/cc grain density. The only prominent trend in the mapping area extends from the northern edge of T.6N., R.9W. through T.7N., R.9W. and T.8N., R.9W. The area of greater than 80 feet of cumulative porosity thickness covers

approximately 2 square miles in T.7N., R.9W., approximately 14 square miles in T.8N., R.9W. and about 2 square miles in T.8N., R.9W. (Figure 3.36).

A net porosity map was constructed for the combined Lower and Upper Medrano sandstone using the same parameters used to make thickness maps for the individual Lower and Upper sandstone units: ≥ 6% density porosity calculated using 2.68 g/cc grain density. The combined Lower and Upper Medrano cumulative net porosity map (Figure 3.38) exhibits a prominent north-south thickening that extends from T.4N., R.7W., through T.5N., R.8W., T.6N., R.8W. and into T.7N., R.8W. A second trend of thicker cumulative porosity extends from the northeast part of T.6N., R.9W. into T.7N., R.9W. and terminates in T.8N., R.9W. (Figure 3.37). The area of combined Lower and Upper Medrano porosity thickness exceeding 100 feet covers approximately 8.5 square miles in T.4N., R.7W., fifteen (15) square miles in T.6N., R.8W., six (6) square miles in T.6N., R.9W., and eight (8) square miles in T.7N., R.9W. (Figure 3.38).

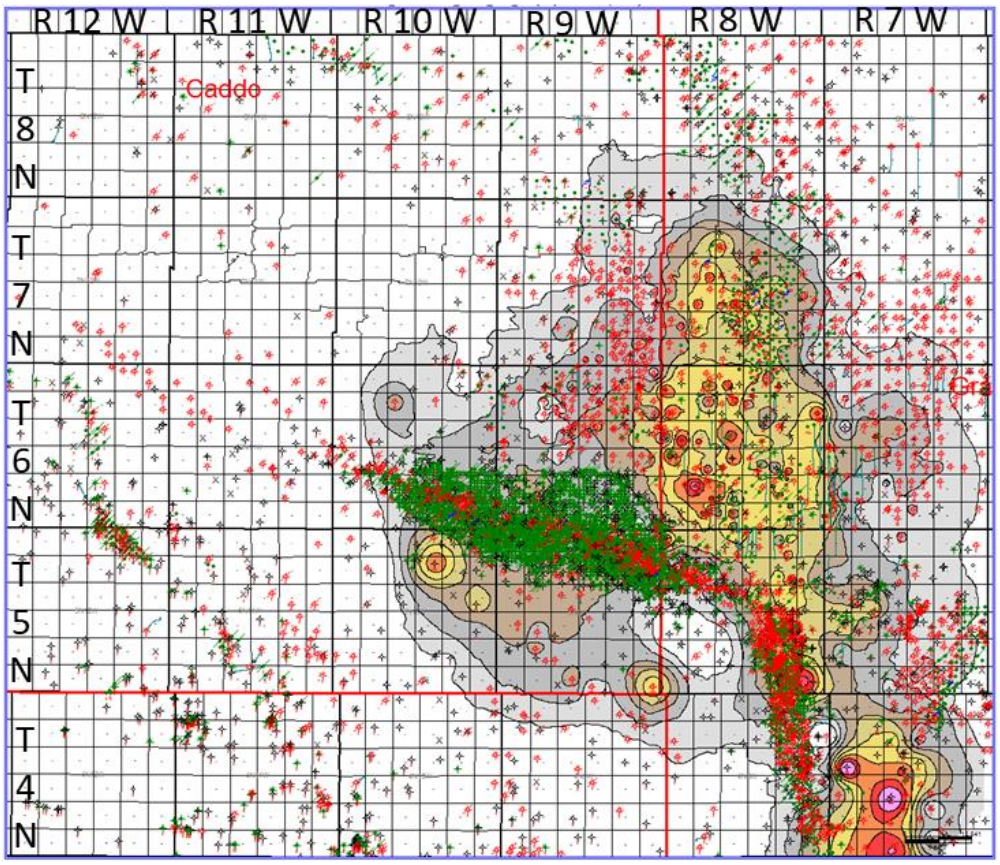

Figure 3.36. Thickness of porosity in the Lower Medrano Sandstone, based on ≥ 6% density porosity (2.68 g/cc grains density). Contour interval is 20 feet with yellow domain representing 80 to 100 feet and orange domain 100 to 120 feet.

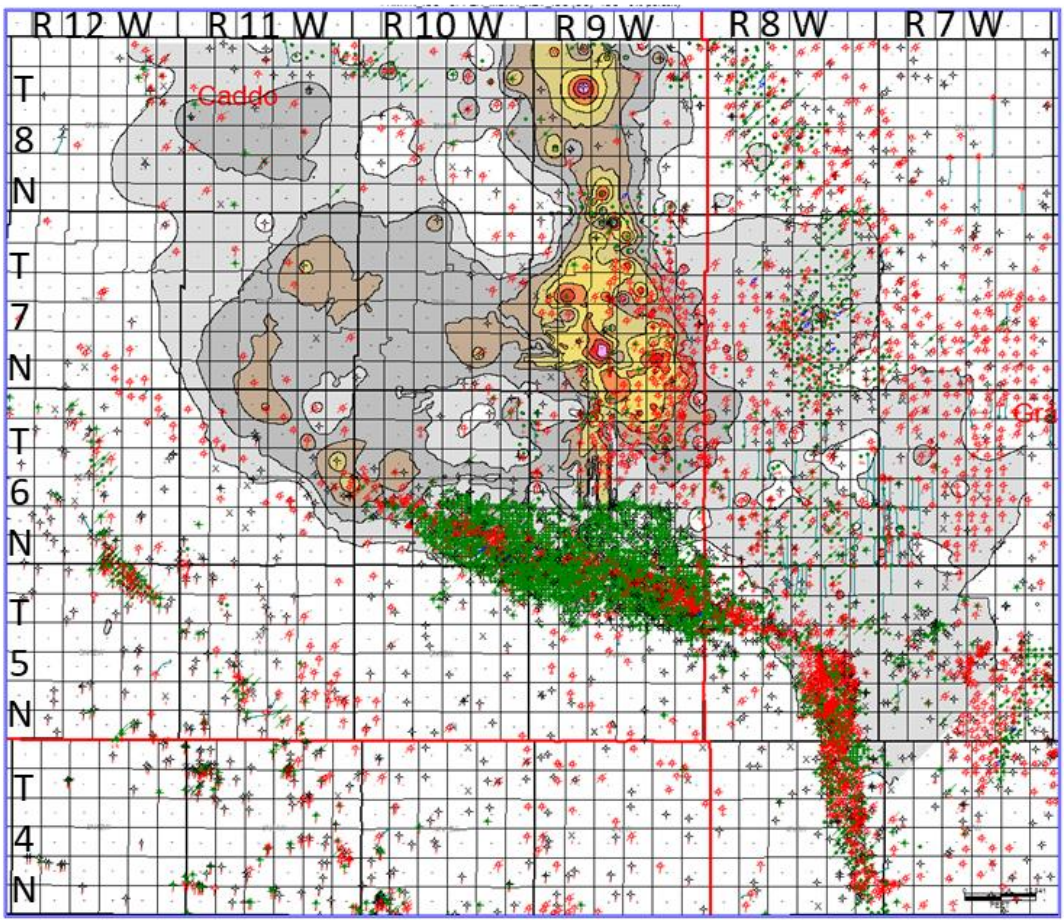

Figure 3.37. Thickness of porosity for combined Lower and Upper Medrano Sandstone, based on ≥ 6% density porosity (2.68 g/cc grain density). Contour interval is 20 feet with yellow domain representing 80 to 100 feet and orange domain 100 to 120 feet. Maximum combined cumulative net porosity thickness is greater than 160 feet in section 27, T.7N., R.9W.

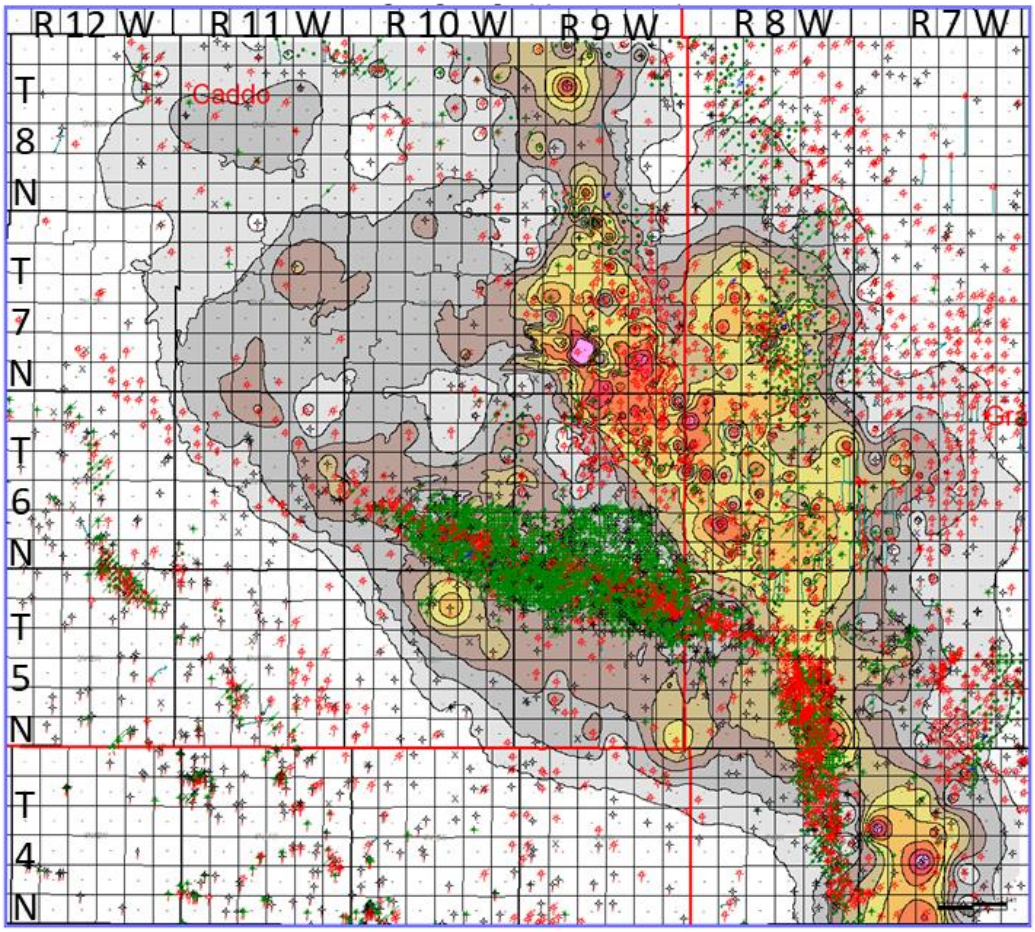

Figure 3.38. Thickness of porosity for combined Lower and Upper Medrano Sandstone, based on ≥ 6% density porosity (2.68 g/cc grain density). Contour interval is 20 feet with yellow domain representing 80 to 100 feet and orange domain 100 to 120 feet. Maximum combined cumulative net porosity thickness is greater than 160 feet in section 27, T.7N., R.9W.

Diagenesis

The Medrano Sandstone underwent multiple episodes of diagenesis that resulted first in a reduction of porosity during burial compaction followed by an episode of porosity enhancement resulting from the dissolution of metastable detrital constituents and finally precipitation of cements, including carbonates and authigenic clays, both of which resulted in a reduction of porosity.

The earliest documented diagenetic product may be calcite cement that precipitated in the bioturbated interval immediately above the Upper Medrano Sandstone in the Schmidt 16 3H core. Calcite cement in the conglomeratic interval of the Upper Medrano Sandstone in the Schmidt core could be early as the zone lacks well developed silica cement, but thin overgrowths occur on a few quartz grains. Based on their scarceness and morphology, these quartz overgrowths could be inherited. The first widespread episode of cementation was silica in the form of syntaxial quartz overgrowths. Silica in solution is generated during compaction as quartz grains contacted each other and dissolution occurred at these contacts. Silica in solution moved into nearby porosity and nucleated on quartz grains generating syntaxial overgrowths. This cement was augmented by silica released along microstylolites. Pseudomatrix formed early as the sandstone compacted, but its temporal relationship with quartz overgrowths is not well defined with the limited number of thin sections. With burial and precipitation of silica cement, primary porosity was reduced to minimal amounts (<1%) as determined by point counting. As a result, visible porosity in the Medrano Sandstone is mostly secondary and the result of dissolution of labile grains including feldspars and sedimentary rock fragments.

Clay minerals occur in the Medrano Sandstone as early detrital grain coating and later authigenic forms that coat grains, bridge pores and partially fill pores. Early grain coating detrital clay is a mixture of illite and chlorite; this early coating was the substrate for later authigenic illite and chlorite. Quartz grains and ooids with detrital grain coatings are common in the Jobe 31-1 (Figures 3.24 and 3.25) and less abundant in the Schmidt 16 3H (Figure 3.35), recognizing the limited sample size. Detrital grain coatings of quartz limited nucleation of silica and formation of syntaxial quartz overgrowth (Figure 3.25).

Authigenic illite occurs as pore bridging (Figure 3.28) and grain coating (Figure 3.24). Enlarged views of ooids shown in Figure 3.26 suggest illite precipitated on the detrital clay substrate, but image quality is poor at high magnification. Authigenic chlorite coats grains, including syntaxial quartz overgrowths (Figure 3.23). Authigenic kaolinite was not recognized

with confidence in thin section, but occurs as partially pore-filling booklets and isolated flakes in SEM image Figure 3.24.

Carbonate cements occur late in the diagenetic history of the Medrano Sandstone. Calcite cement occludes porosity in sandstone with clay-coated grains that limited silica cement (Figure 3.25). Based on the limited sampling and thin sections, dolomite is less prevalent than calcite, but forms areas of cementation that occlude porosity (Figure 3.33) and isolated crystals that partially occlude pores (Figures 3.26, 3.27, 3.28; 3.29).

Calcite cement that appears to predate quartz cement occurs in the Schmidt 16 3H in an interval that lacks detrital clay coatings (Figure 3.38). In other intervals, such as at depth 9,500 feet in the Jobe 31-1, calcite and dolomite appears to replace quartz grains and overgrowths, indicating precipitation of calcite occurred after the main phase of silica cementation (Figure 3.24). Dissolution of quartz and precipitation of carbonates requires alkaline conditions, whereas

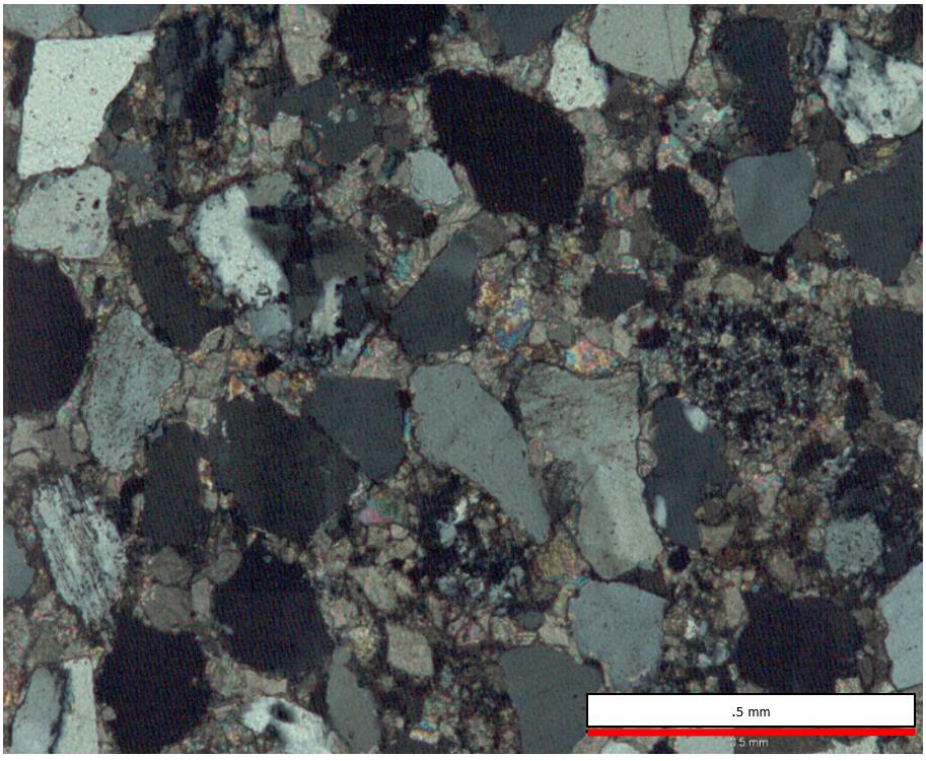

Figure 3.39. Calcite-cemented sandstone with minimal quartz overgrowth or clay-coated grains. Cross-polarized light (CPL). Schmidt 16 3H, depth 9,717 feet. Scale bar is 0.5 mm.

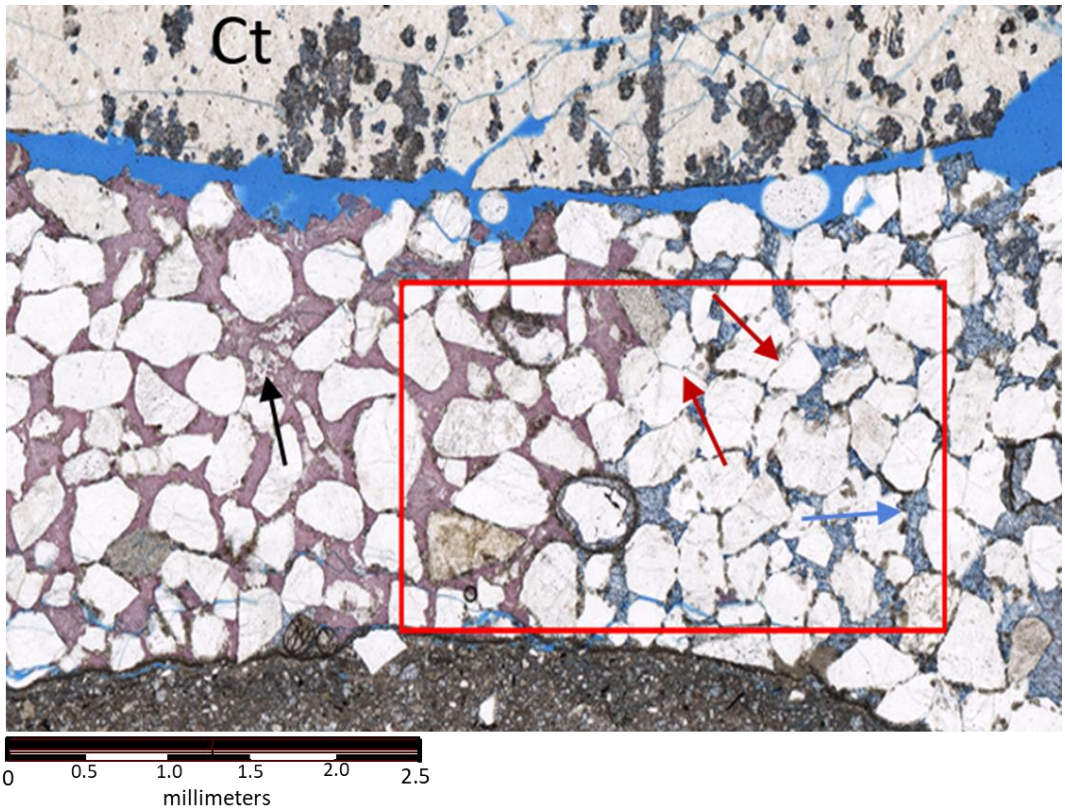

Figure 3.40. Calcite (pink) and dolomite (blue) cement that precipitated after syntaxial quartz overgrowths (red arrows). Quartz grains are irregular and corroded by dolomite (blue arrow) and calcite (black arrow). PPL. Schmidt 16 3H, depth 9,620 feet.

dissolution of feldspar and precipitation of authigenic clay minerals occurs with acidic pore fluids. The change in pore fluid pH from acidic to alkaline can result from introduction of outside fluids or result from the consumption of hydrogen ions (H^+) during dissolution of labile grains such as feldspar. With consumption of H+, pH increases to a point the pore fluid becomes alkaline, favoring dissolution of silica and precipitation of carbonates (Alberta, 1987).

Permeability

Permeability of the Medrano Sandstone was assessed using forty-three (43) NUTECH Log presentations (NUTECH Log) that use conventional data (resistivity, caliper, spontaneous

potential, density and neutron porosity and gamma-ray) obtained from wireline logs, to evaluate multiple rock properties and characterize reservoirs. The newest version of the NUTECH Log presentation consists of 15 tracks (conventional data & NUTECH analysis data) that contain measurements of different parameters necessary to assess properties of the reservoir in question (Figure 3.41). For the purpose of this study, the track indicating permeability (NUPERM) was of primary interest to help identify areas where the Medrano Sandstone contained better quality (higher permeability) reservoir. Representative examples of NUTECH Logs are included, but all NUTECH Logs were utilized to evaluate reservoir quality of the Medrano Sandstone. The NUTECH Log study included calibration of core properties to each associated NUTECH Log, mapping average permeability using values extracted from the 43 wells with NUTECH Logs and comparing structural/stratigraphic relationships of the Medrano Sandstone to mapped permeability.

NUTECH Log analyses demonstrated the high variability in permeability within the Medrano Sandstone reservoir with permeability values ranging from non-existent to >11 millidarcies (mD). The majority of NUTECH logs indicated better reservoir in the Lower Medrano Sandstone interval. A comparison of NUTECH Log analyses for the Jobe 31-1 and Schmidt 16-3H demonstrates the differences in permeability in these respective wells, when porosity values are closer. The average porosity for the Lower Medrano Sandstone in the Jobe 31-1 was 8.6%: the average permeability was .2 md (Figure 3.42). In contrast, the average porosity of the Schmidt 16-3H was 6.2% in the Lower Medrano and < 6% in the Upper Medrano. Average permeability was .021 md in the Lower Medrano interval and non-existent in the Upper Medrano (Figure 3.43). The Schmidt 16-3H has > 200 feet of net sandstone, whereas the Jobe 31-1 has approximately 150 feet of net sandstone, but higher average porosity and permeability.

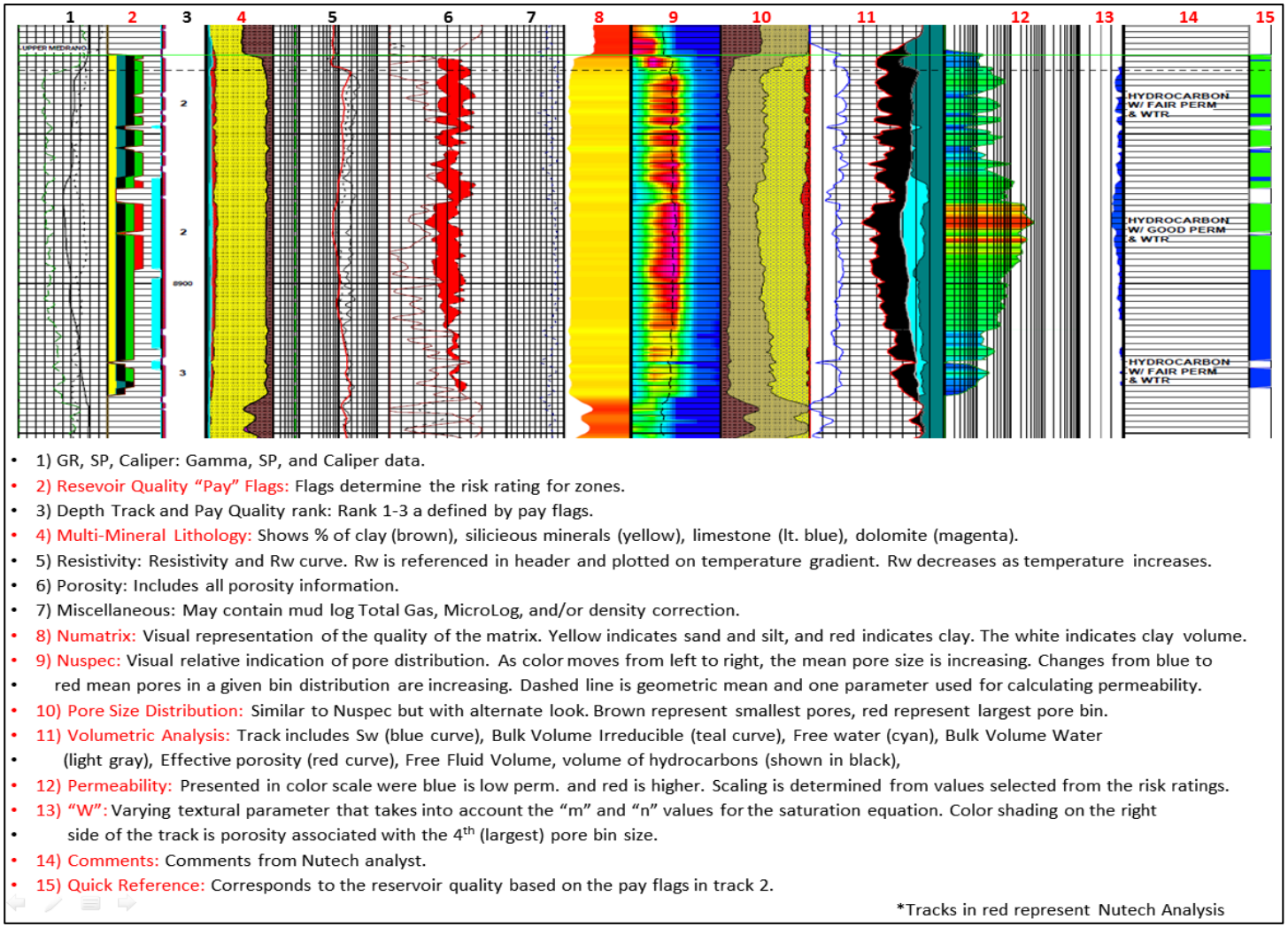

Figure 3.41. Representative NUTECH Log presentation (NUTECH Log) and a description of each of the fifteen (15) tracks that make up the presentation. Parameters highlighted in red are determined from traditional wireline log measurements included in descriptions in black.

Thin section photomicrographs of each core shows the Jobe 31-1 has more intragranular to intergranular porosity due to dissolution of the detrital grains. The Schmidt 16-3H showed dissolution of detrital grains, however the amount of dissolution was much less resulting in roughly 2.4% difference in the measure porosity of the two wells.

A third NUTECH Log from the Dryden-Rider 1 well in section 11, T.5N., R.8W. is shown in Figure 3.43. The Dryden-Rider 1 well has average porosity of close to 8%, peak permeability of 0.2 mD and average permeability of 0.5 mD. According to the NUTECH Log, this sandstone has twenty-seven (27) feet of permeable reservoir (Figure 3.44).

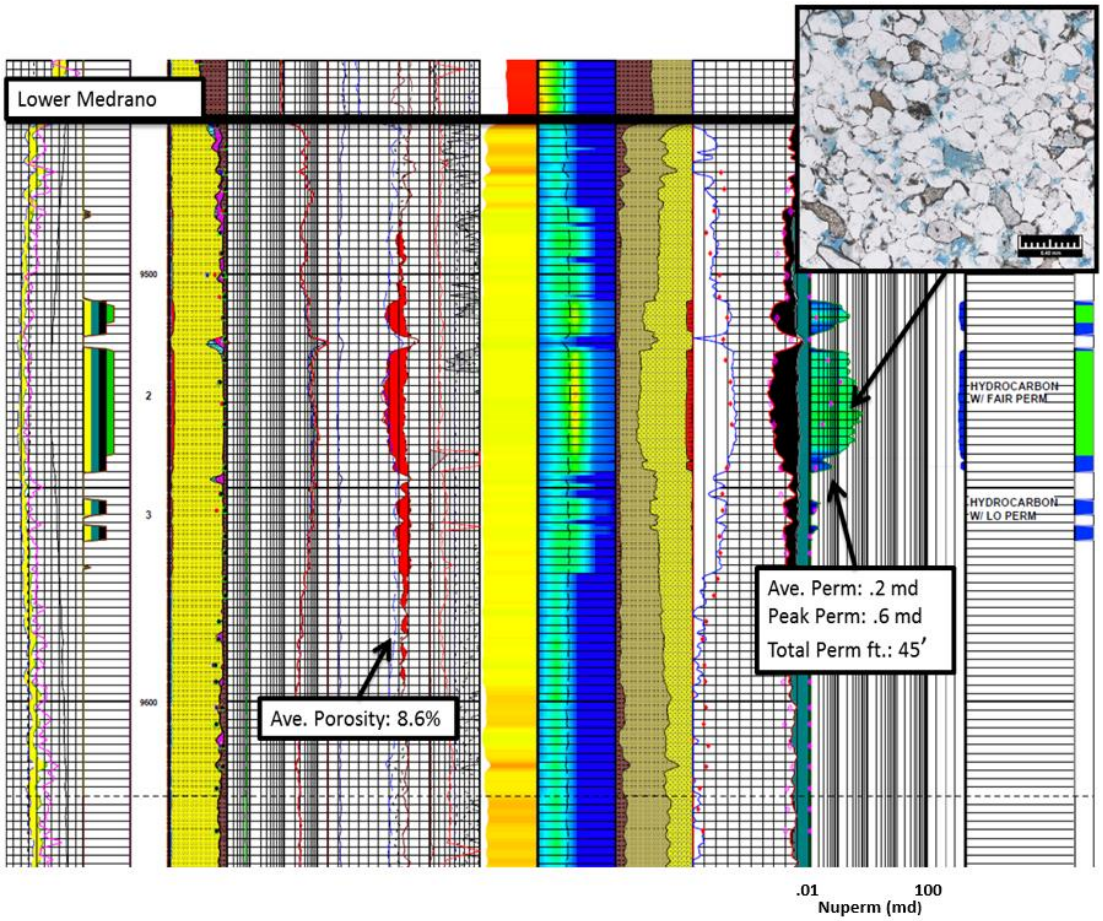

Figure 3.42. Partial NUTECH Log for the Jobe 31-1 cored interval.

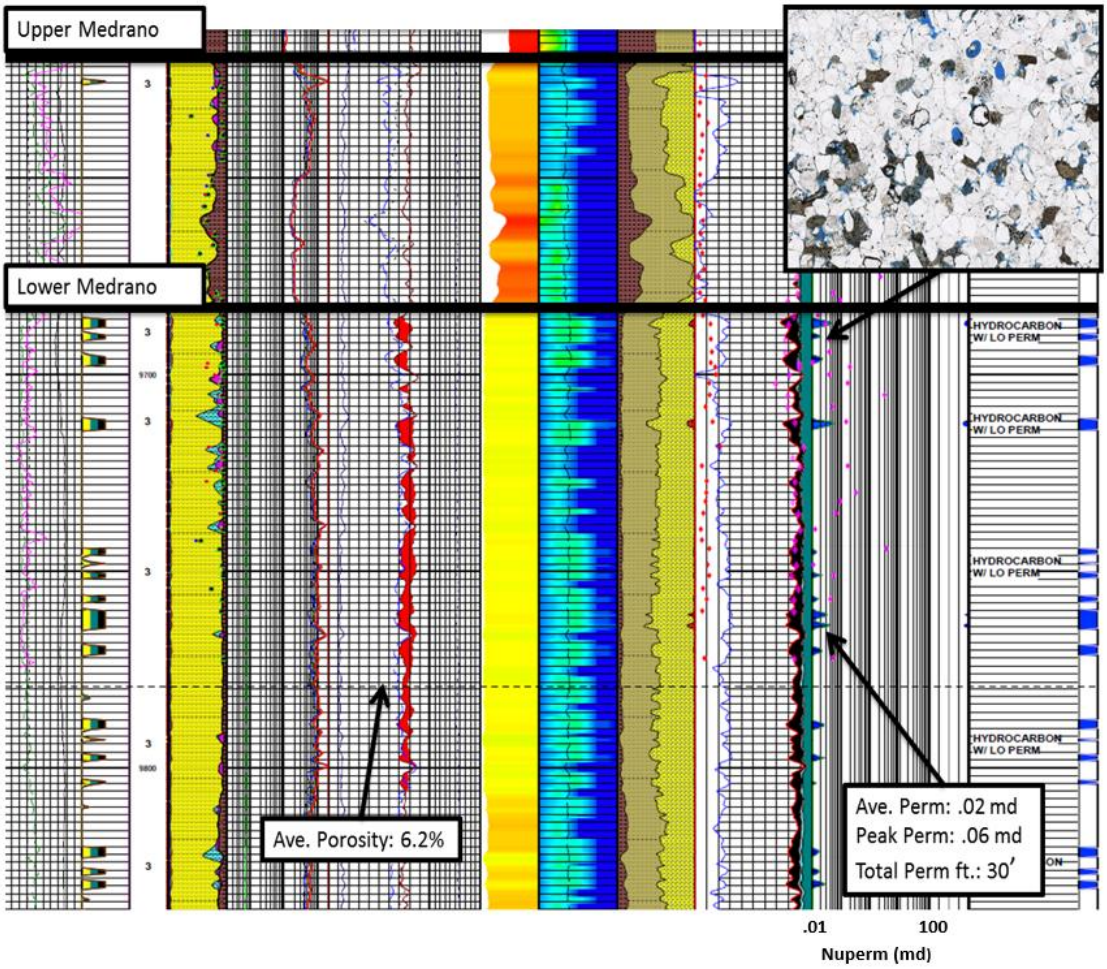

Figure 3.43. Partial NUTECH Log for Schmidt 16 3H. Cored interval 9610 to 9777 feet. Scale bar on inset photomicrograph is 0.4 mm.

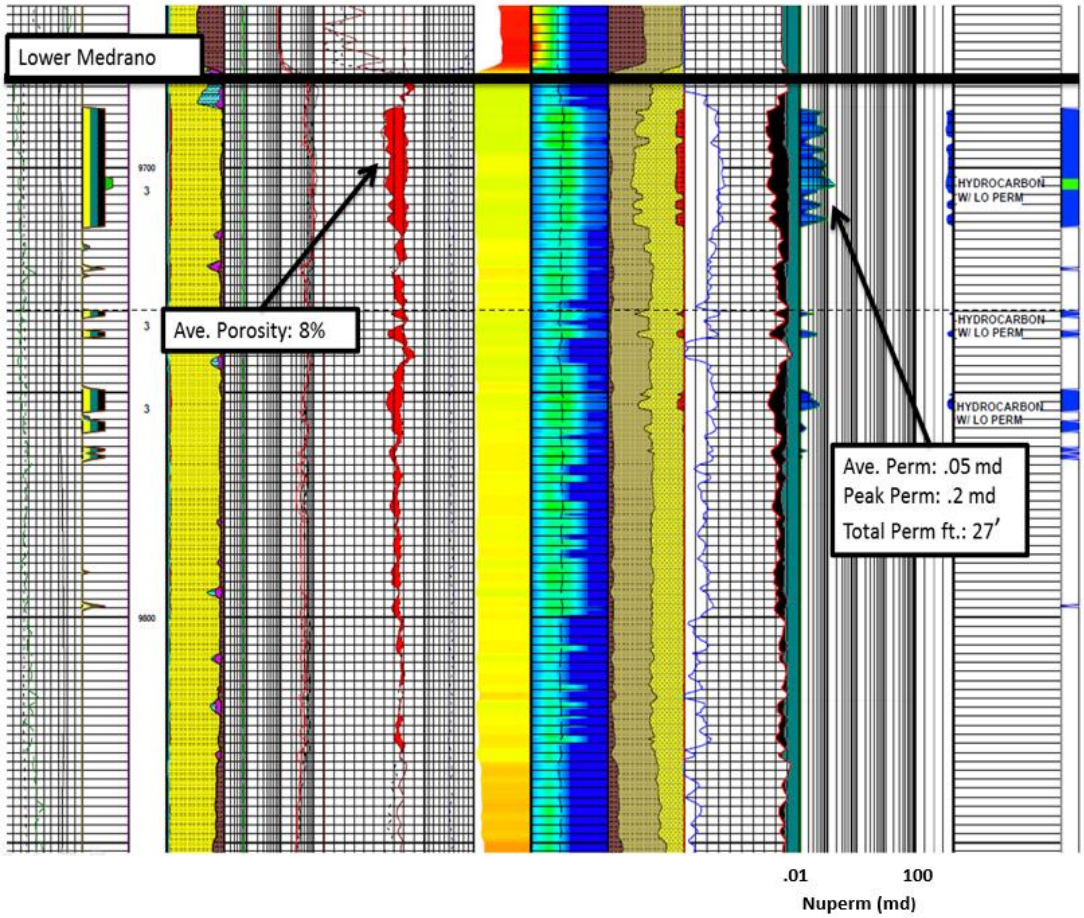

Figure 3.44. Partial NUTECH Log for the Dryden-Rider well in section 11, T.5N., R.8W. This well was not cored.

With respect to the NUTECH logs, reservoir permeability appears to be somewhat linked to porosity. To test the hypothesis that a positive correlation exists between porosity and permeability in the Medrano Sandstone, a cross plot of average permeability against average porosity was constructed (Figure 3. 45). Values for both Lower and Upper Medrano sandstone reservoirs with NUTECH Logs were plotted and the cross plot shows very little correlation between the two parameters. However, if data from the Lower Medrano are separated into a higher permeability domain of > 0.1 millidarcies (mD), a weak positive correlation is evident (Figure 3.45). Porosity averages of the Medrano Sandstone in the available NUTECH Logs ranges from 5-16%, with the average being roughly 8.3%. Permeability averages per well range

from 0 to 2.6 mD, with the average being 0.25 mD. Interesting, the well with the highest average permeability of 2.6 mD, had 9.8% average porosity. In contrast, the well with the highest average porosity of 16%, had an average permeability of 0.09 mD.

Data plotted on the porosity vs. permeability diagram were separated with Lower Medrano data points represented by blue dots, whereas Upper Medrano data are represented by brown triangles. Lower Medrano values tend to have a larger range of both porosity and permeability values with significantly higher upper range porosity values than the Upper Medrano.

A second cross plot of permeability vs. net sandstone or reservoir thickness (Figure 3.46) was generated to test the hypothesis that permeability increases with increasing net sandstone thickness. Values for the Lower Medrano are plotted as blue dots, whereas Upper Medrano data points are brown triangles. Plotted average permeability versus reservoir thickness shows little correlation between these two parameters for either the Lower Medrano or the Upper Medrano. The two higher measured permeability values (> 1 mD) for the Lower Medrano Sandstone occur in reservoir between 50 and 60 feet thick, whereas the two thicker reservoirs (125 – 150 feet thick) have permeability values between 0.2 and 0.7 mD.

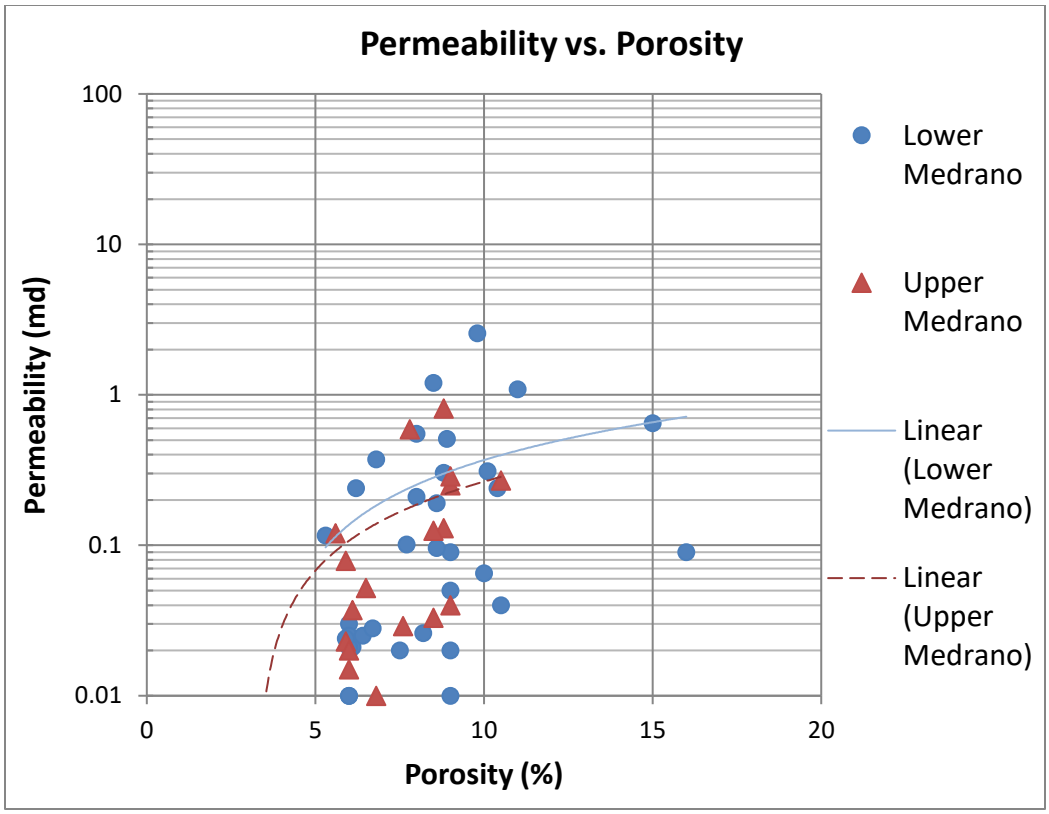

Figure 3.45. Plot of porosity vs permeability for the Lower and Upper Medrano sandstones. A weak positive correlation is evident for the Lower Medrano Sandstone values > 0.1 mD, but computer-generated best-fit line for the Upper Medrano is does not seem to honor data points.

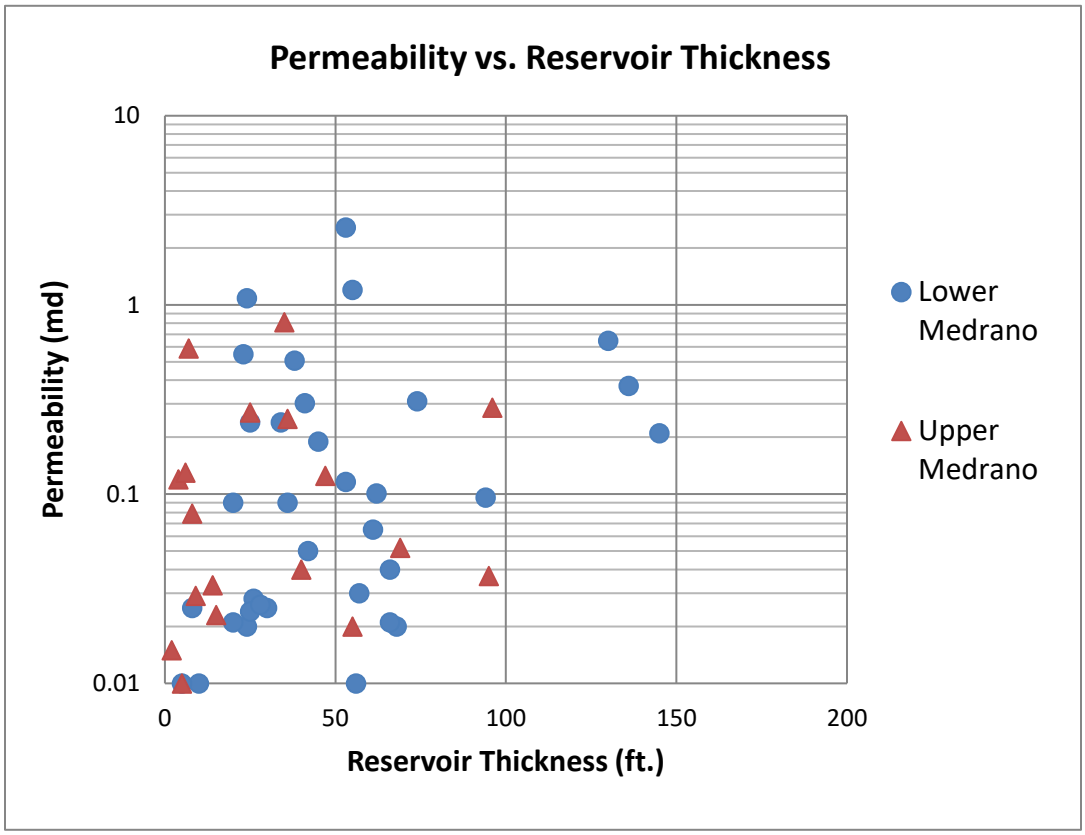

Figure 3.46. Plot of permeability vs reservoir thickness. The scatter of data in this plot indicates no obvious relationship between permeability and reservoir thickness. Permeability data are from minipermeameter.

A reservoir thickness map was constructed using a definition of reservoir as sandstone with ≥6% density porosity and permeability ≥0.1 millidarcies. A permeability cutoff of ≥0.1 millidarcies was used because NUTECH Log determined permeability ≥0.1 mD was defined as “Fair Perm” to “Good Perm” and determined to be “better” quality. This permeability cutoff was used in accordance with the permeability track on NUTECH logs, which determined reservoir intervals ≥0.1 mD correspond to NUTECH Log pay flags. With only 43 NUTECH logs available within the study area, mapping permeability trends with confidence is difficult and contoured trends on permeability thickness maps should be considered speculative.

A bubble map showing average permeability within wells with Nutech logs was created to better show where peak permeability was greatest within the study area. The range for the bubble map was 0-2 mD and the permeability averages were the same averages used for the cross plot of Permeability vs. Porosity (Figure 3.45). The bubble map showed that the greatest average permeability was primarily located in the east-central area of the Medrano Sandstone distribution, which is structurally higher (Figures 3.47; 3.48). However, there are several NUTECH logs for wells in which the Medrano Sandstone is structurally equivalent or lower to these wells in the eastern area that showed greater peak permeability. Wells with greater peak permeability were found closer to the stratigraphic pinch-outs of Medrano sandstone bodies. With this in mind, permeability of the Medrano reservoir may be equally dependent on stratigraphic trapping mechanisms as it is structural trapping mechanisms.

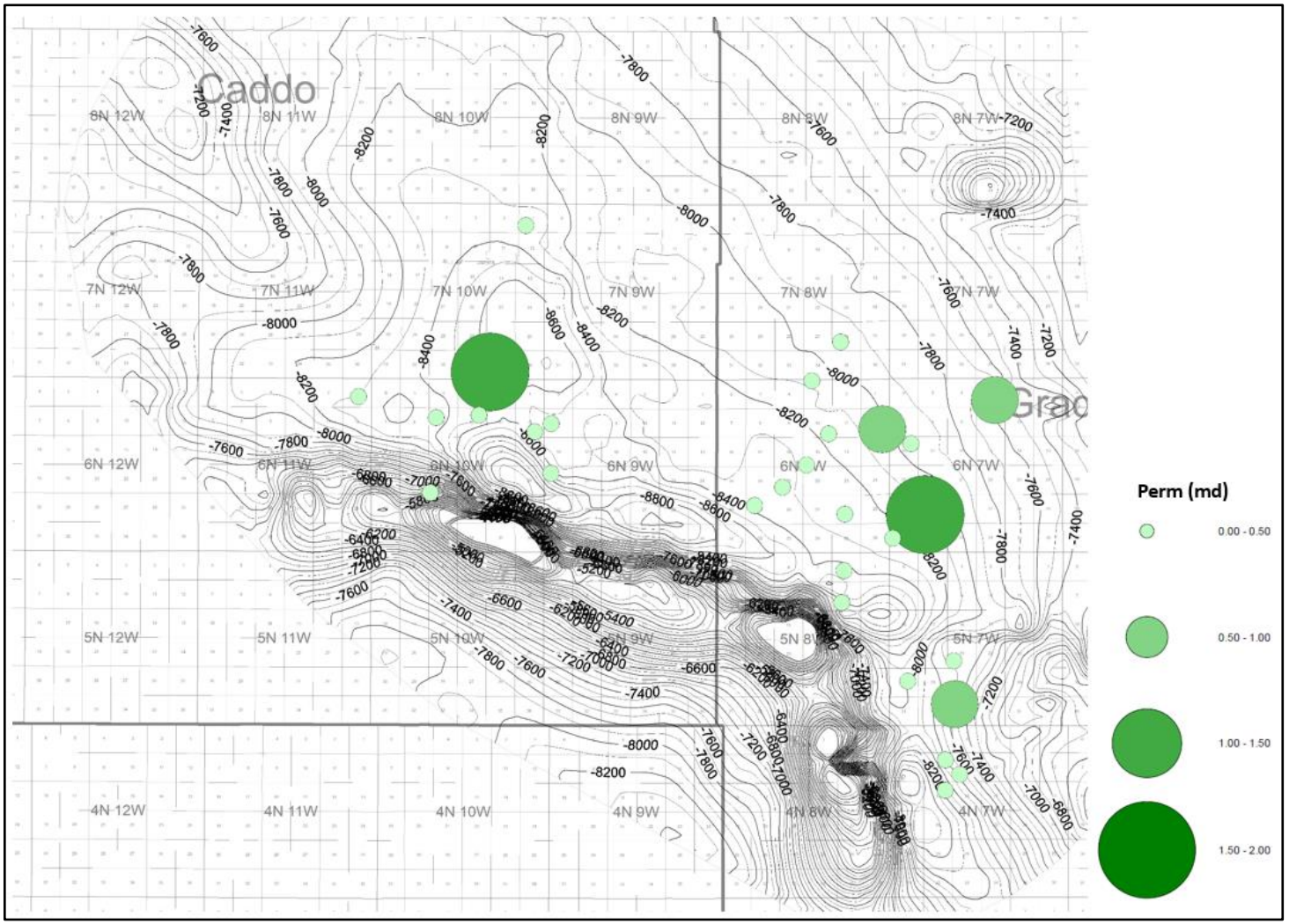

Figure 3.47. Structure map of Medrano Sandstone with Lower Medrano average permeability bubbles.

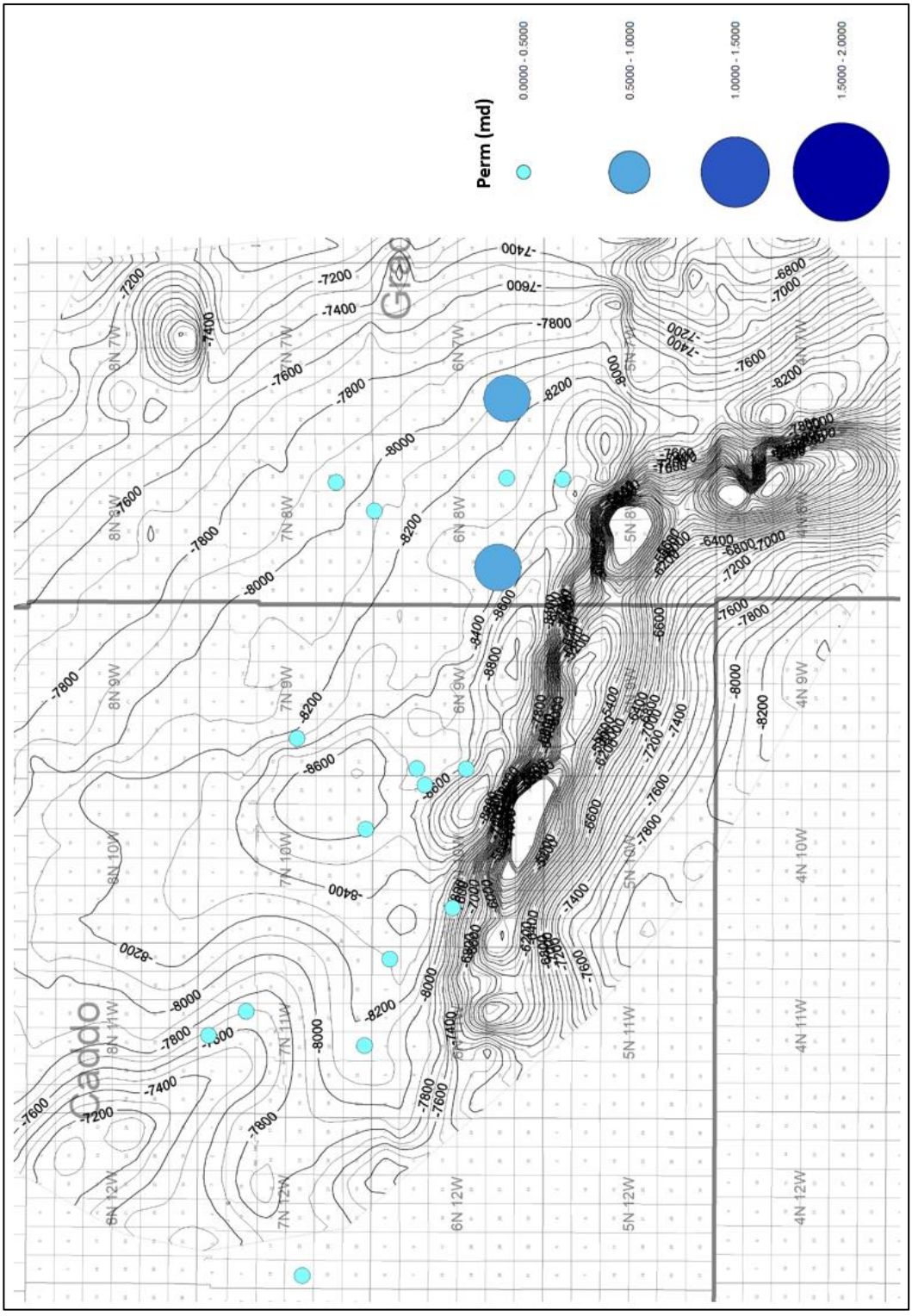

Figure 3.48. Structure map of Medrano Sandstone with Upper Medrano average permeability bubbles.

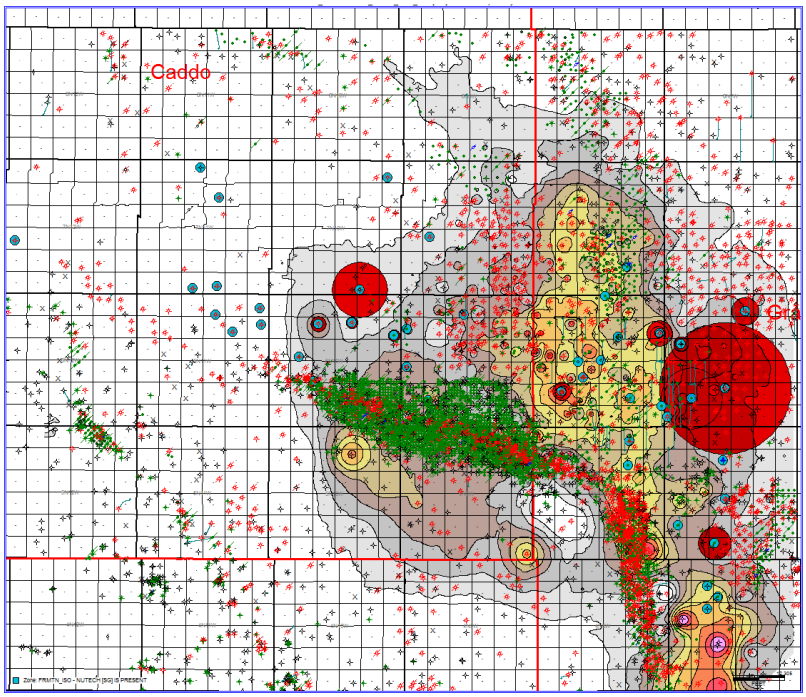

Figure 3.49. Porosity thickness map for the Lower Medrano Sandstone with Lower Medrano average permeability bubbles. See figures 3.47 and 3.48 for bubble scale.

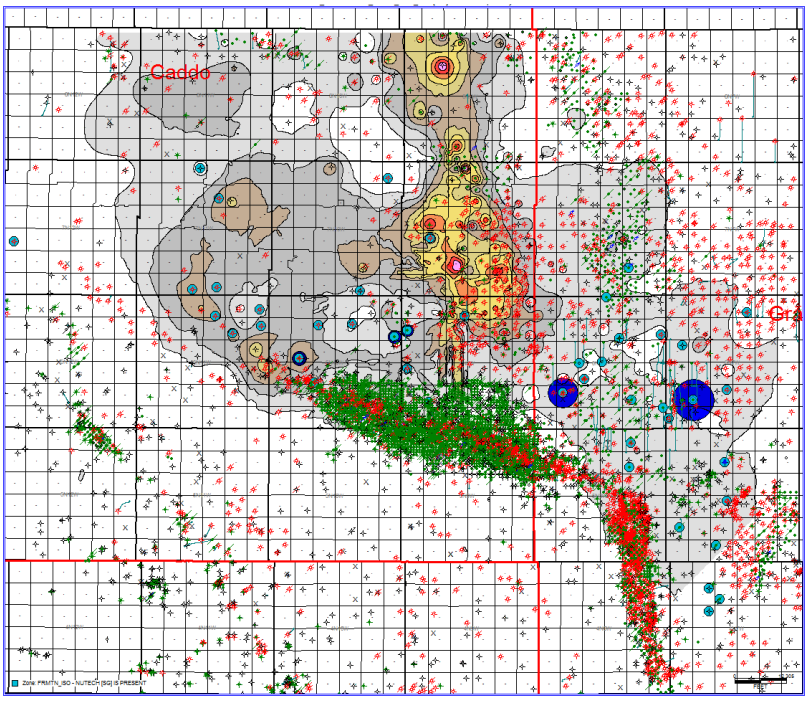

Figure 3.50. Porosity thickness map for the Upper Medrano Sandstone with Upper Medrano average permeability bubbles. See figures 3.47 and 3.48 for bubble scale.

A final map constructed overlapped the electrofacies distribution map with the bubble map of average permeability of the NUTECH logs (Figure 3.52). The map showed high correlations to better reservoirs are in or around the electrofacies of a blocky or FUS signature.

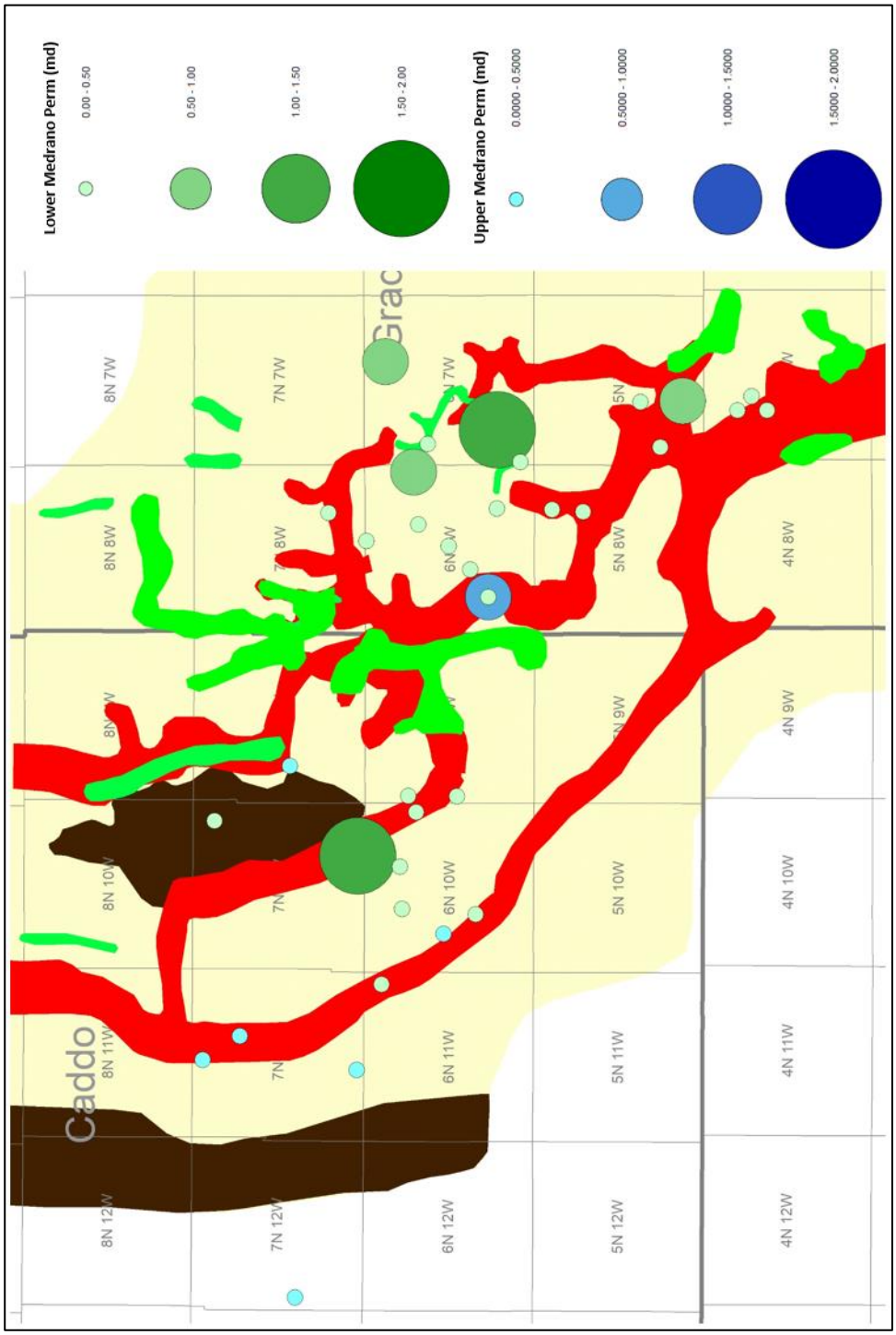

Figure 3.51. Medrano Sandstone electrofacies map with lower and upper Medrano average permeability bubbles.

CHAPTER IV

DISCUSSION AND INTERPRETATION

Using all data and evidence gathered from the gamma-ray log electrofacies signatures, geometry and distribution of the Medrano Sandstone, sedimentary structures found in core, and petrology using thin section samples, the Medrano Sandstone interval appears to represent southeast to northwest progradation, with a possible fluvial system in the southeastern portion of the study area transporting the sediments for a delta complex (Figure 3.37, 3.38; 3.49). Regional distribution of the Medrano sandstone supports a generalized pattern of an elongate delta.

There were multiple gamma-ray electrofacies signatures as well as stacked and hybrid signatures throughout the study area. The dominate gamma-ray electrofacies profile is the coarsening upward signature (CUS) or a funnel shaped wireline log motif. Studies correlating wireline-log signatures to depositional environments (Fisher, 1990; Coleman and Prior, 1982; Brown, 1979; Galloway, 1975) consider the CUS to represent a prograding delta-front environment. Other electrofacies signatures observed include fining upward signatures and cylindrical/blocky signatures. The presence of stacked sequences strengthens the interpretation of a prograding depositional system, and sharp basal contacts between fining-upward motifs and underlying coarsening-upward signatures suggests channels are deposited on older prodelta and delta front sand, silt and muds. Fining-upward signatures in the Upper Medrano interval support the interpretation that fluvial channels and deltaic distributaries extended across the Lower Medrano interval as the system prograded northwesterly into the expanding Anadarko Basin.

By first implementing the 33% or less shale volume estimate modified from the Asquith

and Kyrgowsky (2006) linear gamma-ray response for shale volume estimation, thickness trends of the Medrano sandstones were delineated. Separating the Medrano into individual "Upper" and "Lower" sand intervals shows the growth of these elongate trends through the depositional cycle. The geometry and directional trends of both intervals indicate the source of sediments for the Medrano Sandstone to the southeast and transport toward the Anadarko Basin depocenter. The initial deposition of the Lower Medrano sand was focused in the central area of the study area. The Upper Medrano interval continues this overall trend, but with a slight shift to the northwest due to a lack of accommodation to the southeast where the Lower Medrano accumulated. The deposition of the Medrano was influenced by local bathymetry within the study area. The displayed thin interval trending south to north in the central portion of the study area (Figure 2.6) represents a paleobathymetric high prior to Medrano deposition that reduced accommodation. This paleotopographic high coincides with the no sandstone "No signature" in the north-central portion of the study (T.7N., Rgs. 9 and 10W. and T.8N., Rgs. 9 and 10W.) area seen on the Electrofacies Map (Figure 3.14), as well as the Medrano distribution maps (Figures 3.37; 3.38; 3.49 and 3.50) showing little to no deposition. In contrast, the thicker interval of the Medrano is seen in areas where there was an interpreted paleotopographic low.

The limited core and thin section data do not necessarily support a fluvial-dominated deltaic system. Ooids occur at the very top of the coarsening-upward interval of the Jobe 31-1 at 9500 feet. Furthermore, this interval is burrowed at 9527 feet and below. The fining-upward section above 9496 feet is not so much a change in detrital quartz grain size as it is increasing clay laminae. These thin clay-rich (shale) partings are detected by the gamma-ray tool and give this section a slightly more radiogenic character. Bedding is distorted by soft-sediment deformation common to deposition in a subaqueous environment. The persistent thin and dark clay-rich partings indicate a dependable supply of mud for this sand-rich environment.

Continuous and connected channel systems with well-defined fining-upward signatures associated with fluvial channels are not common in either the Lower or Upper Medrano intervals.

Short sections of channel-filling style log motifs or electrofacies are mapped, but the cylindrical or blocky patterns are more abundant and trend subparallel to the inferred direction of transport. If these blocky/cylindrical log motif trends represent channel-mouth bars or deposits within tidal channels, the Medrano system is likely a wave to tide-dominated delta.

The dominance of the cleaning-upward signature across the mapped area is evidence that wave action or tidal flow were significant forces in shaping Medrano sand deposits. Core data are limited for the Medrano Sandstone, but evidence of cross stratification, winnowing of clay, decreasing bioturbation and bidirectional cross stratification in the upper portion of cored coarsening-upward intervals support wave and tidal processes. Integrating mapped sandstone distribution, inferred geometries of sandstone bodies from wireline logs and biogenic and sedimentary features in the two available cores support a tentative interpretation of the Medrano Sandstone as a northerly prograding, wave- or tide-dominated deltaic complex.

Chert conglomerate at the top of the Upper Medrano sandstone interval in the Schmidt 16 3H represents a higher-energy event interpreted as a storm deposit or wave ravinement surface. This storm may have occurred in the Ouachita Orogen and transported chert pebbles from the highland into the fluvial system that sourced the Medrano delta. The presence of detached mud drapes and rip up clasts suggests higher energy events were common during Medrano deposition. On the other hand, the highly burrowed intervals in the lower section of the coarsening-upward intervals, in the shale and silty sandstone section that separates the Upper and Lower Medrano sandstone bodies and the Upper Medrano Sandstone indicate that quiet water and a stable substrate that supported a healthy biota were common.

The inclusion of ooid grains, where the nucleus of the ooid was quartz grains, found in a number of thin section samples indicate wave action was common during deposition of the Medrano sands. However, it has been suggested by Seale (1982) that the ooid grains originally formed east of the study area as part of the Belle City Limestone (carbonate shelf equivalent of the Medrano) and were transported into the study area. Bryozoan and crinoid fragments in the

Schmidt 16 3H indicate close proximity to a shallow-water setting where normal marine fauna flourished (Scholle and Ulmer-Scholle, 2003). Siderite nodules are not an indicator of depositional environments because of the multiple environments that precipitate siderite. However, being more common in the finer grained shales and silts point to siderite precipitation occurring in a post-oxic prodelta environment with low concentrations of organic matter and low sedimentation rates (Stonecipher, 1999). The abundance of subrounded quartz grains and the lack of Wichita-Amarillo granitic material in the thin sections support a more distal Ouachita Mountains source for Medrano sediments, whereas a more proximal source is not supported. Based on the current evidence, the Ouachita Mountains are considered to be the main source for the Medrano detrital grains.

Depositional Model

The integration of all data provided for the project allow inferences regarding the depositional processes operating during Medrano time. As previously mentioned, the Medrano Sandstone consists primarily of cleaning-upward sandstone that is burrowed and contains occasional other marine indicators such as ooid and normal marine bioclasts. Based on the limited thin section data, bioclasts are not adequately abundant to classify these cleaning-upward sandstones as shoreface. In addition, bi-direction cross stratification is observed in both cores, suggesting tidal ebb and flow. In some sections of the core, soft-sediment deformation masks apparent indication of tidal ebb and flow, whereas others are distinct and easily recognized. Tidal laminates are not observed in these sandstones, but burrowing is pervasive in the quieter-water sections and varies in intensity.

The Medrano interval exhibits characteristics of a prograding delta, but seems to lack a well developed fluvial or distributary channel system. Without core through rock exhibiting the cylindrical/blocky log motif and the best example of a fining-upward interval, any interpretation of the Medrano Sandstone system will remain tentative and subject to modification as additional data become available. The depositional environment is interpreted as a prograding deltaic

system, with significant tidal influence. Other environments considered for the Medrano consisted of nearshore marine environment such as longshore bar and barrier bar, but these were not supported by data. Significant consideration was given to a beach/shoreface environment, but the lack of skeletal fragments was not supportive. The lower section of the Medrano Sandstone in both cores was dominated by black to dark gray interbedded shale and siltstone laminae and bioturbation that occurred in a marine environments where strong wave, current, and tidal energy was negligible.

The geometry inferred from gamma-ray signatures was that of a coarsening-upward sequence (funnel shaped), which is interpreted as a delta-front deposit where the advancing sands from the delta are deposited on top of the prodelta silt and mud. Examined wireline logs showed a sharp shale contact on top of the Lower and/or Upper Medrano sandstone (where present) or a stacked sequence with a fining-upward motif in sharp contact with the coarsening-upward motif below. The abrupt contact with the overlying shale on numerous well logs was interpreted as a transgressive event that took place after the deposition of the Lower Medrano sand. Blocky (cylindrical) gamma-ray signatures were interpreted as distributary channel mouth bars or accumulations in tidal channels (Figure 4.1). The distribution of the combined Lower and Upper Medrano electrofacies summarizes the Medrano distribution pattern and illustrates some of the issues posed in the discussion.

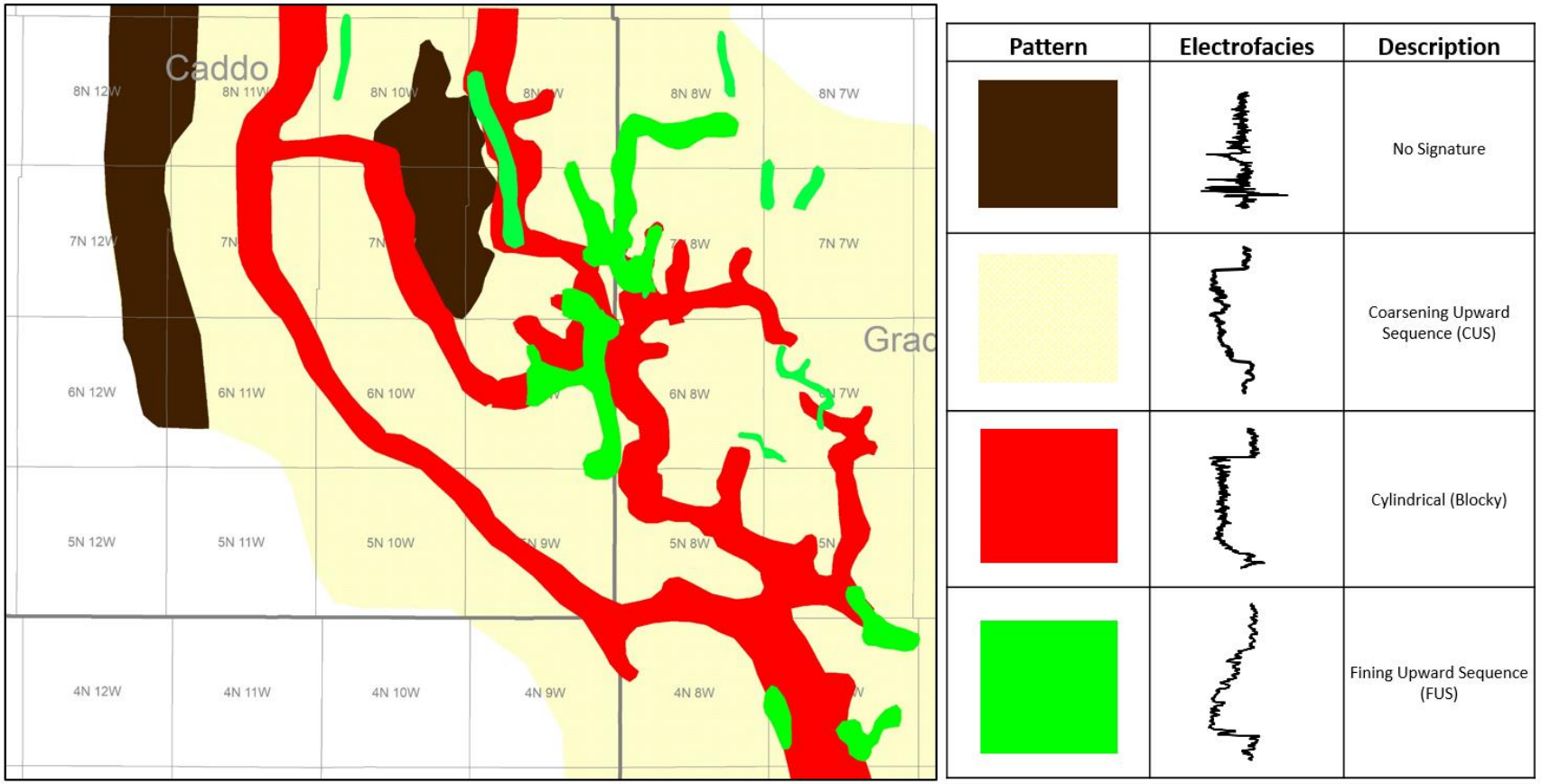

Figure 4.1. Schematic representations of various electrofacies found throughout study area within the Medrano sandstone interval. The depositional relationship between the Lower Medrano and Upper Medrano sandstones is shown in Figure 4.2.

The abundance of subrounded quartz grains and the absence of distinct detrital grains such as metamorphic rock fragments associated with the Appalachian source and granitic rock fragments associated with the Wichitan source, gives insight to the source of detrital grains and the length and/or temporal duration of their transport. Preliminary data for another Hoxbar Group sandstone, the Marchand Sandstone (unpublished data, 2020) supports an ultimate Appalachian source for detrital quartz and zircon. Metamorphics are not observed in this sandstone and it is hypothesized that the quartz and zircon were likely recycled following their deposition in and subsequent liberation by erosion of Ouachita strata. This episode of deposition and erosion provided the time and environment for chemical dissolution of metamorphic detrital grains, resulting in a quartz-rich sandstone with minor feldspar or chert. Storms transported chert pebbles from the Ouachita highlands toward the depocenter, whereas normal flow did not. The lack of granitic fragments in thin section samples does not support a proposed secondary source from the Wichita-Amarillo Uplift to the south.

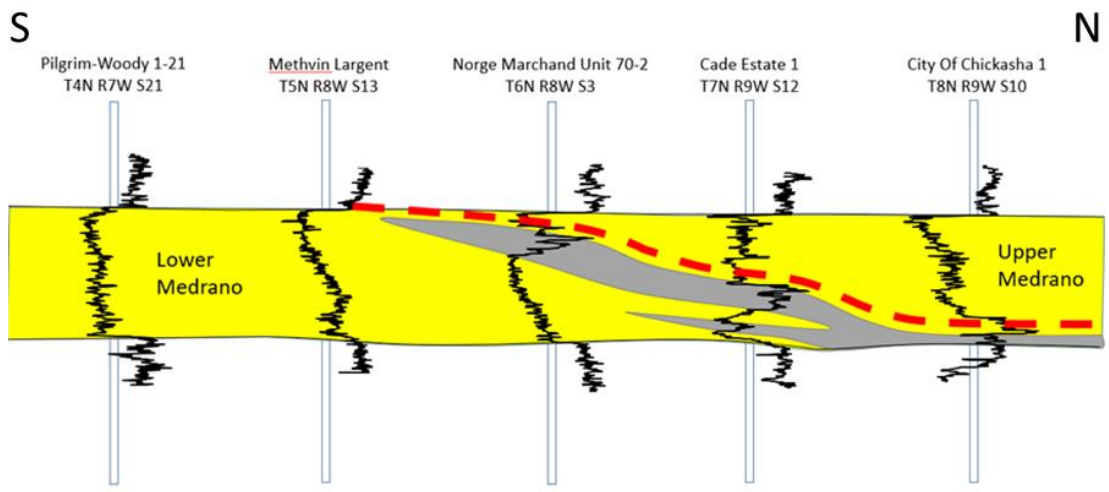

Figure 4.2. Schematic showing depositional relationship between Lower and Upper Medrano sandstone bodies.

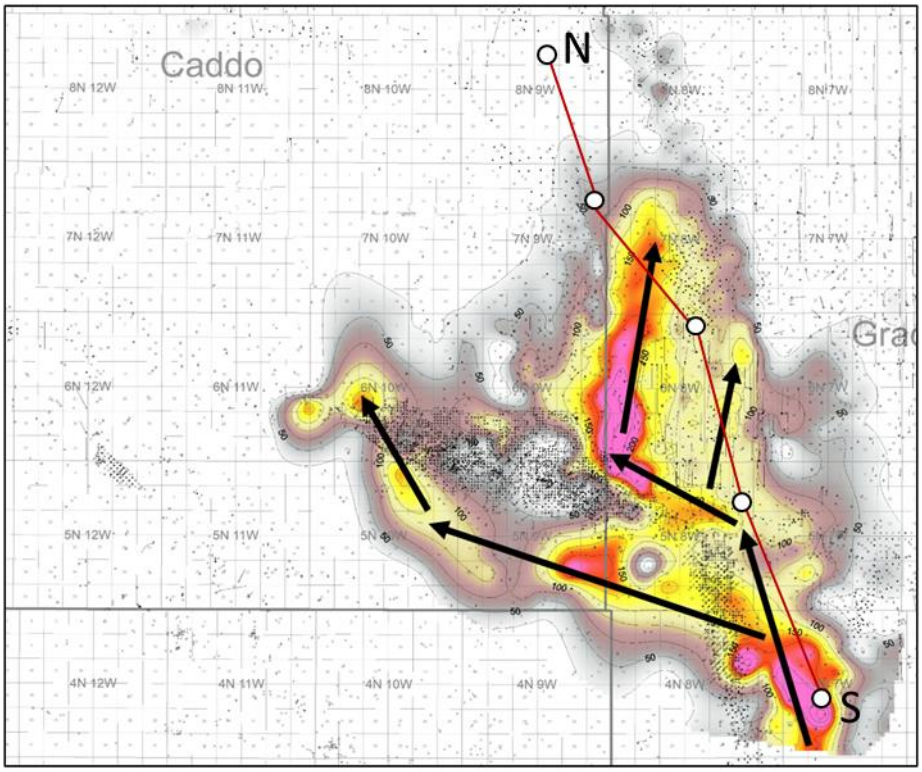

Figure 4.3. Thickness map of Lower Medrano Sandstone (≥67% sandstone) showing proposed direction of sediment transport. Cross section N-S is Figure 4.2.

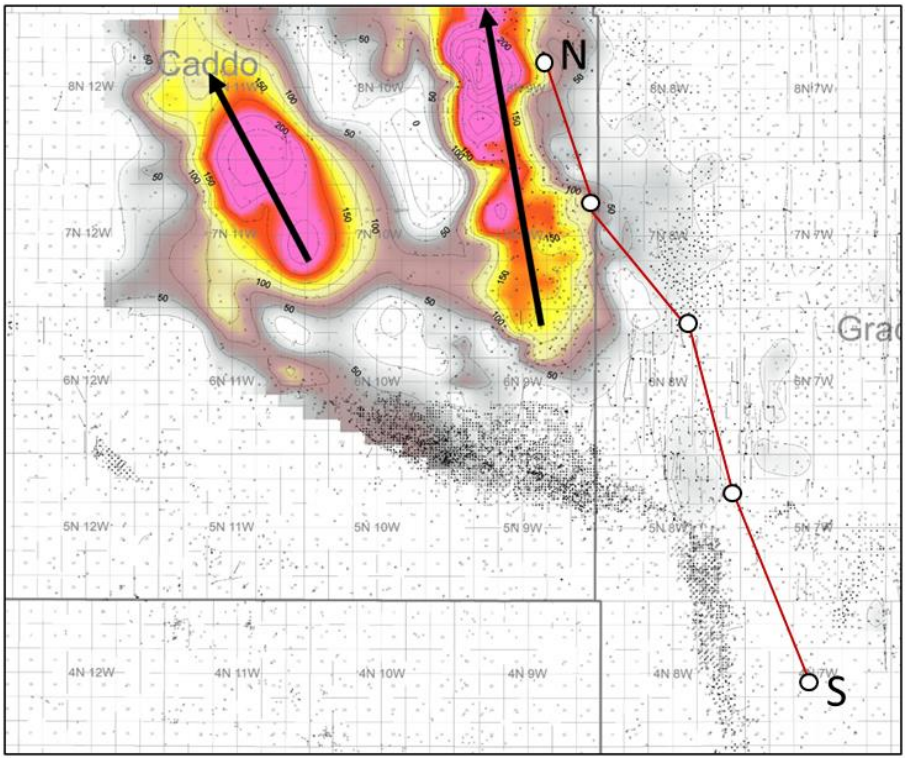

Figure 4.4. Thickness of net Upper Medrano Sandstone using a sandstone cutoff of (≥67% sandstone) showing proposed direction of sediment transport. Cross section N-S is Figure 4.2.

A second hypothesis is that constant reworking in a tidal environment allowed the chemical weathering of most labile grains, resultling in quartz-rich sand. The Medrano Sandstone has depositional features and distribution patterns that suggest a tide-dominated deltaic setting (Goodbred and Yoshiki, 2011; Dalrymple et al., 2003). Modern analogs considered for the depositional environment include the Ganges-Brahmaputra delta. Similarities are seen where macrotidal currents are major drivers in shaping the deltaic deposits into elongate sand bodies. The tide dominated portion of the Brahmaputra delta contains sand bodies that extend several miles (Figure 4.5), much like the distribution of Medrano sand bodies that are interpreted as tidal bars and tidal shoals. A high tidal range in the Bay of Bengal (>10 ft) results in strong tidal currents, which have fashioned a network of interconnecting channels, many of which exceed 100 feet in depth (Figure 4.5). Laterally continous sand bodies are not typical in this type of delta, and the continuity of the sands seen in the Medrano reflect this type of depositional process. Other modern tide-dominated deltas included the Fly River delta and the Indus River delta, both of which exhibit depositional characteristics similar to the Medrano in that these deltas consists of elongate fingerlike protrusions of sands and isolated sand bodies lying seaward of the shoreline (Figure 4.6) witih minimal preservation of fluvial deposits.

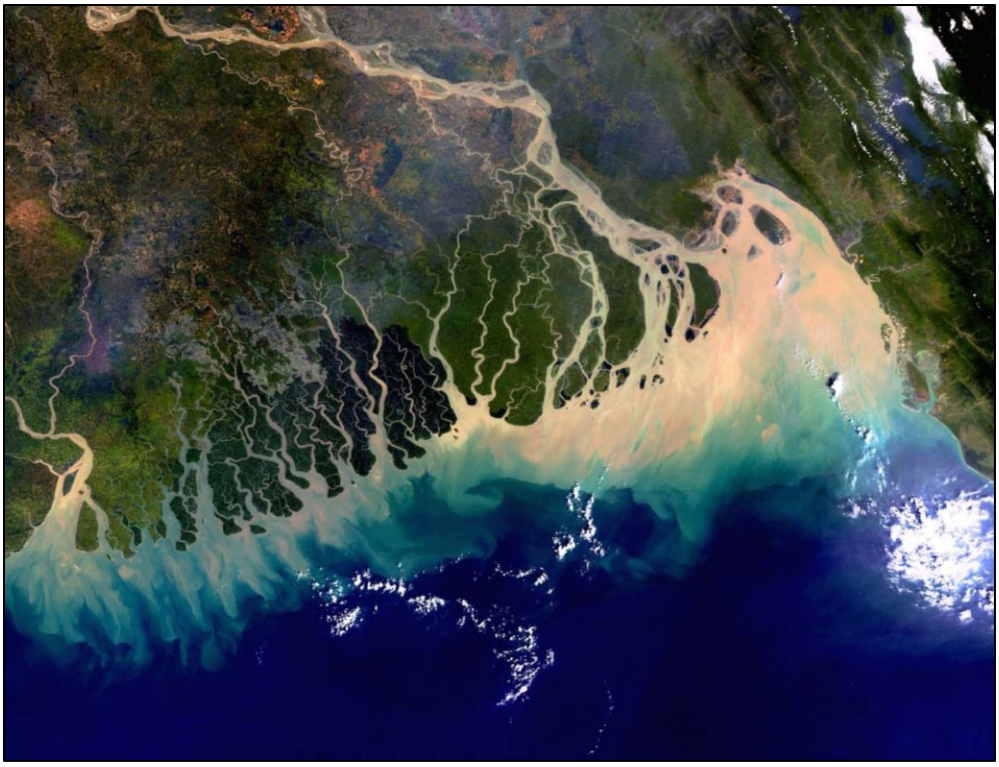

Figure 4.5 Satellite image of the Bay of Bengal showing elongate sand bodies off the shoreface of the Brahmaputra delta.

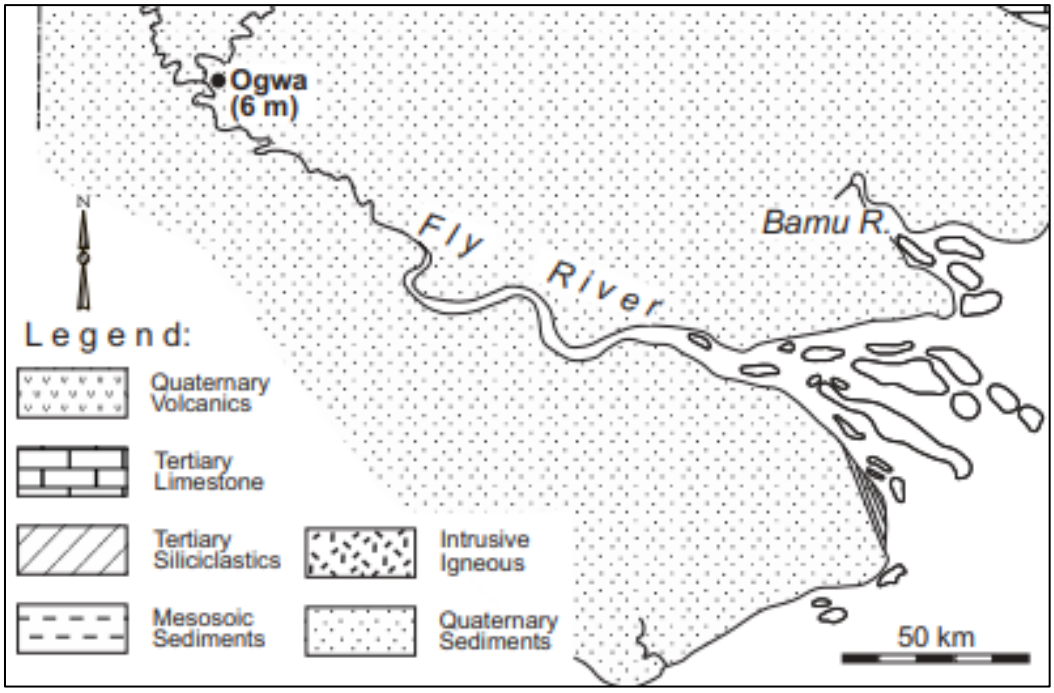

Figure 4.6. Fly River delta schematic depicting tide-dominated elongate bodies seaward of river mouth (Dalrymple et al., 2003).

Sequence Stratigraphy

To better understand depositional processes, the Medrano interval and adjacent stratigraphic intervals were interpreted in a sequence stratigraphic framework. An ideal vertical succession of facies is representative of one complete rise and fall of sea level. Calibrating core data from the Schmidt 16 3H and Jobe 31-1 wells to their associated wireline logs was the first step in defining sequences. The next step was extrapolation using existing wireline logs within the study area to expand the stratigraphic framework. The gamma-ray curve was used in conjunction with the resistivity curve to provide the most accurate lithostratigraphic interpretation.

Prior to Medrano deposition, the area experienced a period of relatively low sea-level associated with deposition of the Hedlund Sandstone. Immediately following Hedlund deposition, flooding occurred and a transgressive-systems tract (TST) developed and relatively radiogenic (marine) shale formed that has an average gamma-ray value > 100 API units. With continued transgression, a maximum flooding (MFS) and condensed section (CS) formed (Figure 4.7). These occur within the shale-dominated interval and set the stage for the following highstand systems tract (HST) by providing accommodation for deposition of Lower Medrano sediments. During the relatively stable sea level of the highstand systems tract, the Lower Medrano sediment dispersal system prograded northward and filled accommodation. The highstand systems tract terminated with the shallowest water section in the coarsening-upward sandstone. Neither core shows evidence of a marked decline in sea level in this part of the basin, so it is believed that sediment supply slowed as subsidence continued and the Lower Medrano coarsening-upward sandstone was flooded and covered with the highly burrowed silt and mud that formed the shale that separates the lower and upper Medrano intervals. Subsidence slowed and/or sediment supply increased and Upper Medrano sediments were transported across the Lower Medrano coastal plain and deposited to the northwest as a lowstand clastic wedge. This lowstand event culminates with the deposition of the Upper Medrano chert conglomerate.

Widespread flooding associated with the Wade interval transgression inundated the Upper Medrano surface. Conglomerate and bioclasts at the top of the Medrano sandstone could represent coarser material deposited along the wave ravinement surface. As transgression progressed, water deepened and deposited marine mud with similar gamma-ray signature as the TST shale at the base of the Medrano interval. The shale section at the base of the Wade interval likely contains the maximum flooding surface (MFS) and is succeeded by a highstand systems tract which is marked by the progradation of the Wade Sandstone coarsening-upward sandstone (Figure 4.7).

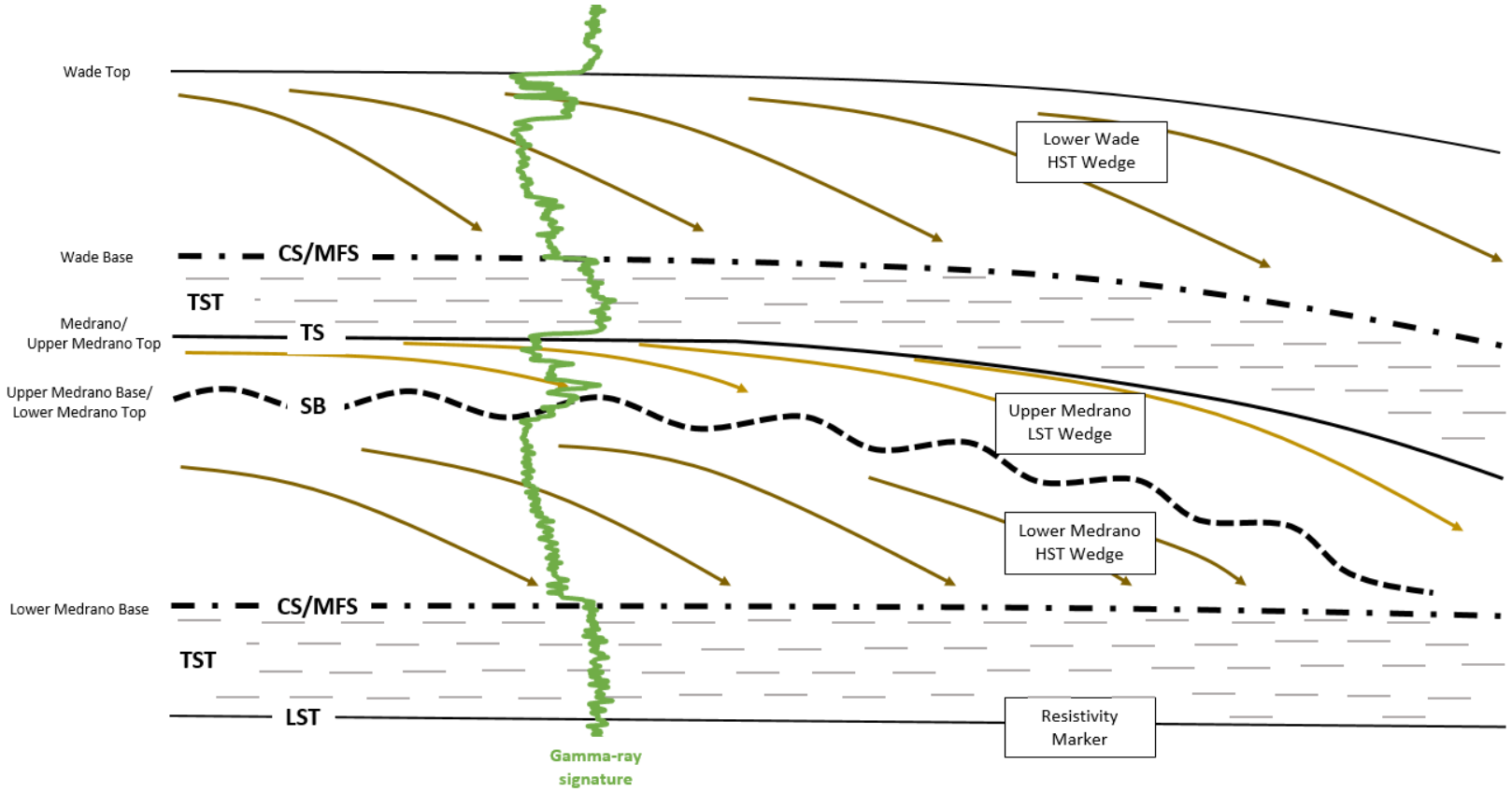

Figure 4.7. Sequence Stratigraphy diagram of the Medrano sandstone with superimposed Gamma-ray signature.

CHAPTER V

CONCLUSIONS

An objective of this research was to establish the depositional environment for the Medrano Sandstone and determine if better reservoir properties were linked to specific depositional facies. Abundant wireline log data allowed for the mapping of generalized electrofacies, but a lack of rock data hampered efforts to establish a link between specific depositional facies and reservoir quality, and construct a depositional model. The conclusions listed below reflect the findings based on data currently available and it is hoped that these conclusions will be supproted, refined or modified if more data become available. As of the completion of this work on the Medrano Sandstone, the following conclusions are proposed to address the depositional processes, diagenesis and reservoir properties.

1. Cored Medrano Sandstone contains sedimentary and biogenic features characteristic of marginal marine settings as well as ooids and normal marine bioclasts in selected samples.

2. Core calibrated electrofacies are limited to cleaning/coarsening upward intervals, a subtle fining-upward interval and several mudrock (shale and siltstone) intervals, which contain indicators of shallow marine or marginal marine environments including fossils and bioturbation.

3. Detrital composition of Medrano sandstone samples is mostly quartz arenite and litharenite, whereas conglomerate near the top of the Upper Medrano Sandstone is chert litharenite.

4. Sandstone distribution patterns trend south-southeast to north-northwest with the Lower Medrano Sandstone accumulating in the southern part of the study area and the Upper

Medrano Sandstone accumulating in the southern part of the study are and the Upper Medrano Sandstone accumulating in the northern part.

5. The distribution pattern of electrofacies for both the Lower and Upper Medrano sandstones is interpreted as an elongate prograding deltaic complex, but it should be noted that core were not available in the more distinct fining-upward sandstone or the cylindrical/blocky sandstone motifs that represent “channel like” distribution patterns.

6. It is proposed that Medrano sandstone was deposited in a northerly prograding deltaic complex that was tidal-dominated.

7. Lower Medrano deposition filled accommodation in the southern part of the study area and forced Upper Medrano deposition to the northwest toward the basin axis.

8. The proposed source for detrital grains in the Medrano Sandstone is the Ouachita Mountains, a conclusion based on composition of the Medrano Sandstone being dominantly quartz with minor amounts of feldspar and chert, the absence of metamorphic rock fragments and Wichitan granitic rock fragments and the occurrence of chert pebble conglomerate in the Upper Medrano Sandstone.

. 9. The dominant porosity type in the Medrano Sandstone is secondary resulting from the dissolution of feldspar and chert, whereas primary porosity occurs only in trace amounts as a result of burial, compaction and cementation.

10. Porosity is limited in the Medrano Sandstone as a result of removal of labile grains during sediment recycling or reworking in the tide-dominated system. Removal of these metastable grains prior to deposition eliminated their potential for dissolution to form secondary pores during burial.

11. Permeabiltiy ranged from non existent to 11 millidarcies and exhibited no apparent correlation to porosity except a weak correlation when porosity values exceeded 8%.

12. Higher permeability reservoirs in the Medrano Sandstone as determined by NUTECH are associated with cylindrical/blocky and fining-upward log motifs, but this pattern was not

consistent across the area and a number of wells with those motifs contain low permeability sandstone.

13. Other higher permeability reservoirs were linked to stratigraphic and structural features seen within the Medrano deposition.

REFERENCES

Adler, F.J., 1971 “Petroleum Potential of the Anardarko Basin and Central Okalhoma Area”. American Association of Petroleum Geologists Memoir 15, Vol. 2. p. 1061-1072.

Alberta, P. L., 1987, Depositional facies analysis and porosity development in the (Pennsylvanian) upper Morrow chert conglomerate “Puryear” member, Roger Mills and Beckham counties, Oklahoma: unpublished M.S. thesis, Oklahoma State University, 134 p.

Asquith, George, and Krygowski, Daniel, 2006, “Basic Well Log Analysis”. 2nd Edition. American Association of Petroleum Geologists Methods in Exploration Series, No. 16.

Boyd, Dan T. “Stratigraphic Guide to Oklahoma Oil and Gas Reservoirs,” Oklahoma Geological Survey, 2008.

Boeckman, Charles H., 1958, “A Subsurface Study of the Lower Pennsylvanian Sediments of Northern Grady and Caddo Counties, Oklahoma” The Shale Shaker Digest II, Vol. VI-VIII. p. 97-114.

Brown, L. F. Jr., 1979, “Deltaic Sandstone Facies of the Mid-continent” Tulsa Geological Society, 2006.

Cain, C. L., 2018, Deciphering the Cleveland Sandstone stratigraphic framework: differentiating the Kiefer and Owasso sandstone complexes, north-central Oklahoma, unpublished M.S. thesis, Oklahoma State University, 111 p.

Coleman, J. M., and Prior, D. B., 1982, “Deltaic Environments of Deposition”; in Scholle,
P. A., and Spearing, D., ed., “Sandstone Depositional Environments”. American Association of Petroleum Geologists Memoir No. 31, p. 139-178.

Coleman, J.M., and Wright, L.D., 1975, “Modern River Deltas: Variability of Processes and Sand Bodies”, Models for Exploration: Houston Geological Society, p. 99 – 149.

Dalrymple, Robert W., Baker E. K., Harris, P. T. and M. G. Hughes, 2003, “Sedimentology and Stratigraphy of a Tide-dominated, foreland-basin delta (Fly River, Papua New Guinea)”. SEPM Special Publication No. 76, p. 147-173.

Fisher, W. L., 1990, “Delta Systems and Oil and Gas Occurrence”. Bureau of Economic Geology, The University of Texas at Austin. p. 13-26.

Fisher, W.L., and McGowen, J.H., 1969, “Depositional Systems in Wilcox Group (Eocene) of Texas and Their Relation to Occurrence of Oil and Gas”. American Association of Petroleum Geologists Bulletin, Vol. 53, No. 1. p. 30-54.

Folk, R. L., 1974, Petrology of sedimentary rocks: Hemphill Publishing Company, Austin Texas, 132 p.

Galloway, William E., 1975, “Process Framework for Describing the Morphologic and Stratigraphic Evolution of Deltaic Depositional Systems”. Houston Geological Society, 2007. Deltas: Models for Exploration. p. 87-98

Goodbred, Steven L. and Saito Yoshiki, 2011, “Tide-Dominated Deltas”; in Davis Jr. and Dalrymple, Robert, “Principles of Tidal Sedimentology.” p. 129-149

Harlton, Bruce H., 1960, “Stratigraphy of Cement Pool and Adjecent Area, Caddo and Grady Counties, Oklahoma” Bulletin of the American Association of Petroleum Geologists Vol. 44, No. 2. p. 210-226.

Henry, M.E., and Hester, T.C., 1995, “Anadarko Basin Province (058)”, *in* Gautier, D.L., Dolton, G.L., Takahashi, K.I., and Varnes, K.L., eds., 1995 National assessment of United States oil and gas resources on CD-ROM: U.S. Geological Survey Digital Data Series 30, 51 p., accessed April 20, 2011, at *http://energy.cr.usgs.gov/oilgas/noga/1995.html*.

Herrmann, Leo A., 1961, “Structural Geology of Cement-Chickasha Area, Caddo and Grady Counties, Oklahoma” Bulletin of the American Association of Petroleum Geologists Vol. 45, No. 12. p. 1971-1993.

Johnson, Kenneth S., 1988, “Geologic Evolution of the Anadarko Basin, in Anadarko Basin Symposium” Oklahoma Geological Survey Circular 90. p. 3-12

Jordan, L, 1957, “Subsurface Stratigraphic Names of Oklahoma” Oklahoma Geological Survey, Guide Book VI. p. 132.

Krumme, G.W. and Visher, G.S., 1972, The Seminole Formation in Tulsa County. Tulsa Geological Society, Digest, 37: p. 103-112

Lange, Edward Bernard Jr., 1984, “Middle Hoxbar (Missourian) from Shelf to Basin in the Northeastern Anadarko Basin” Limestones of the Mid-Continent. (1984). p. 273-306.

Moore, George E., 1979, “Pennsylvanian Paleogeography of the Southern Mid-continent” Pennsylvanian Sandstones of the Midcontinent: Tulsa Geological Society, p. 2-12.

Rascoe, B., and Adler, F.J., 1983, “Permo-carboniferous Hydrocarbon Accumulations, Mid-Continent, U.S.A”. American Association of Petroleum Geologist Bulletin. Vol. 67. No. 6. p. 979-1001.

Rascoe, B. Jr., and Adler F. J., 1987, “Permo-Carboniferous Hydrocarbon Accumulations, Mid-Continent U.S.A.” Tulsa Geological Society Special Publication No. 3.

Sawyerr, Olumuyiwa A., 1973, " Subsurface Stratigraphic Analysis, Lower Hoxbar Group (Pennsylvanian), Dutton-Verden-Norge-Trend, Caddo and Grady Counties, Oklahoma" The Shale Shaker Digest VII, Vol. XXI-XXIII. p. 217-242.

Scholle, Peter A., and Ulmer-Scholle, Dana S., 2003, "A Color Guide to the Petrography of Carbonate Rocks: Grains, Textures, Porosity, Diagenesis". American Association of Petroleum Geologists Memoir No. 77.

Seale, John D., 1982,"Depositional Environments and Diagenesis of Upper Pennsylvanian Marchand Sandstone on South, East and Northeast Flanks of the Anadarko Basin" The Shale Shaker Digest X Vols XXX-XXXII. P. 322-343.

Shelton, John W. "Models of Sand and Sandstone Deposits: A Methodology for Determining Sand Genesis and Trend" Bulletin 118, Oklahoma Geological Society

Smirnova, N. V., 1959. "Types of Cement and Their Effect on Permeability of Sandy Rocks" Petroleum Geology: A digest of Russian literature of Petroleum Geology. Vol 3. p. 413-419.

Stonecipher, Sharon A., 1999, "Genetic Characteristics of Glauconite and Siderite: Implications For The Origin of Ambiguous Isolated Marine Sandbodies". Society for Sedimentary Geology. Publication No. 64. p. 191-204.

Taylor, A. M. and R. Goldring, 1993, Description and analysis of bioturbation and ichnofabric: Journal of the Geological Society, v. 150, p. 141-148.

US Geological Survey (USGS), 2020, U.S. geologic names lexion (Geolex) National Geologic Maps Database: https://ngmdb.usgs.gov/Geolex/search

Waller, Bryan R., 1994, "Depositional Environment, Petrology, Diagenesis and Petroleum Geology of the Cottage Grove Sandstone, North Concho Field, Canadian County, Oklahoma: (Part 1)" The Shale Shaker Digest XIII Vols. XXXX-XXXXIV. p. 265-275.

Waller, Bryan R., 1994, "Depositional Environment, Petrology, Diagenesis and Petroleum Geology of the Cottage Grove Sandstone, North Concho Field, Canadian County, Oklahoma: (Part 2)" The Shale Shaker Digest XIII Vols. XXXX-XXXXIV. p. 276-286.

White, Howard, Kirkland, R., Glassman E. and G. Schnerk, 1999, "Revisiting Pennsylvanian Reservoir Architecture – Chitwood, Norge, and Northeast Verden Fields, Caddo and Grady Counties, Oklahoma. AAP Midcontinent Section Meeting. p. 212-219.

APPENDICES

APPENDIX A

Core Box Photos

EOG Resources Jobe 31 No. 1

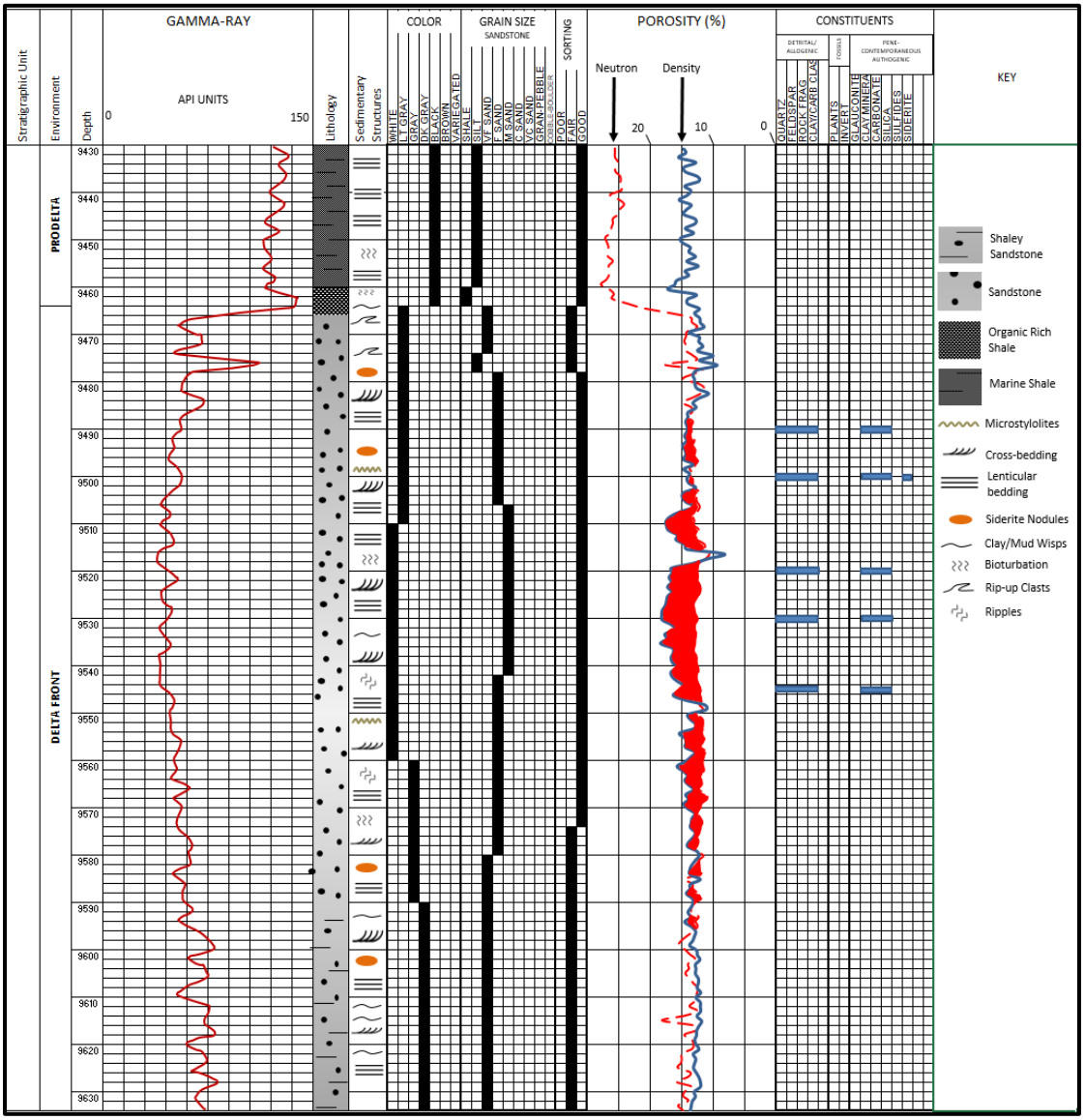

Jobe 31-1: Lithologic log with gamma-ray and porosity curves.

Core Photographs EOG Resources Jobe 31 No. 1: Depths: 9430 – 9634 feet.

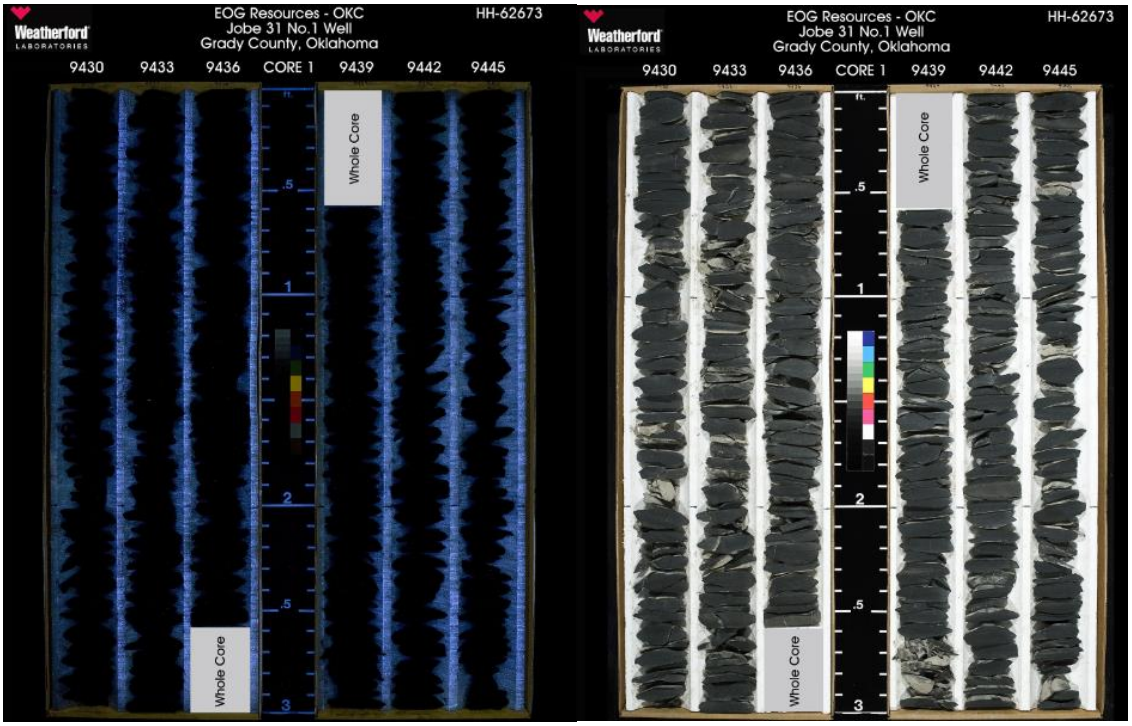

Core photograph 9430-9448 feet. Left: ultraviolet light. Right: normal light

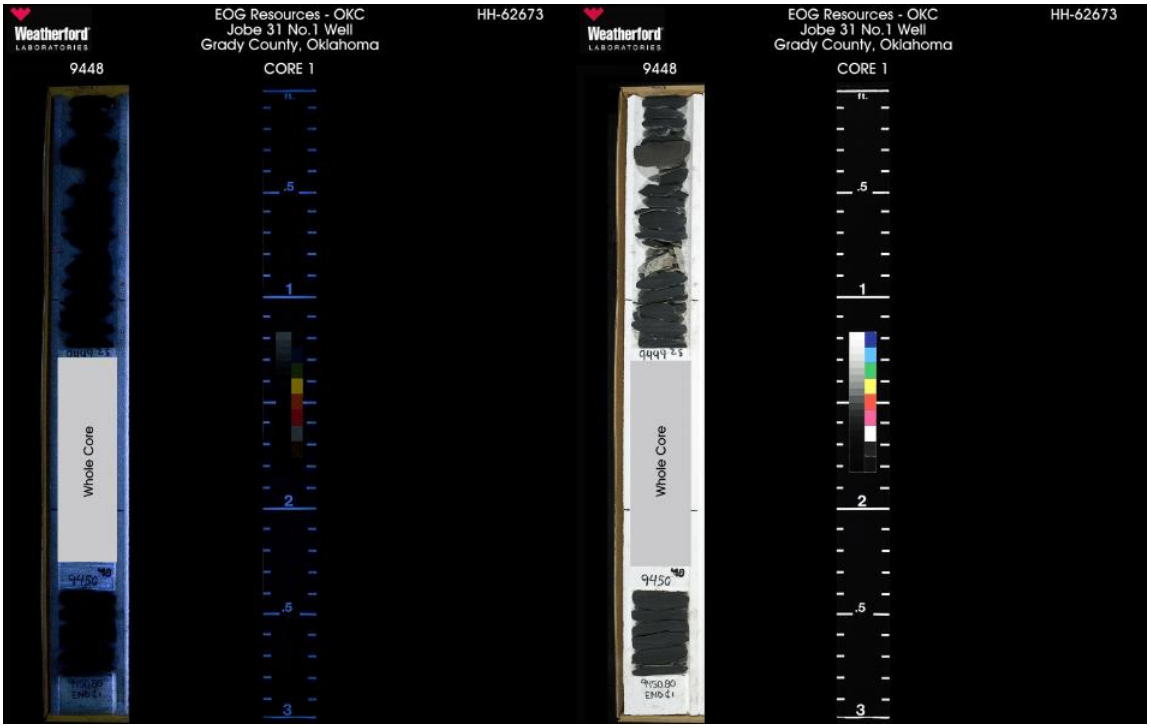

Core photograph 9448-9450.8 feet. Left: ultraviolet light. Right: normal light

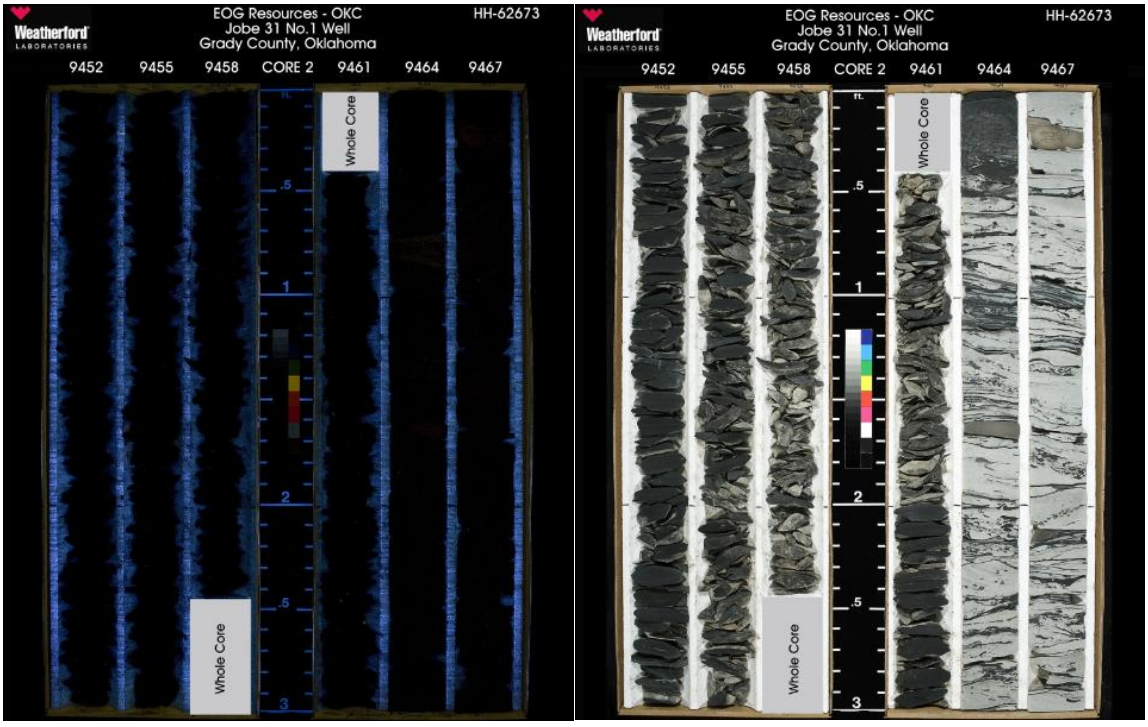

Core photograph 9452-9467 feet. Left: ultraviolet light. Right: normal light

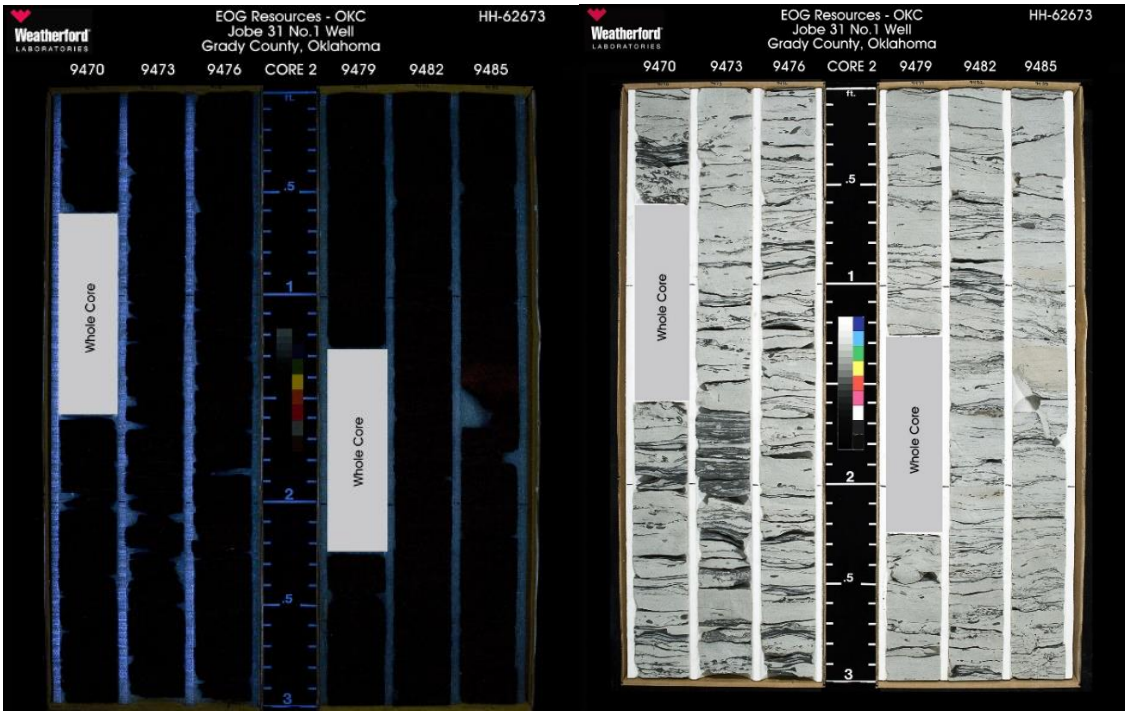

Core photograph 9470-9488 feet. Left: ultraviolet light. Right: normal light

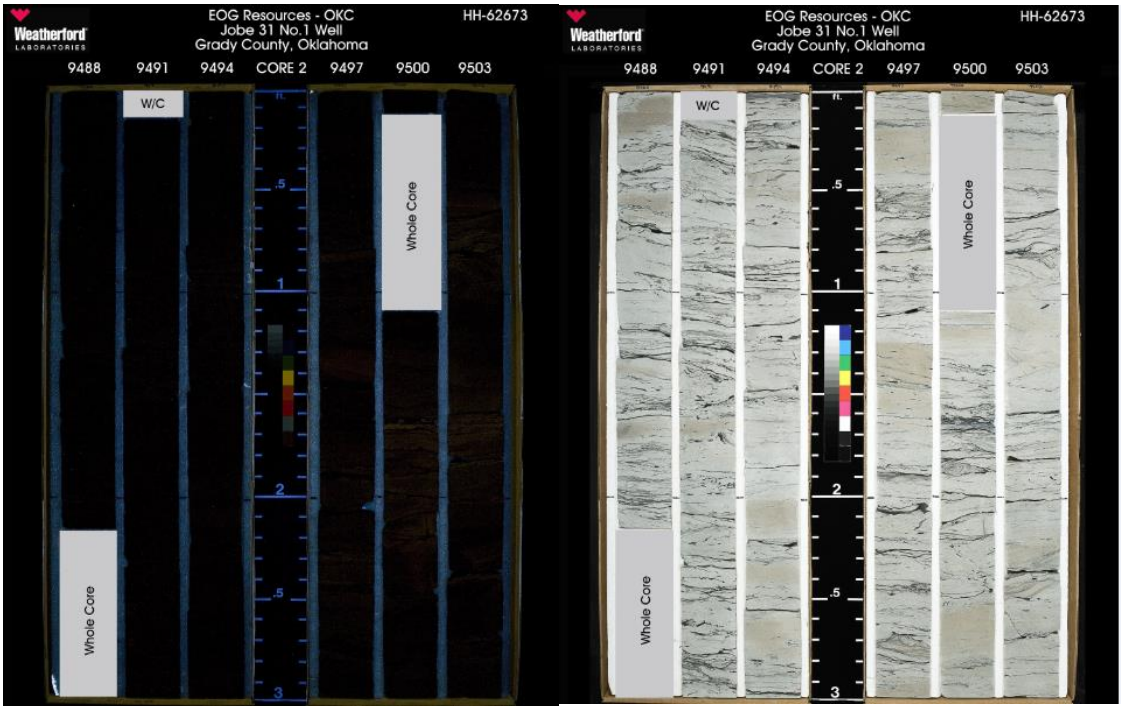

Core photograph 9488-9506 feet. Left: ultraviolet light. Right: normal light

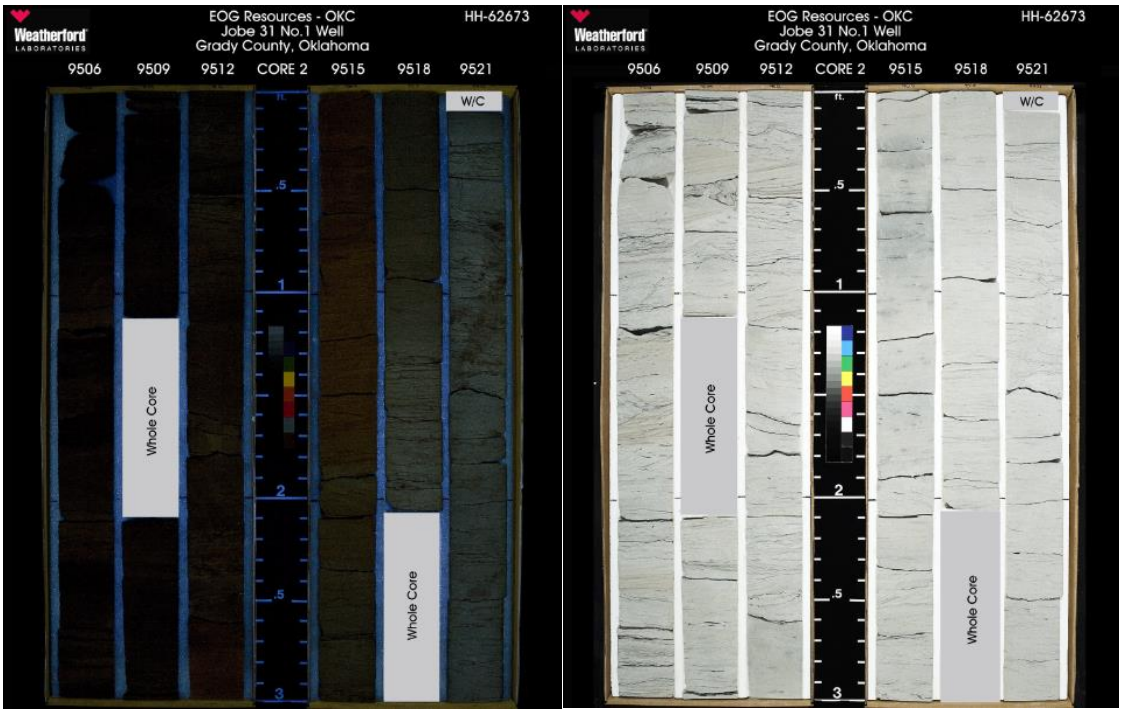

Core photograph 9506-9524 feet. Left: ultraviolet light. Right: normal light

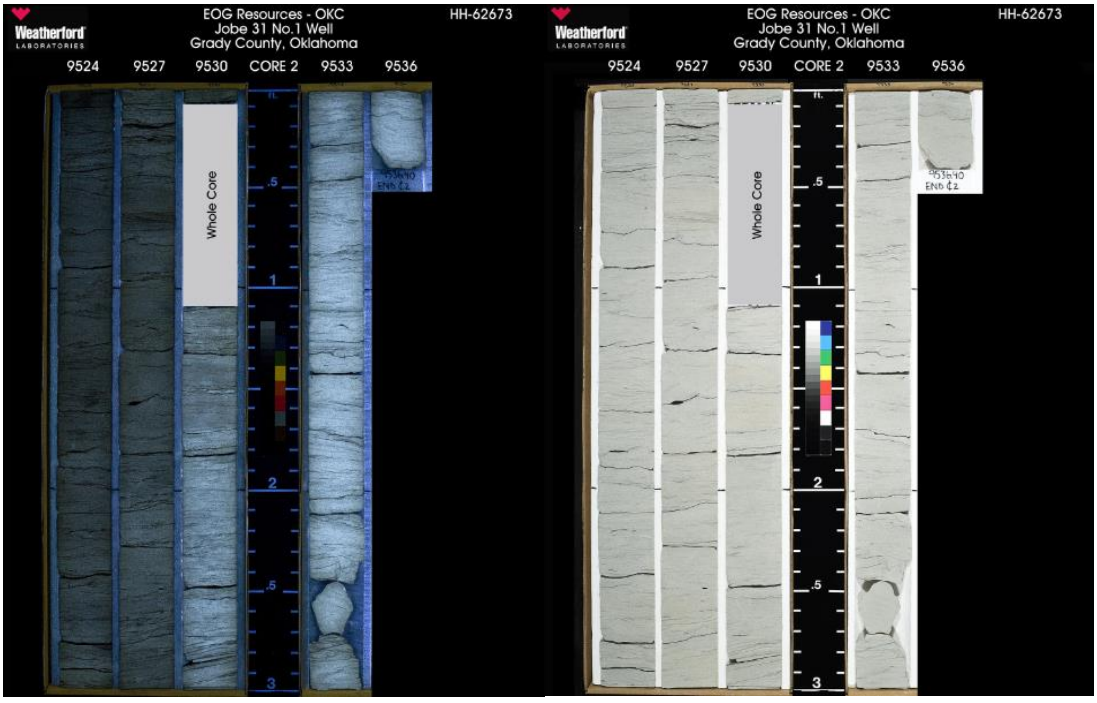

Core photograph 9524-9536.4 feet. Left: ultraviolet light. Right: normal light

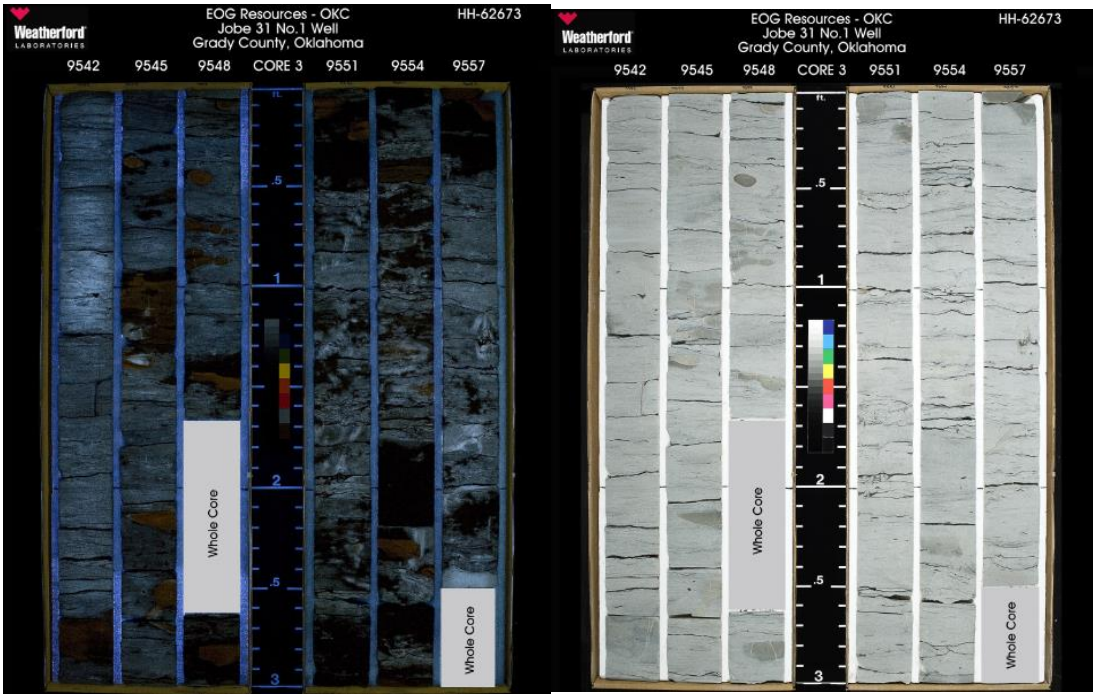

Core photograph 9542-9560 feet. Left: ultraviolet light. Right: normal light

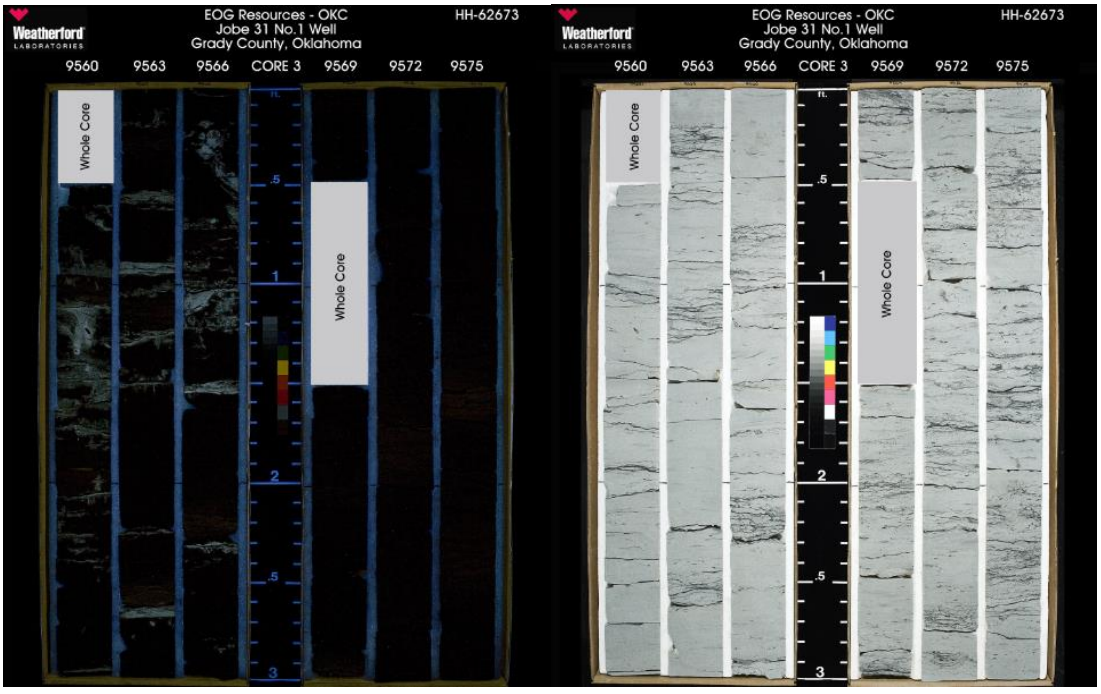

Core photograph 9560-9578 feet. Left: ultraviolet light. Right: normal light

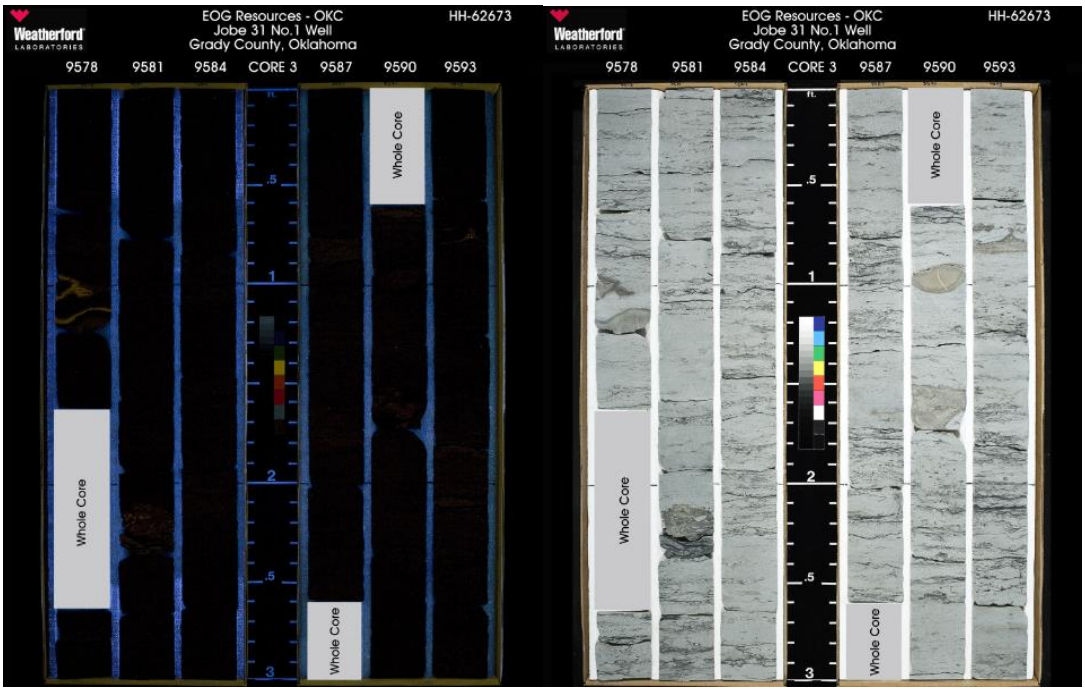

Core photograph 9578-9596 feet. Left: ultraviolet light. Right: normal light

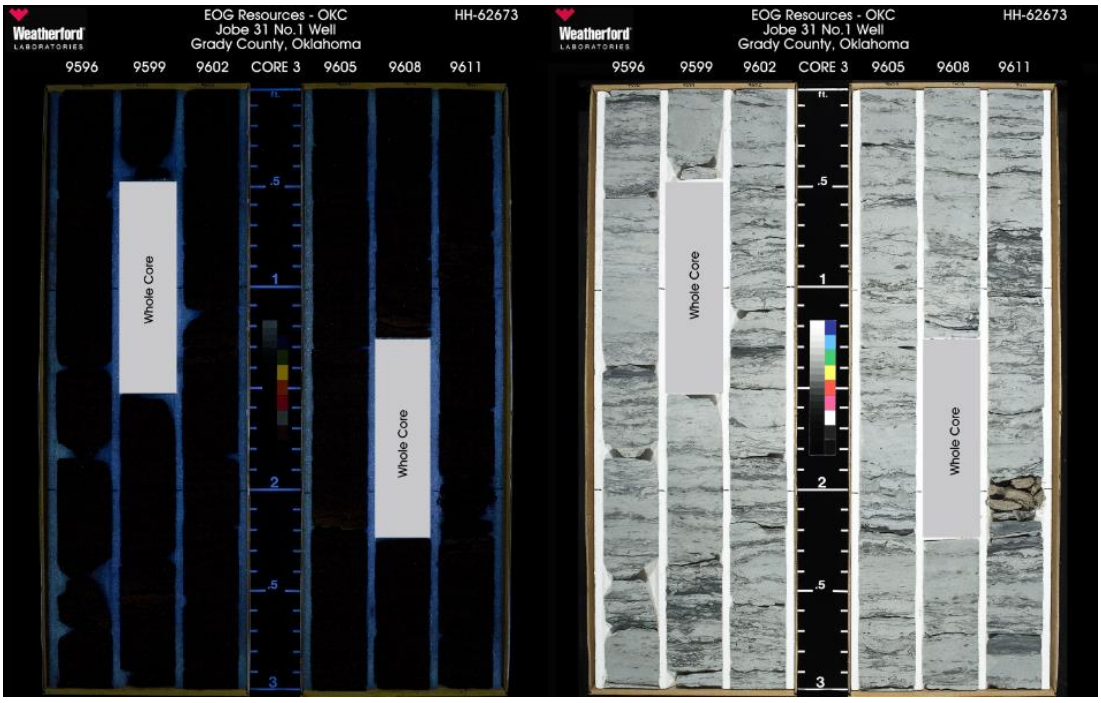

Core photograph 9596-9614 feet. Left: ultraviolet light. Right: normal light

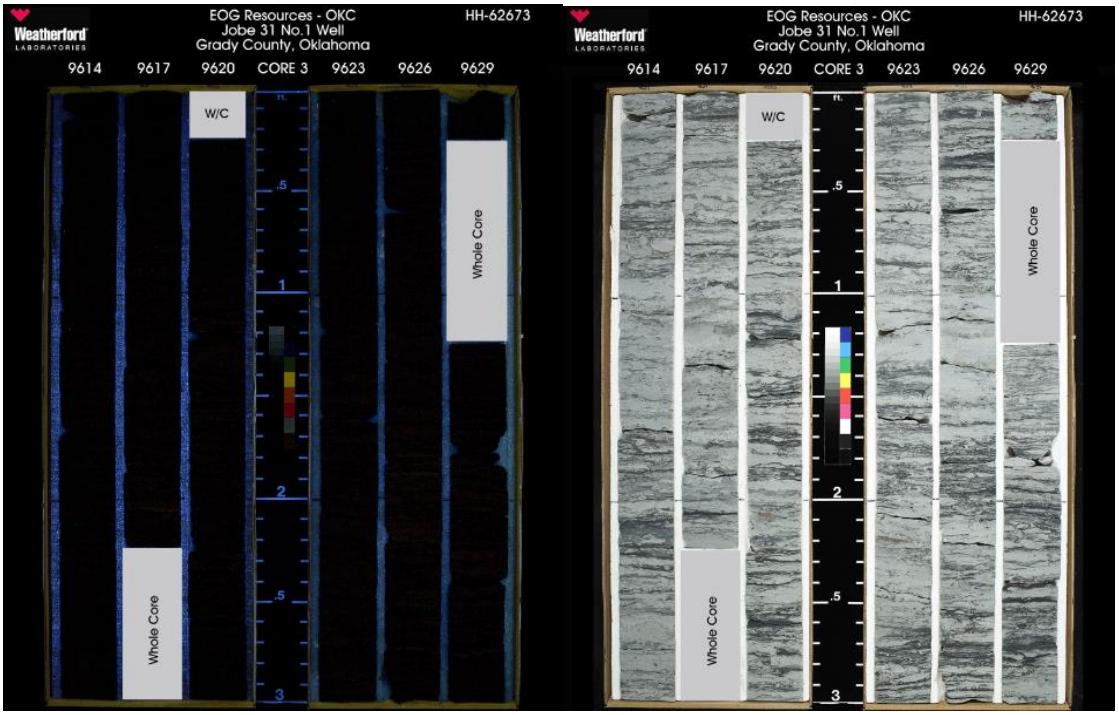

Core photograph 9614-9632 feet. Left: ultraviolet light. Right: normal light

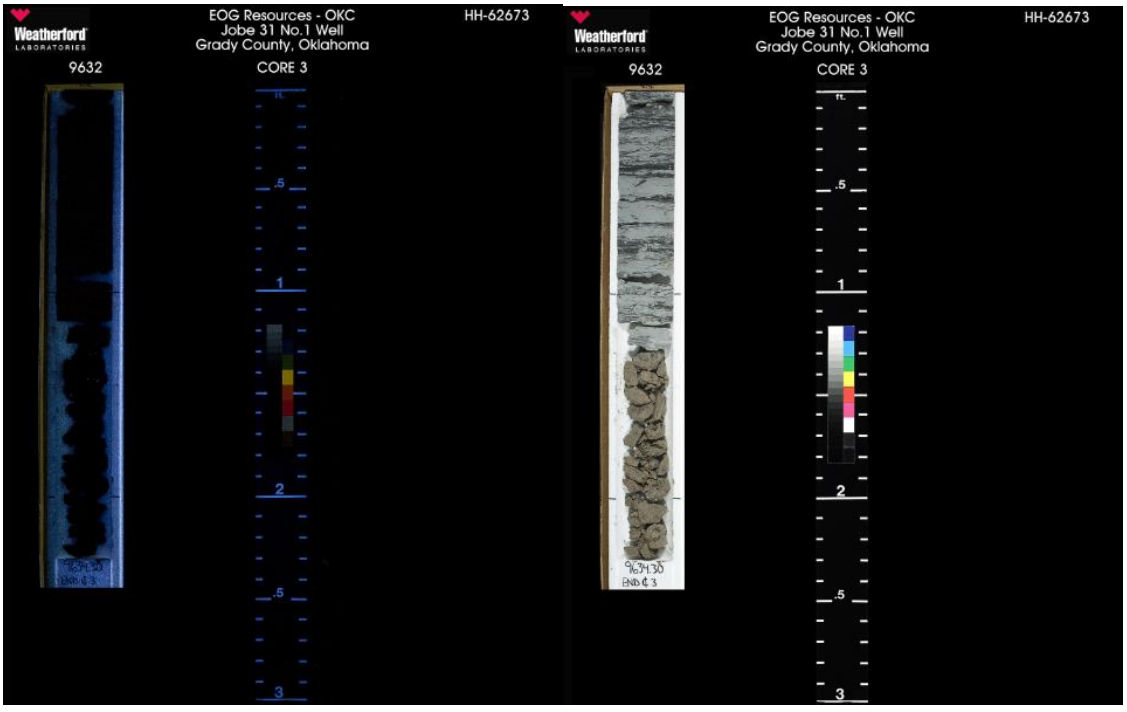

Core photograph 9632-9634 feet. Left: ultraviolet light. Right: normal light

EOG Resources, Schmidt 16 3H

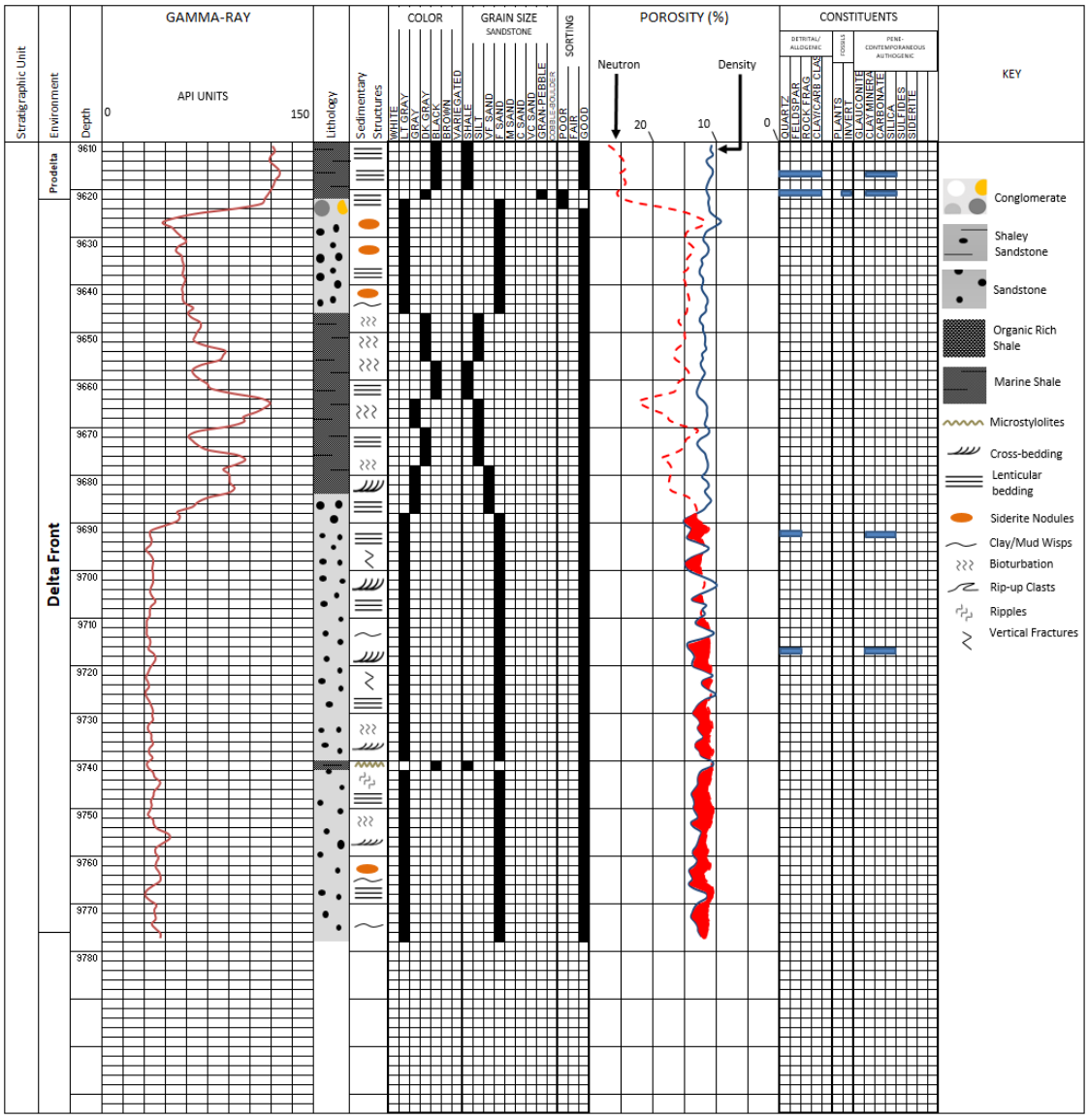

Schmidt 16 3H: Lithologic log with gamma-ray and porosity curves.

Core Photographs EOG Schmidt 16 No. 3H. Depth: 9608 – 9774 feet

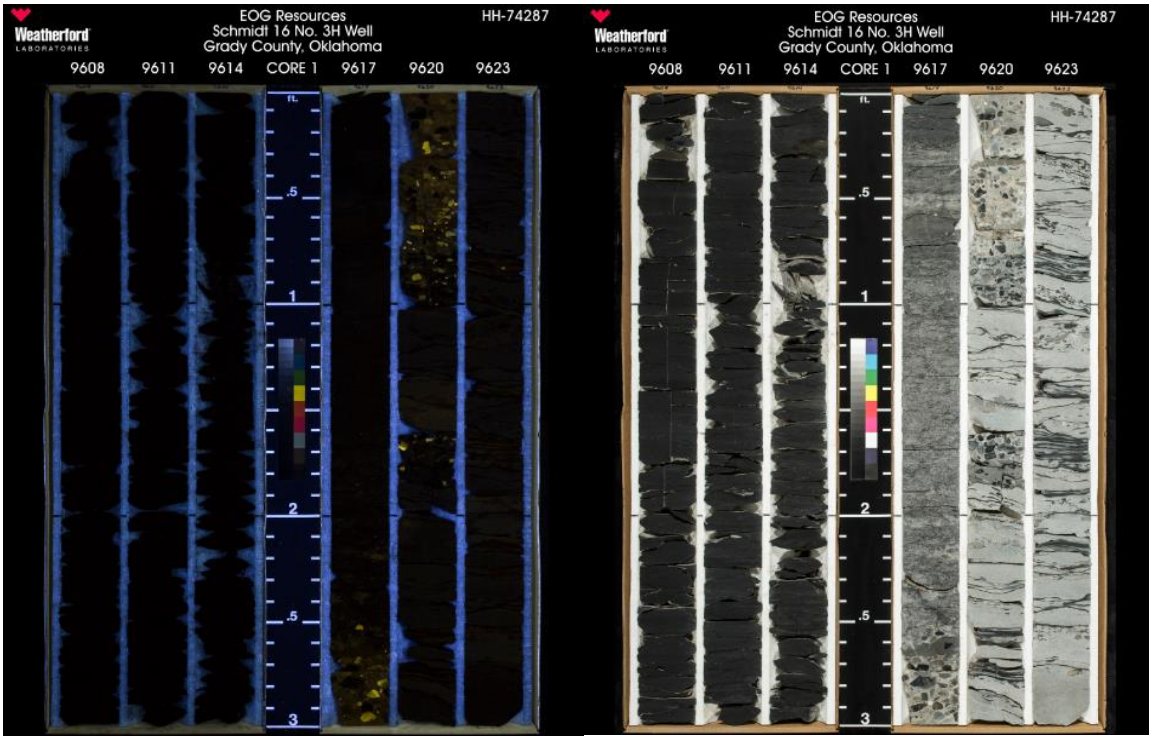

Core photograph 9608-9626 feet. Left: ultraviolet light. Right: normal light

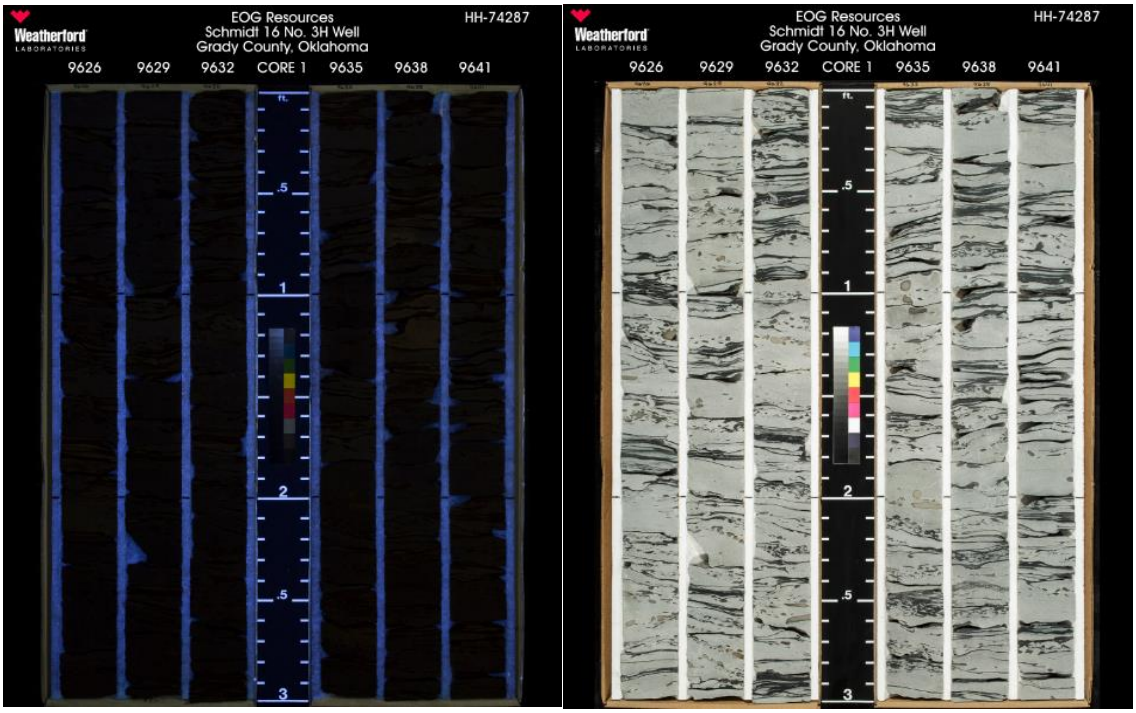

Core photograph 9626-9644 feet. Left: ultraviolet light. Right: normal light

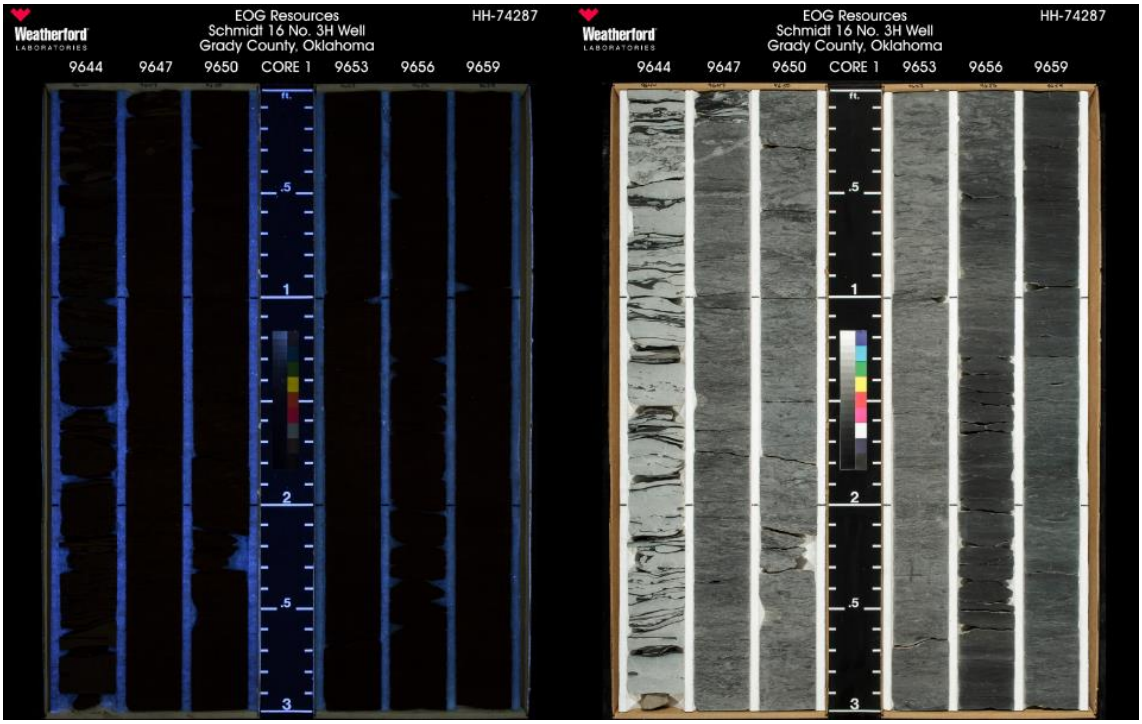

Core photograph 9644-9662 feet. Left: ultraviolet light. Right: normal light

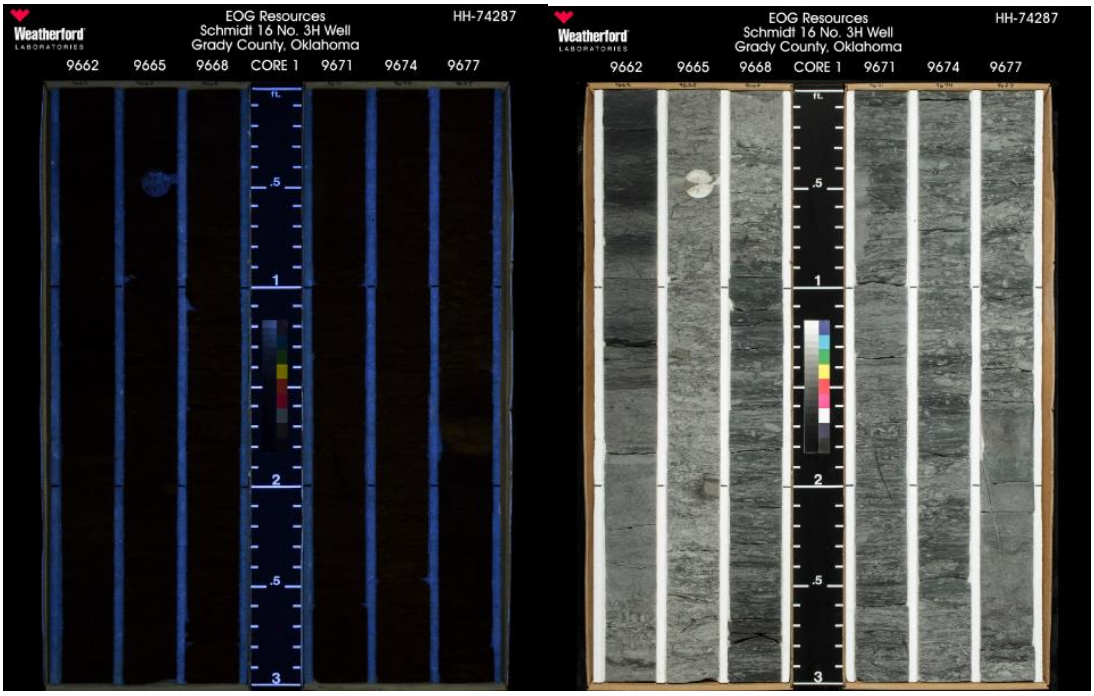

Core photograph 9662-9680 feet. Left: ultraviolet light. Right: normal light

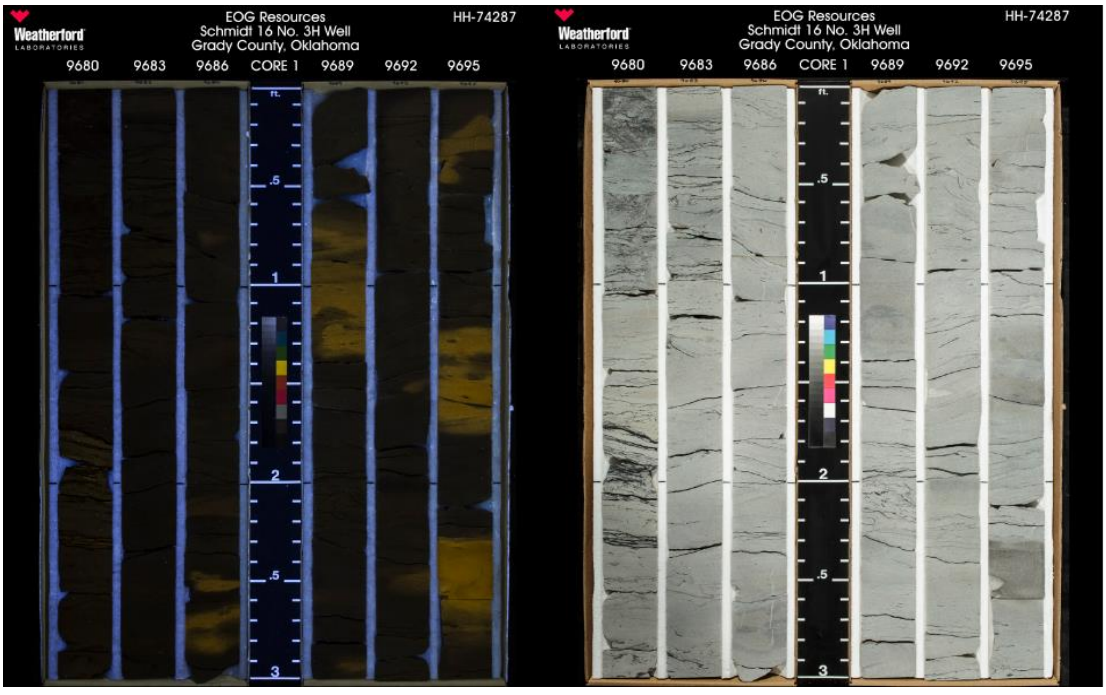

Core photograph 9680-9698 feet. Left: ultraviolet light. Right: normal light

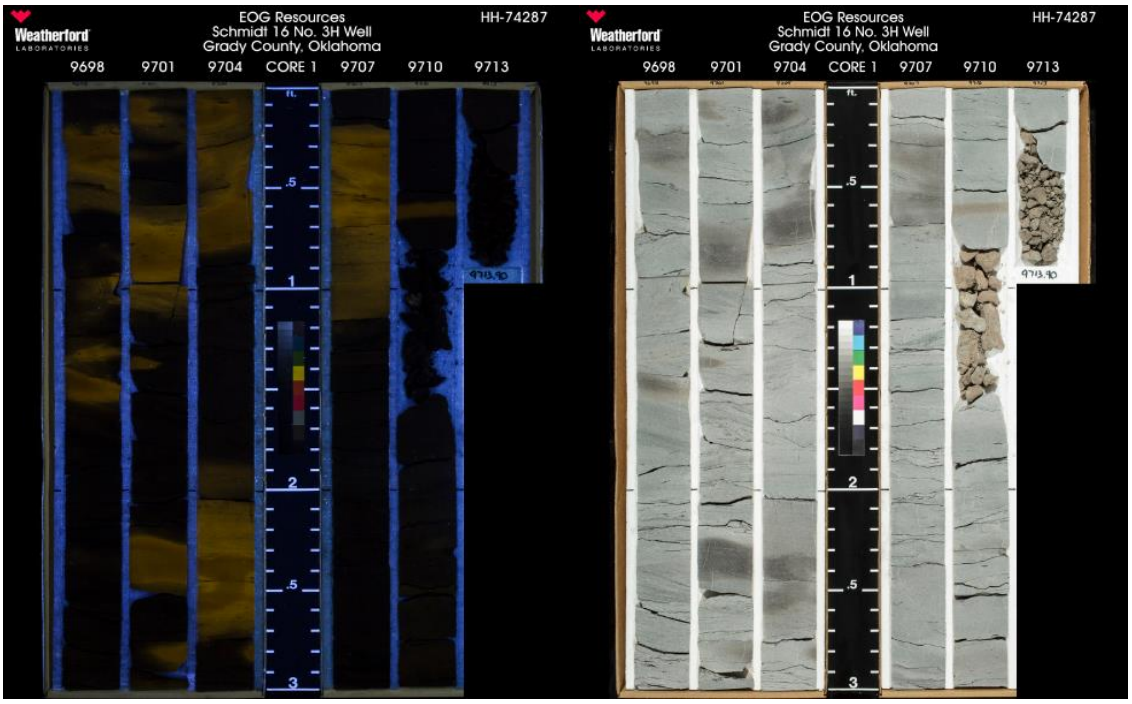

Core photograph 9698-9714 feet. Left: ultraviolet light. Right: normal light

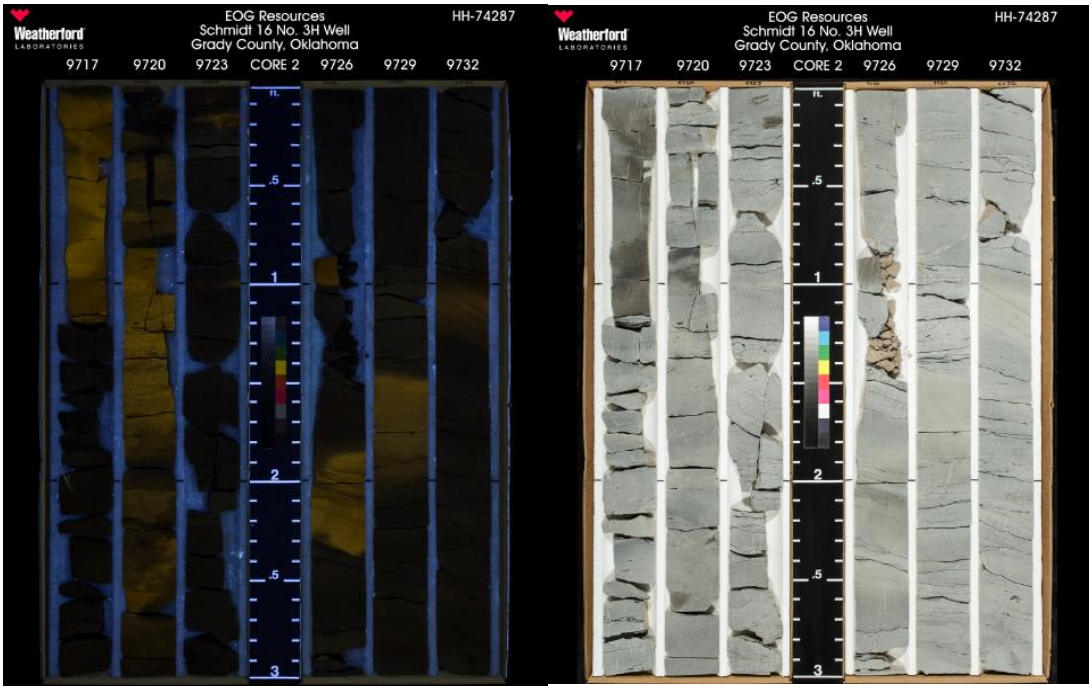

Core photograph 9717-9735 feet. Left: ultraviolet light. Right: normal light

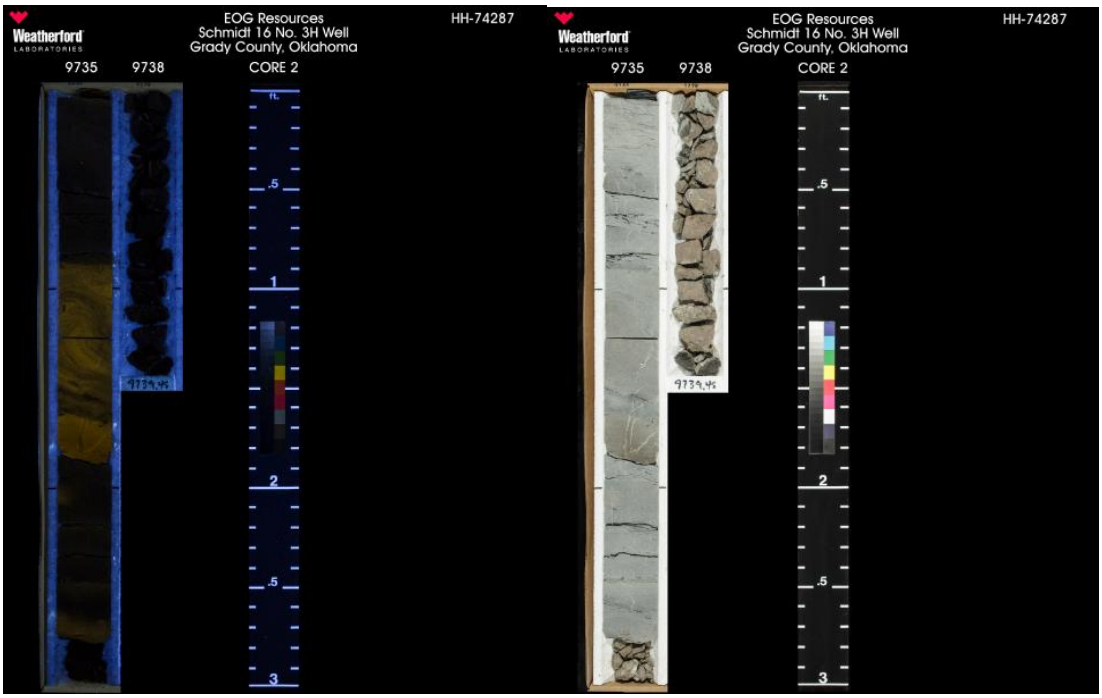

Core photograph 9735-9739.45 feet. Left: ultraviolet light. Right: normal light

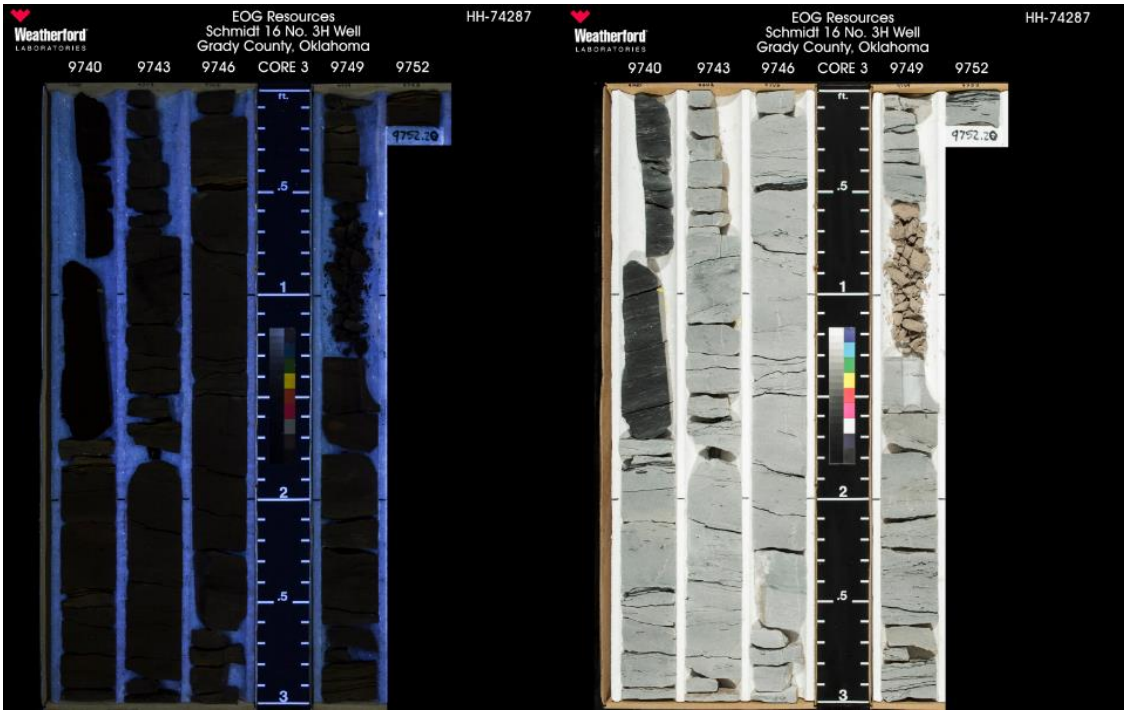

Core photograph 9740-9752 feet. Left: ultraviolet light. Right: normal light

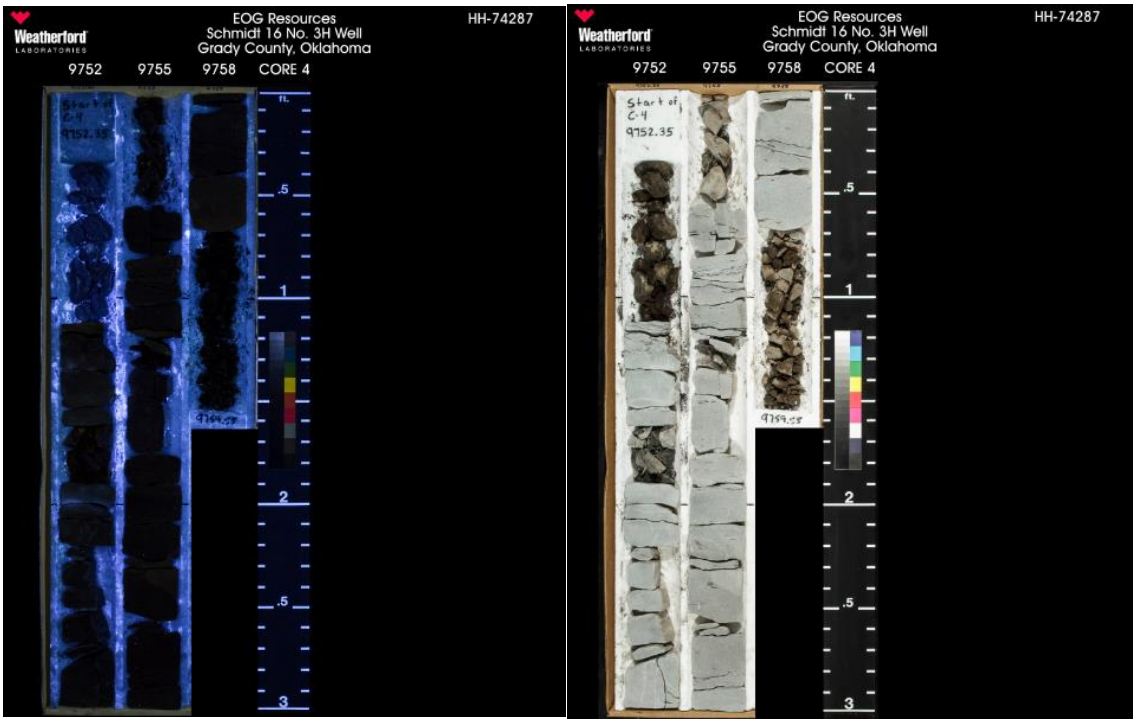

Core photograph 9752-9759 feet. Left: ultraviolet light. Right: normal light

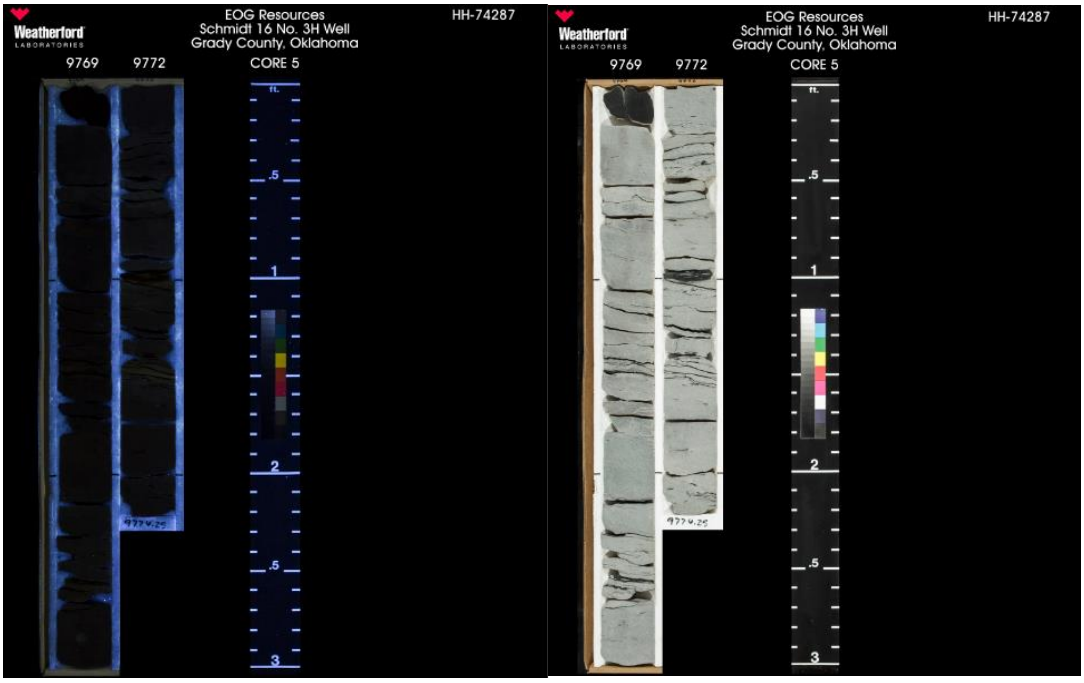

Core photograph 9769-9774 feet. Left: ultraviolet light. Right: normal light

APPENDIX B

Cross Sections of Study Area

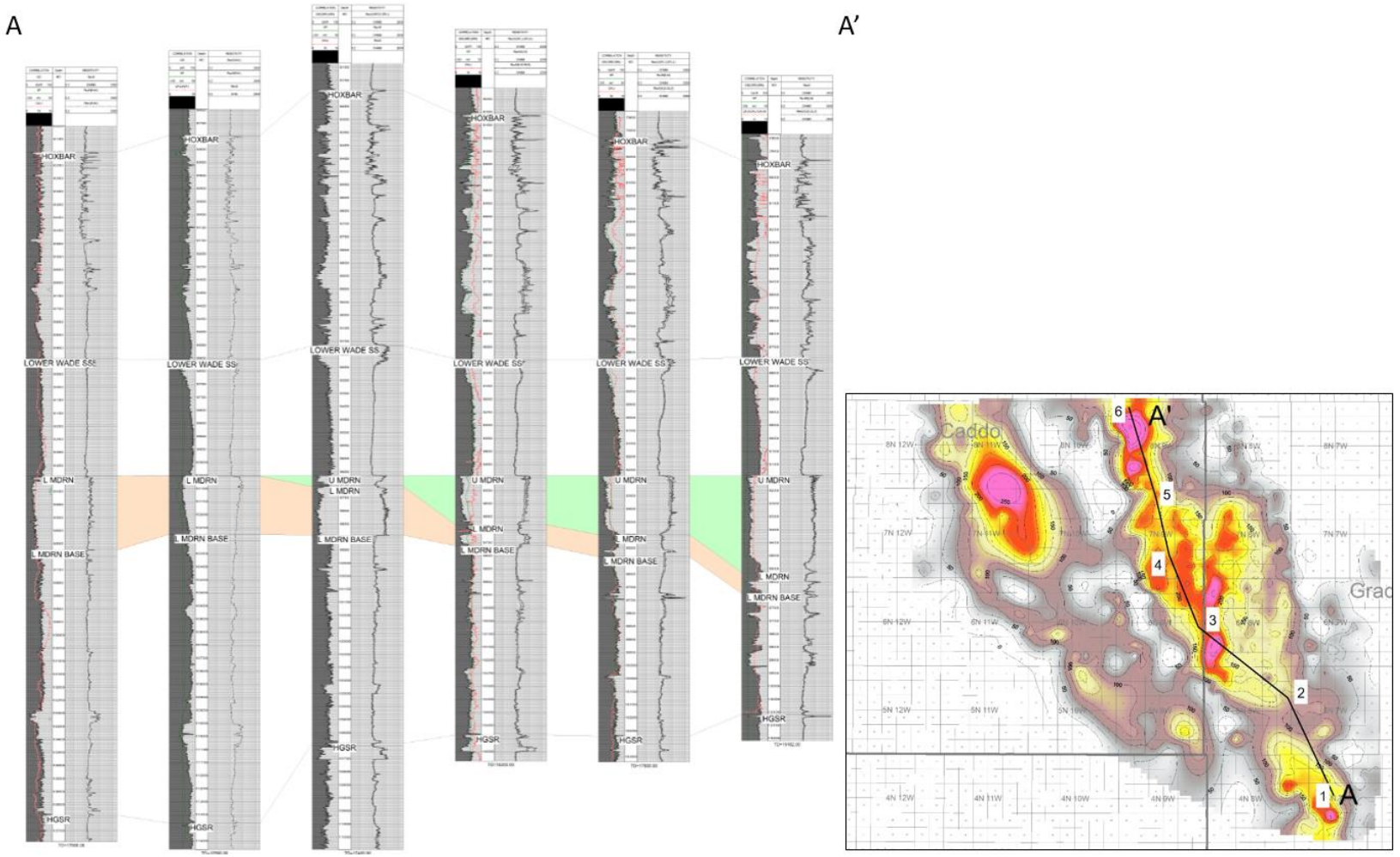

Stratigraphic Cross-Section A-A' showing distribution relationship of Lower and Upper Medrano Sandstone. Datum is top of Medrano interval.

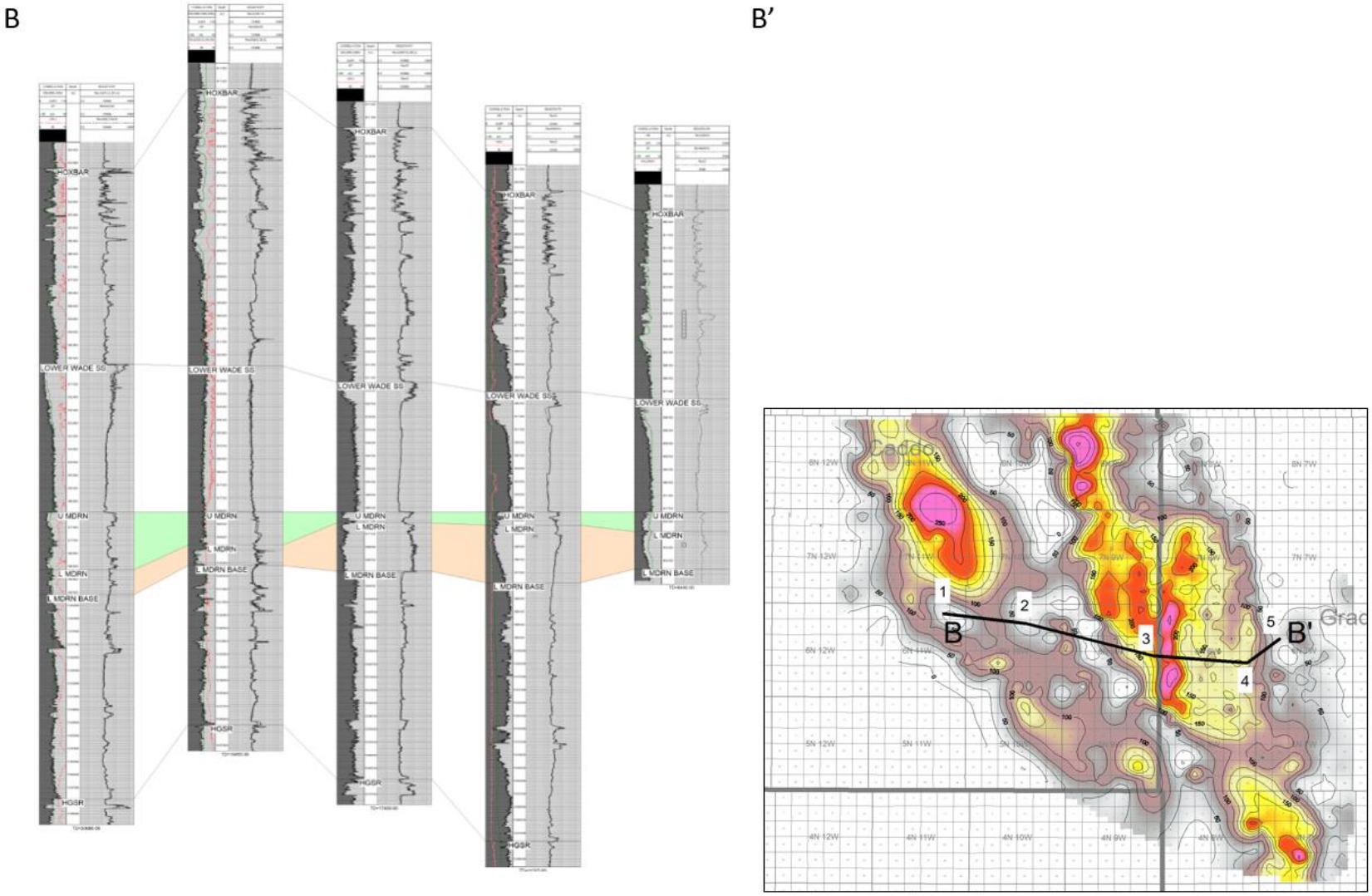

Stratigraphic Cross-Section B-B' showing distribution relationship of Lower and Upper Medrano Sandstone. Datum is top of Medrano interval.

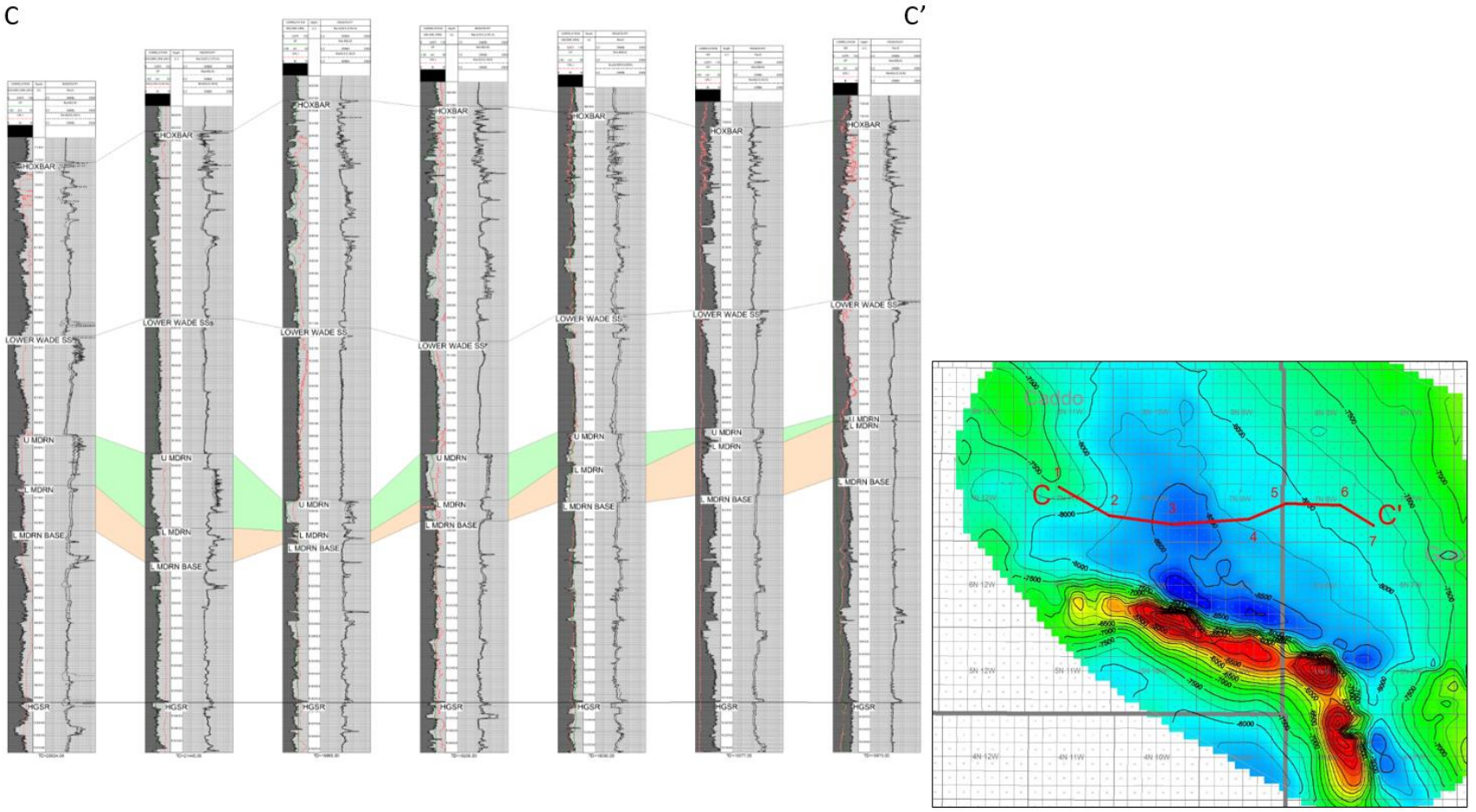

Stratigraphic Cross-Section C-C' showing internal stratigraphy of the Medrano Sandstone. Datum is Hogshooter marker.

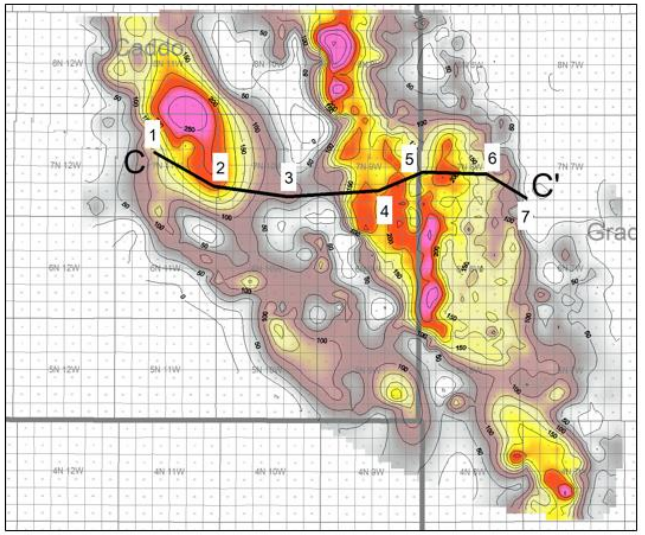

Stratigraphic Cross-Section C-C' showing distribution relationship of Lower and Upper Medrano Sandstone. Datum is top of Medrano interval.

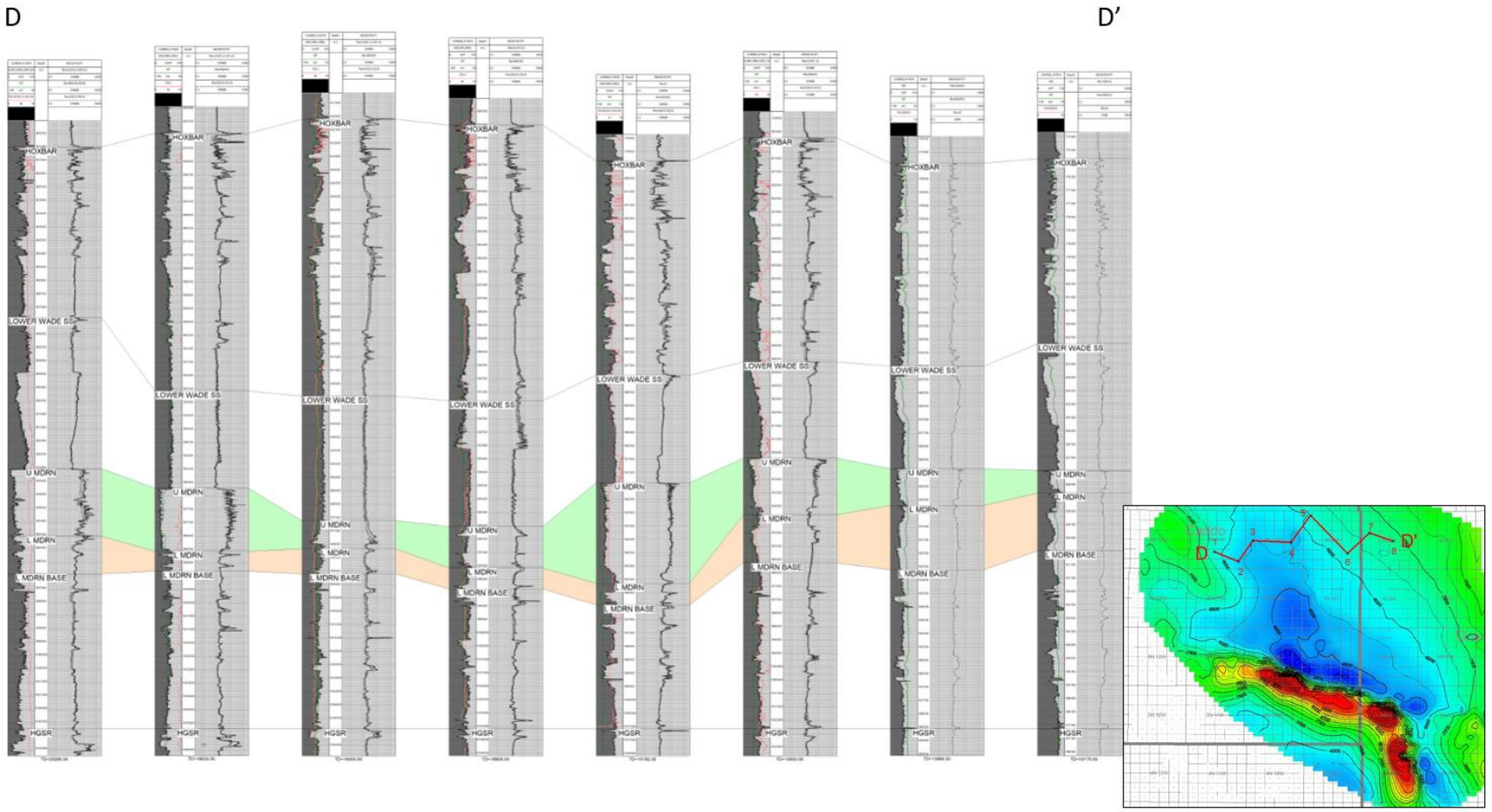

Stratigraphic Cross-Section D-D' showing internal stratigraphy of the Medrano Sandstone. Datum is Hogshooter marker.

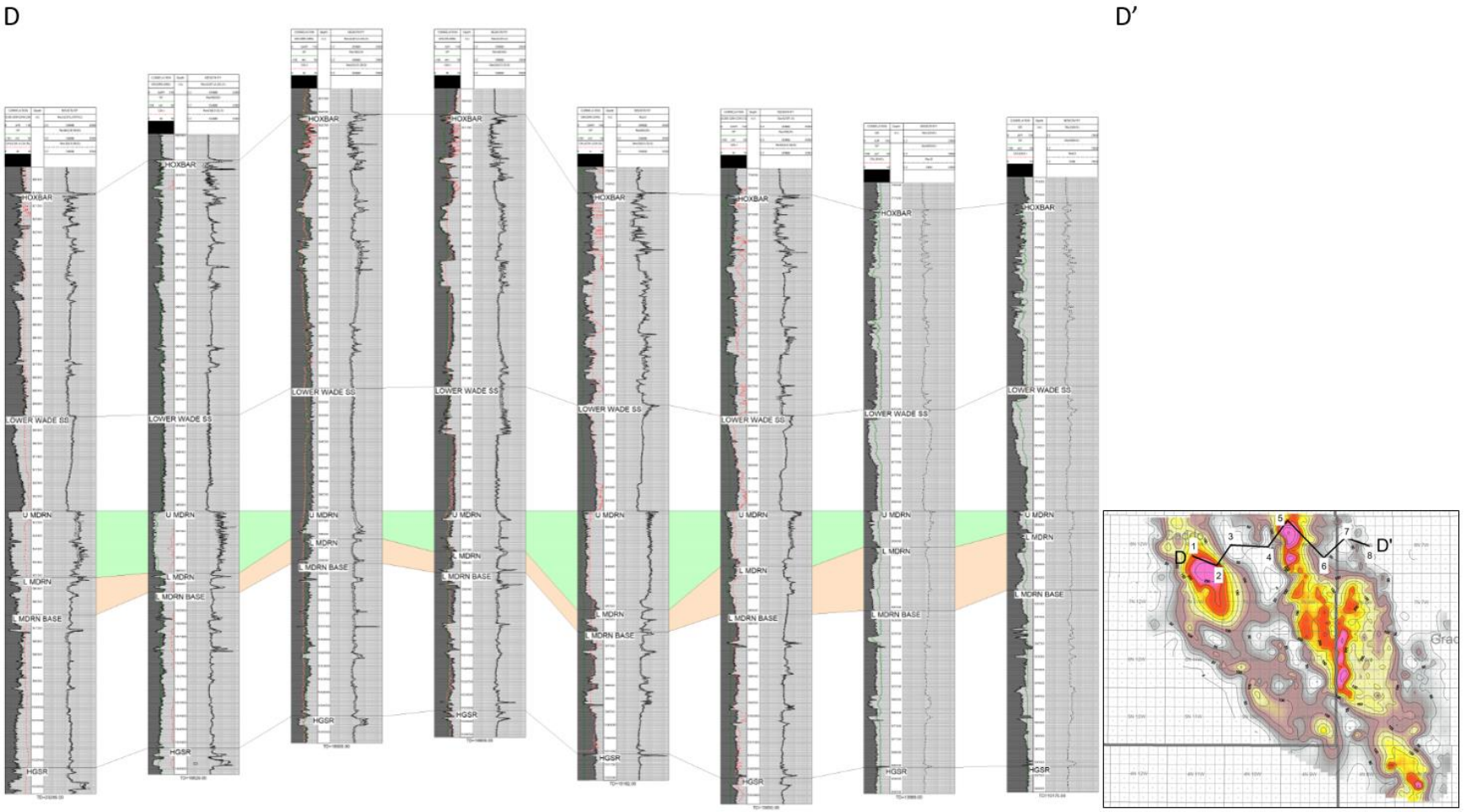

Stratigraphic Cross-Section D-D’ showing distribution relationship of Lower and Upper Medrano Sandstone. Datum is top of Medrano interval.

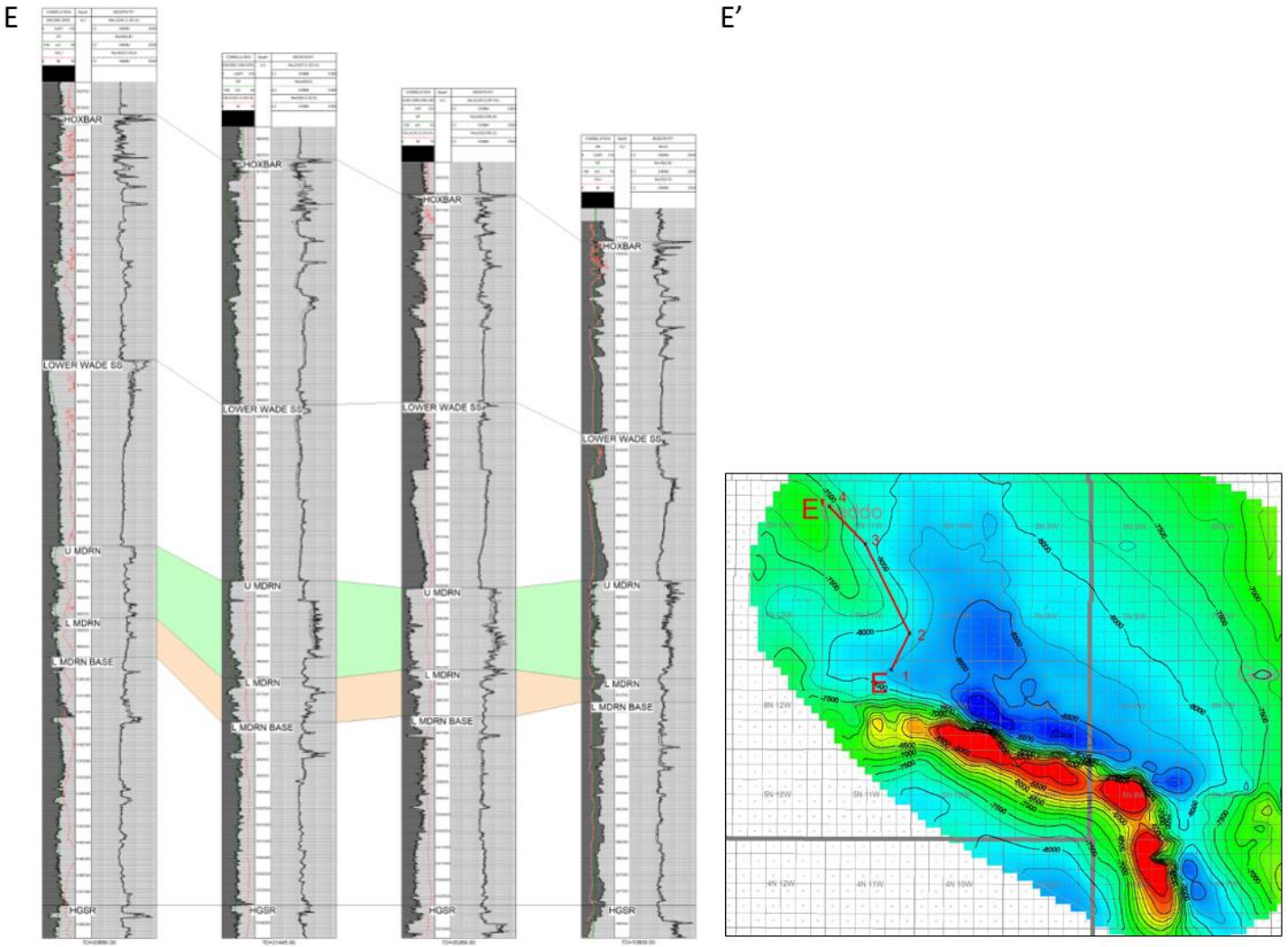

Stratigraphic Cross-Section E-E' showing depositional relationships for the Upper and Lower Medrano Sandstone. Datum is Hogshooter marker.

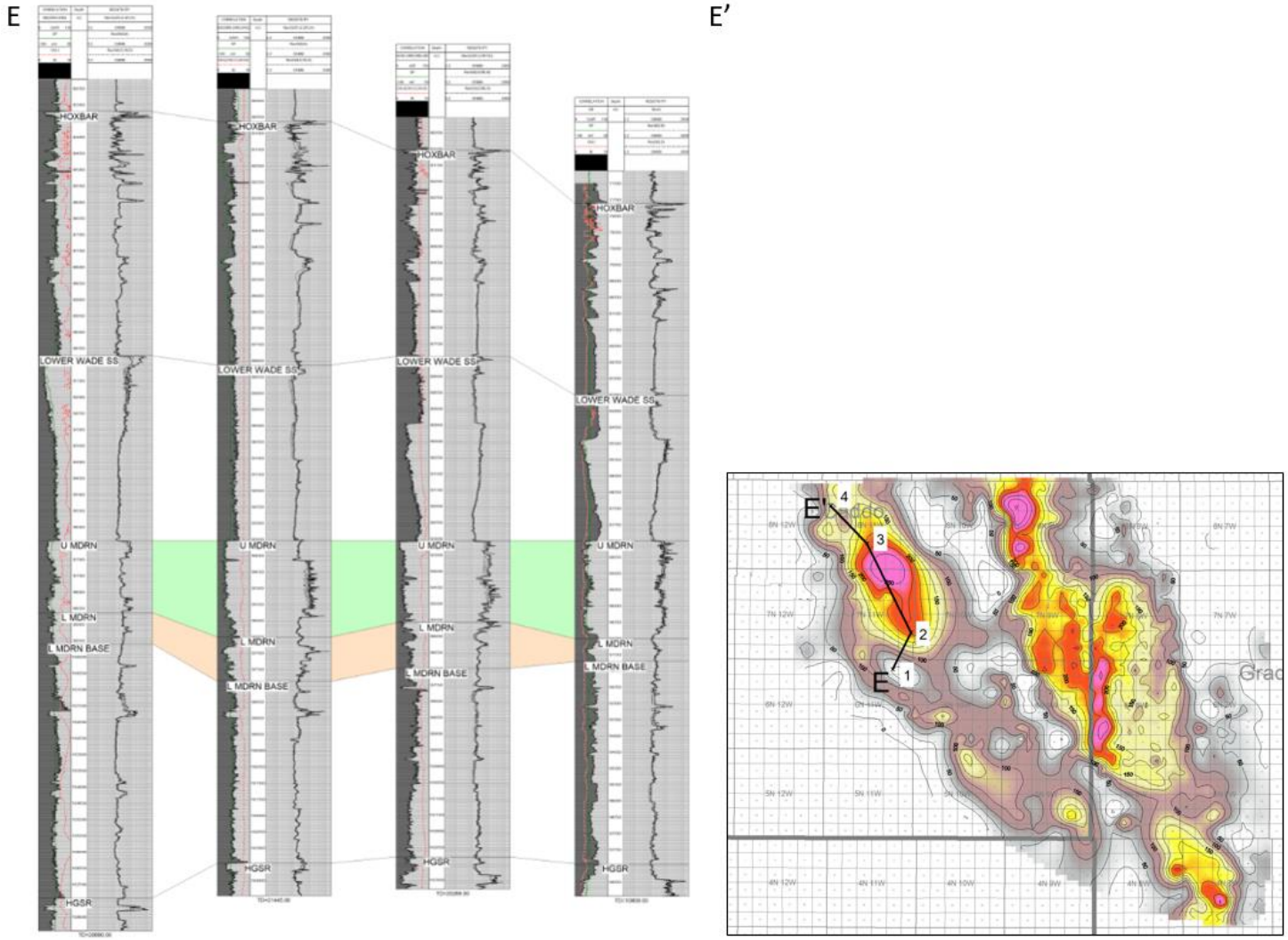

Stratigraphic Cross-Section E-E' showing distribution relationship of Lower and Upper Medrano Sandstone. Datum is top of Medrano interval.

VITA

Sean Christopher Ganes

Candidate for the Degree of

Master of Science

Thesis: DEPOSITION ENVIRONMENT AND RESERVOIR CHARACTERISTICS OF THE MEDRANO SANDSTONE, SOUTHERN OKLAHOMA HOXBAR OIL TREND (SOHOT)

Major Field: Geology

Biographical:

Education:

Completed the requirements for the Master of Science in Geology at Oklahoma State University, Stillwater, Oklahoma in December, 2020.

Completed the requirements for the Bachelor of Science in Geology at Oklahoma State University, Stillwater, Oklahoma in 2012.

Experience:

Geologist: Unit Petroleum Corporation
Geologist/Geoscience Manager: Chisholm Oil and Gas Operating, LLC

Professional Memberships: AAPG, TGS, OCGS